LABORATORY INDENTATION TESTING OF POLYCRYSTALLINE ICE: AN INVESTIGATION OF FRACTURE

THOMAS R. MACKEY

Laboratory Indentation Testing of Polycrystalline Ice: An Investigation of Fracture

by

Thomas R. Mackey, B. Eng., B.Sc.

A thesis submitted to the School of Graduate Studies
in partial fulfillment of the requirements for the degree of
Master of Engineering

Faculty of Engineering and Applied Science
Memorial University of Newfoundland
December 2005

St. John's Newfoundland Canada

Your file Votre référence
ISBN: 978-0-494-30482-2
Our file Notre référence
ISBN: 978-0-494-30482-2

Abstract

For industries working in artic and sub artic waters ice load is a major concern. Ice has an inherently varying mechanical nature related to material randomness caused by such things as internal flaws, grain size variation, varying growth history, varying temperature, among others. Due to theses uncertainties, accurate estimation of ice load is difficult. The objective of this report is to present the results of a laboratory test program designed to increase the knowledge of the material behaviour of ice. Work such as this will eventually allow the high degree of conservatism in ice load estimates to be reduced, leading to more economical design.

The report provides a relevant review of ice mechanics and ice load design. For design, two pressure area relationships are shown, one for local area and one for the global area. These are probabilistic tools, based on full scale data; this is currently necessary due to an incomplete understanding of the mechanisms occurring during an ice-structure interaction process. Presently there exists an inability to effectively predict the behaviour of ice using physics based numerical models.

The main objective of the report is to describe and present the results from an indentation test series completed as a joint collaboration between Memorial University and The Institute for Ocean Technology. The series consisted of small scale indentation tests (see test matrix below) designed to provide insight into the changing behaviour of ice under varying loading conditions. It is believed that an indention test can be used as a model of a spatially stationary, single, high pressure zone. It is proposed that a strong understanding of the mechanics occurring during an indention test can be used to further understand full scale interactions of ice with structures, which consist of many high pressure zones randomly distributed across the area of interaction.

			Number of Tests		
Indenter Diameter	Indenter Speed (mm/sec)		Indenter distance to the edge		
			Center (10 cm from edge)	Intermediate (5cm from edge)	Edge (2 cm from edge)
10 mm	5.0	Fast	**1**	**1**	**1**
10 mm	1.0	Medium	**1**	**1**	**1**
10 mm	0.1	Slow	**1**	**1**	**1**
20 mm	10.0	Fast	**1**	**1**	**1**
20 mm	2.0	Medium	**1**	**1**	**1**
20 mm	0.2	Slow	**1**	**1**	**1**

A high speed video camera was used in the analysis of the tests; this is a recent development in the study of ice mechanics in the laboratory arising from past observations during load tests in which qualitatively suggested that ejected ice appeared to be linked to load trace spike/drop sequences. The high speed imagery was used to correlate load trace events (i.e. load spikes/drop sequences, etc) with visual events. It was shown that large fractures or spalls are correlated with load drop spikes. It has also been demonstrated that "spiky" load graphs are related to repetitious spalling throughout the test (effective clearing of material from under the indenter) while smoother load graphs are related to continuous but small extrusion (ineffective clearing of material form the indenter).

Post test analysis of the tested samples (thin sectioning) provided evidence of damage mechanisms during testing. Evidence for micro-cracking, inter-grain boundary cracking, crushing, and recrystallization were all present in zone beneath the indenter. This is consistent with the current mechanics description of a high pressure zone, providing confidence in the current ice structure interaction models.

Acknowledgements

Ian Jordaan, his friendship and guidance are gratefully acknowledged. Ian is a skilled and graceful writer, and has always encouraged that I strive to improve this aspect of my work. It is hoped that I have.

Much appreciation is also extended to NRC-Institute for Ocean Technology, it was with great pleasure that I took advantage of the research equipment available at the cold room facilities located there. This was made possible through the assistance of Ahmed Derradji and Austin Bugden.

Contents

List of Figures

List of Tables

Chapter 1 Background

1.1 Introduction

Offshore activity related to the oil and gas industry in the East Coast of Canada is currently thriving. The Canada-Newfoundland and Labrador Offshore Petroleum Board (CNLOPB) estimates (May 19, 2004) the total amount of potential recoverable oil is 2055.6 million bbls; the total amount of potential recoverable gas is 9646 billion cu.ft.; and the total amount of potential recoverable natural gas liquids is 436 million bbls (see Table 1-1 and Figure 1-1).

Table 1-1: Reduced version of "Petroleum Reserves and Resources- Newfoundland Offshore Area" showing potential resources for areas of high interest.

Field	Oil million bbls	Gas billion cu. ft.	NGL million bbls
Grand Banks			
Hibernia	865	1320	160
Terra Nova	354	44.9	3
Hebron	325	-	-
Whiterose	283	2722	96
West Ben Nevis	34	-	-
Sub-Total (all Grand Banks)	2056	5402	313
Labrador Shelf			
Sub-Total (all Labrador Shelf)	0	4244	123
Total	2055.6	9646	436
"Resources" are volumes of hydrocarbons, expressed at 50% probability of occurrence, assessed to be technically recoverable that have not been delineated and have unknown economic viability. (http://www.cnlopb.nl.ca/ Dated: May 19, 2004)			

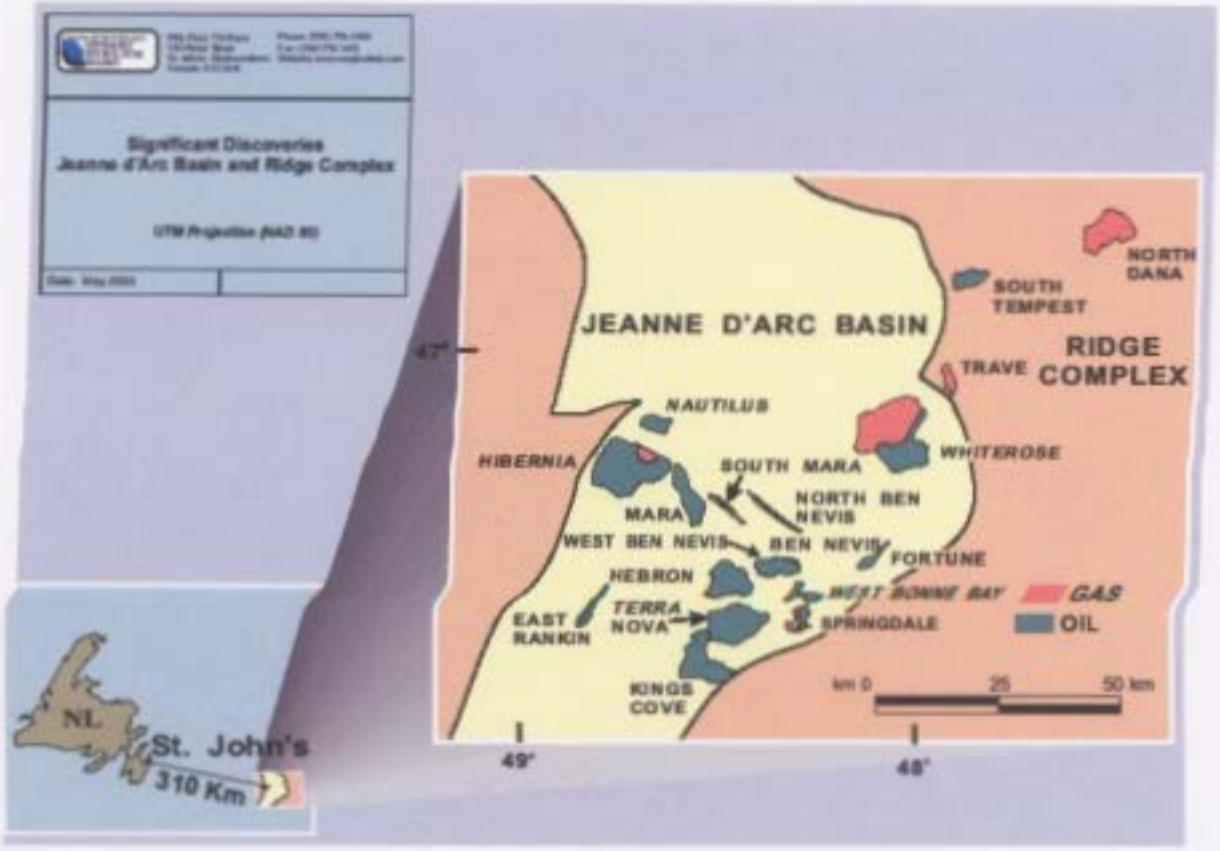

Figure 1-1: Significant Discoveries of the Jeanne d'Arc Basin and Ridge Complex (from http://www.cnlopb.nl.ca/)

The offshore industry is anticipated to continue expanding over the next few decades with exploration proceeding rapidly into new frontiers including deeper waters offshore Newfoundland and Labrador and the Arctic. Ice is a significant environmental factor in these regions. Moreover, there are also a growing number of offshore oil and gas regions in the world where ice is a significant, often dominant, design condition. These include many areas in Norway, Russia, China, and Alaska. While ice is an important design criterion for ships and offshore structures, there are many technical challenges to overcome. The most significant challenge facing a designer is the selection of the level of structural strengthening, which is itself dependent on knowledge of the local loads. One

must recognize that to fully understand the role of ice in the generation of local loading, it is equally important to understand the contribution of ice to global loading.

At a recent PERD (Program of Energy Research and Development) workshop held in St. John's (Oct. 1-2 2002) involving a number of major players in the oil and gas industry (Petro-Canada, Chevron Texaco, Terra Nova, Exxon Mobil, Canship Ugland, Norsk Hydro), serious concerns were raised about the presence of icebergs 6-8 months every year in those areas. Among the various challenges facing offshore activities, iceberg issues, such as detection, forecasting, management and ice-structure interaction, were deemed to be the most critical. Ice considerations dominate the design of offshore production systems and are of great importance in the design of sub-sea installations. In March 2004 during a steering committee meeting for "Ice Data Analysis and Mechanics for Design Load Estimation (IDA)" – a project currently being completed at Memorial University of Newfoundland – in which representatives from all industry partners were in attendance, ice failure processes and ice mechanics was discussed at length. Industry partners showed particular interest in this area, and noted that more experimental work was needed to fully address these issues.

These series of discussions identified a need for greater experimental ice research and led to a proposal being submitted to Petroleum Research Atlantic Canada (PRAC) and Natural Sciences and Engineering Research Council of Canada (NSERC). The proposal entitled "Experimental Study of Ice Failure Processes for Design Load Estimation" was approved and is collaboration between ice researchers at Memorial University of

Newfoundland and The National Research Council of Canada-Institute for Ocean Technology (IOT). The research presented in this thesis was completed as a portion of this large project.

For the readers benefit, a brief explanation of IDA is provided. In this project, researchers at Memorial University are analyzing a complete set of available data bases to estimate ice forces and pressures on offshore structures, giving a solid foundation for the development of constitutive and numerical models. The project involves the determination of ice pressures on engineered structures, using probabilistic analysis and incorporating the most recent data on ice loads and stresses. IDA is being conducted by MUN, NRC Institute for Ocean Technology (St. Johns), the Canadian Hydraulics Center (Ottawa), and C-CORE with industry partners; Chevron Canada Resources, Husky Energy and Petro-Canada.

1.2 Scope

This research has been divided into the following tasks:

I. A brief review of ice design load estimation

II. A literature review of relevant ice structure and mechanics

III. A detailed discussion of the laboratory scale indenter tests completed for this project, which is the pilot test portion (i.e. phase 1) of the large project "Experimental Study of Ice Failure Processes for Design Load Estimation".

Chapter 2 Structure and Mechanical Behaviour of Ice

2.1 Introduction

The primary goal of ice research is to produce a model capable of accurately estimating the behaviour of ice during ice-structure interactions. This goal is achievable only through a strong understanding of the material being studied and the mechanics involved. It will also require a model that takes into account all aspects of deformation in the ice occurring as a result of the interaction. This section aims to provide a review of some of the aspects of this broad subject. The reader is referred to Sanderson (1988) and Michel (1978) for a more comprehensive historical discussion of ice mechanics.

2.2 Ice Crystal Structure

Ice possesses 12 different crystal structures, plus two amorphous states. At common pressures the stable phase is termed ice I. There are two closely related variants: hexagonal ice Ih, whose crystal symmetry is reflected in the shape of snowflakes, and cubic ice Ic. Ice Ih is obtained by freezing water and is the form considered in ice engineering; ice Ic is formed by depositing vapour at low temperatures ($\approx$ -130°C).

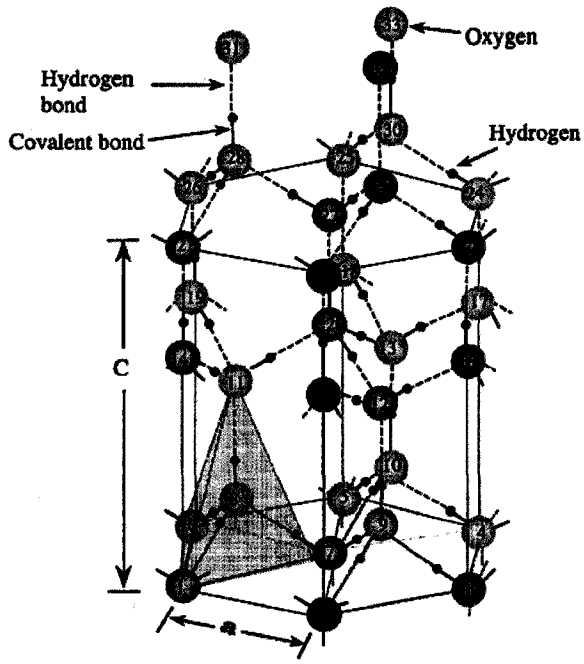

Figure 2-1: Crystal structure of Ice (Schulson, 1999)

Figure 2-1 shows the crystal structure of regular ice. Each water (H_2O) molecule has four nearest neighbours arranged near the vertices of a regular tetrahedron centered about the molecule of interest. The oxygen atom of each molecule is strongly bonded to two hydrogen atoms (by covalent bonds), while the molecules are weakly bonded to each other (by hydrogen bonds). The oxygen atoms are well bonded in layered hexagonal symmetry, but less well attached from layer to layer (having 3 bonds within a layer, but only 1 across to the next layer). This defines a weaker "basal plane" parallel to the crystal structure along which deformation can take place. The direction perpendicular to the basal plane is referred to as the c-axis.

The lattice parameters near the melting point are a = 0.4523 nm and c = 0.7367 nm. The c/a ratio (1.628) is very close to the ideal ratio (1.633) and is independent of temperature.

The ice Ih unit cell is relatively open (packing factor less than 0.34), this accounts for ordinary ice being less dense than water (Pounder, 1965).

2.3 Mechanics

This section will provide a brief review of classical constitutive theories of material behaviour followed by a discussion of how these theories might be applied to ice.

Elastic solids

In purely elastic materials stress and strain are directly related. Elastic deformation is reversible and can be modeled effectively using Hooke's law (Timoshenko and Goodier, 1951) using the following for extension and shear respectively.

$$\sigma = E\varepsilon \qquad \textbf{Equation 2-1}$$

$$\tau = G\gamma \qquad \textbf{Equation 2-2}$$

where E, the elastic modulus (also known as Young's modulus), and G, the shear modulus, are material constants characterizing the stiffness of the material.

Poisson's ratio (ν) is a material parameter that characterizes the contraction in the lateral directions when a material is extended. It is the negative of the ratio of lateral strain to axial strain. For an isotropic elastic material (i.e., an elastic material for which the properties are the same along all directions) there are only two independent material constants. The relation between these three moduli is given by,

$$G = \frac{E}{2(1+\upsilon)}$$ **Equation 2-3**

Viscoelasticity

Viscoelasticity is the term used to describe a material that displays a time-dependent material response, where the stress response of that material depends on both the strain applied and the strain rate at which it was applied (i.e. stress is a function of strain rate). Unlike elastic solids, which have a unique response, a viscoelastic material has an infinite number of possible responses that are directly depended on the strain-rate.

Interesting points about viscoelasticity are as follows (Lockett, 1972):

- If the stress is held constant, the strain increases with time (creep).
- If the strain is held constant, the stress decreases with time (relaxation).
- The effective stiffness depends on the rate of application of the load.
- If cyclic loading is applied, hysteresis occurs. (Physically, a hysteresis is any cause-and effect phenomenon where the effect depends, in one way or another, on the history of the cause). The area in the hysteresis loop is a function of loading rate. Under repetitive loading, a viscoelastic material will heat up.
- Rebound of an object following an impact is less than 100%.

Viscoelastic behaviour is commonly modeled by combinations of springs and dashpots. A spring is used to represent elastic deformation, and similarly a dashpot to represent viscous flow. The simplest manner in which to construct a viscoelastic model is to combine one of each component either in series or in parallel. The most common models

used to represent this are the Maxwell and the Kelvin-Voigt Spring-dashpot (Figure 3-2); both models show that stress is a function of strain and strain-rate represented by,

$$\sigma = \sigma\left(\varepsilon, {}^{d\varepsilon}/_{dt}\right)$$ **Equation 2-4**

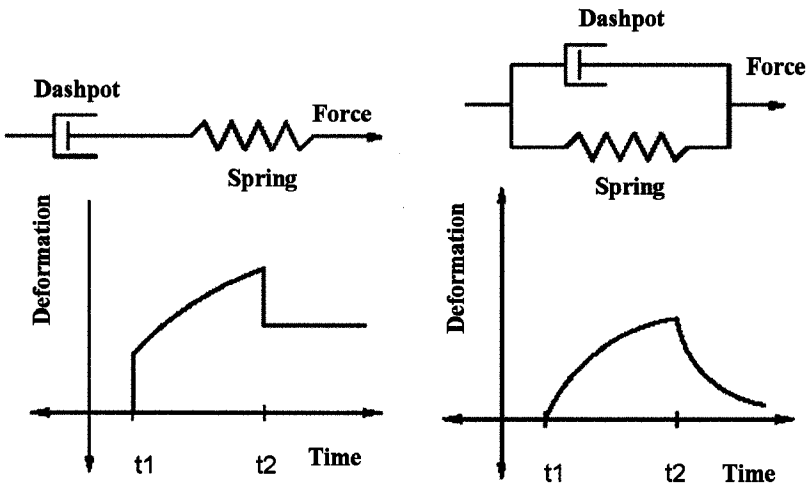

Figure 2-2: A schematic representation the Maxwell (left) and the Kelvin-Voigt (right) spring dashpot models and graphs showing qualitative, viscoelastic behaviour graphs for each.

2.4 Discussion of General Ice Mechanics

The deformational behaviour, failure mechanism, and strength of ice are highly influenced by the strain rate – where the ranges of strain may be classified as ductile, transitional and brittle. At very high rates of loading, stresses are influenced by strain-rate effects, impact velocity and the ability to effectively clear material.

Granular ice has typically been treated as an isotropic material in engineering problems. The elastic modulus is determined from reading the initial tangent value from a stress strain curve obtained from a very rapid test. Since it is accepted that ice deformation contains a creep component, this will lead to inaccuracies that can be minimized by taking high frequency measurements during testing.

Material constants are known to vary with temperature, and Glen (1975) provided a temperature–dependant equation for ice. This variation is often assumed to be negligible (Sinha, 1979).

As mentioned above, ice will creep when subjected to low rates of loading or to sustained loads. When these strains are slowly increased, a ductile failure is reached where the maximum stress obtained is referred to as the yield strength. Figure 2-3 below (scanned from Michel 1978) illustrates the effect of different strain rates on the strength of ice.

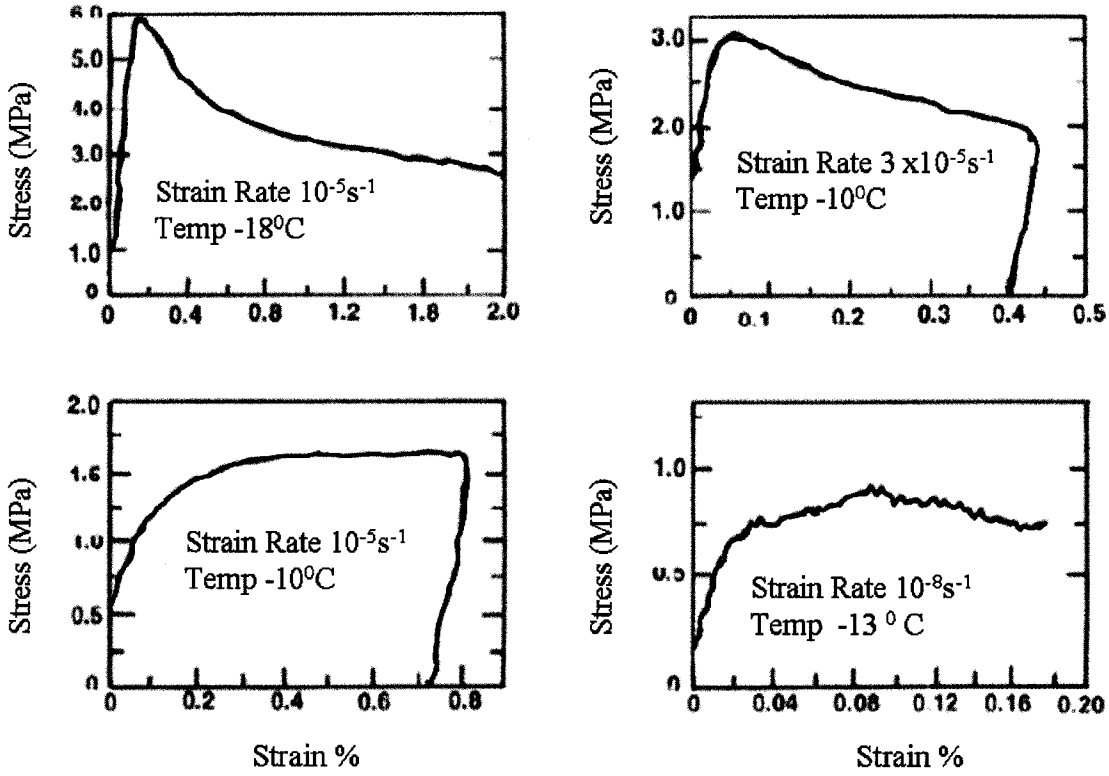

Figure 2-3: Effect of different strain rates on the yield strength of ice (from Michel 1978)

By examining the typical creep curves for ice under a constant load (Figure 2-4) and a constant deformation rate (Figure 2-5) in tension and compression, we can see that ice exhibits the classical primary, secondary and tertiary creep at low stress or low strain rate.

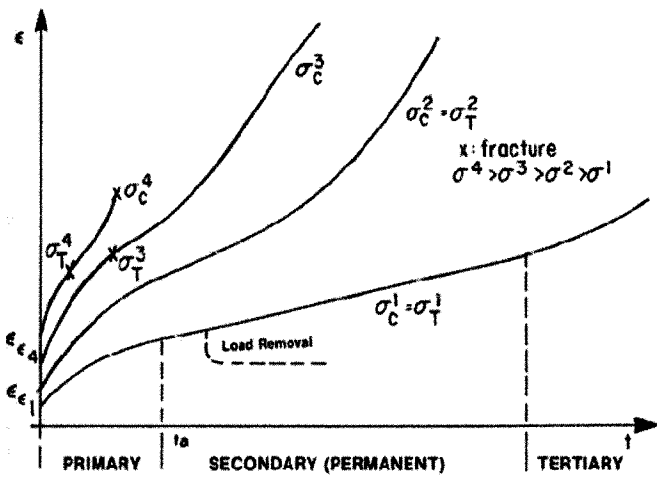

Figure 2-4: Typical creep curves for ice under a constant load in tension and in compression (from Michel 1978).

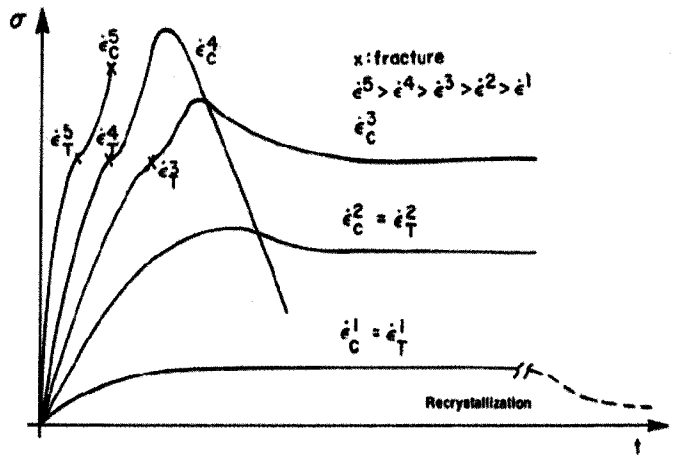

Figure 2-5: Typical creep curves for ice under a constant deformation rate in tension and in compression (Michel 1978).

Figure 2-6 is an example of a graph showing ice behaviour at a high strain rate. It illustrates that tests at higher stress levels or higher strain rates do not exhibit all stages of classical creep due to sudden brittle failure (Michel, 1978). At high strain rates, dislocation velocities are too slow to allow ductile behaviour so that the mechanisms of fracture initiation and propagation control the strength in this range of strain rates. In the brittle domain, behaviour before fracture is essentially elastic, and strength is determined by grain size and temperature, not by strain rate. A compressive discussion regarding the effect of hydrostatic and triaxial stress states on the mechanical behaviour of ice is beyond the scope of this thesis, but can be found in of the Michel (1978).

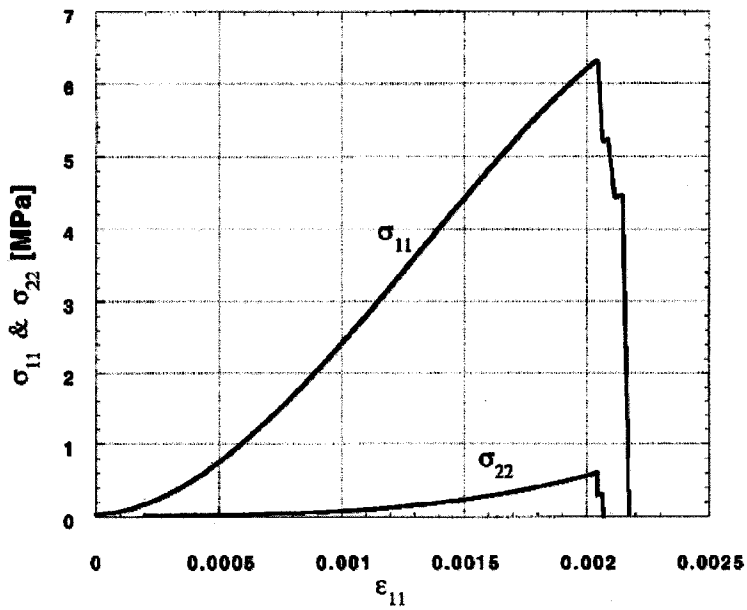

Figure 2-6: Graph from Schulson (1999) illustrating a transition in the material behaviour of ice under compression from elastic to brittle.

Fracture mechanics and spalling

It is well documented that at the speeds associated with ice structure interactions, the loading can become dynamic and cyclic. This was particularly well illustrated during the deployment of the Molikpaq in the Canadian Beauforte Sea (Jefferies and Wright 1988), when dynamic loading caused by interaction with a large ice floe produced a significant structural reaction. The phenomenon of dynamic ice loading has traditionally been explained by the majority of the ice engineering community as a result of fracture processes closely related to the presence of high pressure zones. Peyton (1966) and Blenkarn (1970) were among the first to study this process. It is acknowledged that dynamic loading will also have a dependency on the type of structure involved with the contribution made by the structure dictated by its level of compliance.

Damage mechanics and layer formation

Jordaan (2001) has developed a model that utilizes damage mechanics to explain the cyclic loading associated with ice interaction events. This model uses the presence of a "damage layer" occurring at the site of contact. The mechanical process taking place in the layer is directly related to the loading condition, and the spatial and temporal location of the high pressure zone (Figure 2-7). At the edges of a high pressure zone, where confinement pressures are lowest, micro-fracturing will occur. Within the high pressure zone, where confinement pressures are highest, the energy associated with the interaction will be manifested into crystal defects, pressure melting and recrystallization processes.

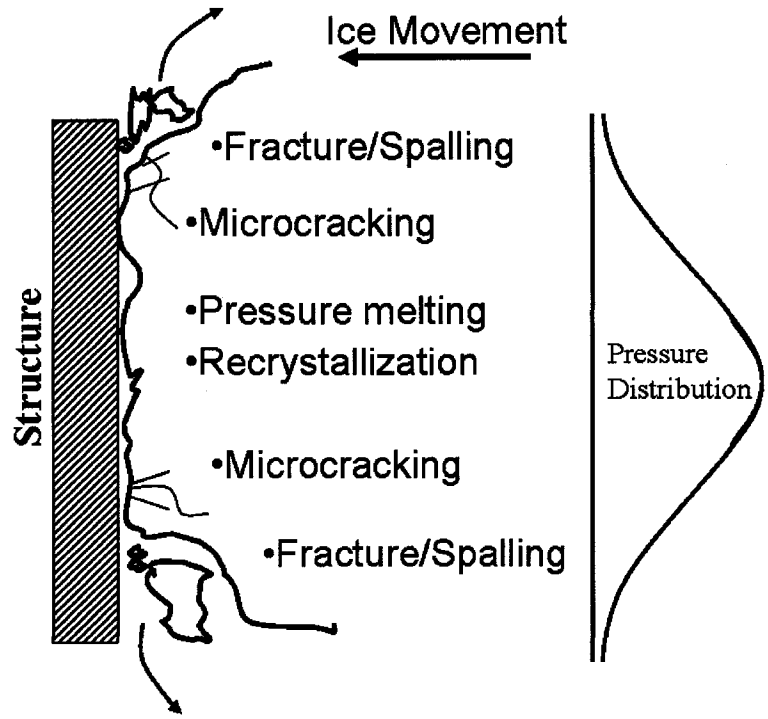

Figure 2-7: Zones of damage associated with high pressure zones (HPZ's).

Although the model described by Jordaan (2001) contains more complexity than that normally considered within the ice engineering community, it is built upon some rather early work. Barnes and Tabor (1966) were among the first to recognize recrystallized texture and pressure melting at the ice-indenter interface, and that these processes were somewhat dependent on temperature. During a later test series, Barnes et al. (1971) provided convincing thin sections (Figure 2-8) showing a recrystallized texture that manifested at the surface of a single crystal during sliding experiments. During this same

time period Offenbacher et al. (1972) also provided evidence of recrystallization during cone penetration tests (Figure 2-9).

This theory has also been supported from evidence collected during other indentation projects as will be discussed in further detail later.

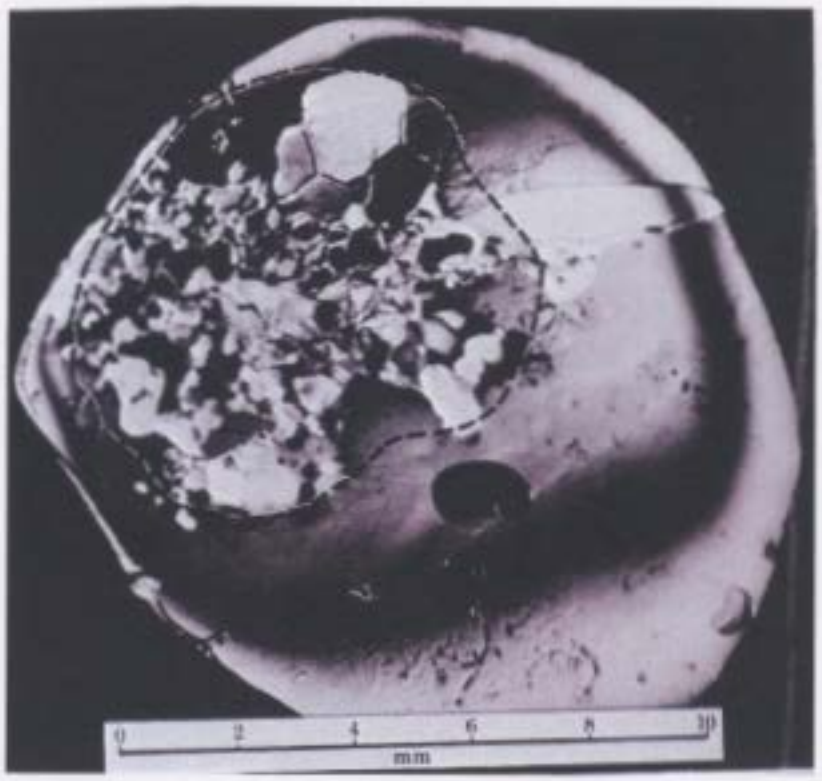

Figure 2-8: A thin section of the contact zone examined through cross polaroids. The ice was originally a single crystal with a basal plane normal to the direction of sliding. The broken line outlines the area of recrystallization (from Barnes et al., 1971).

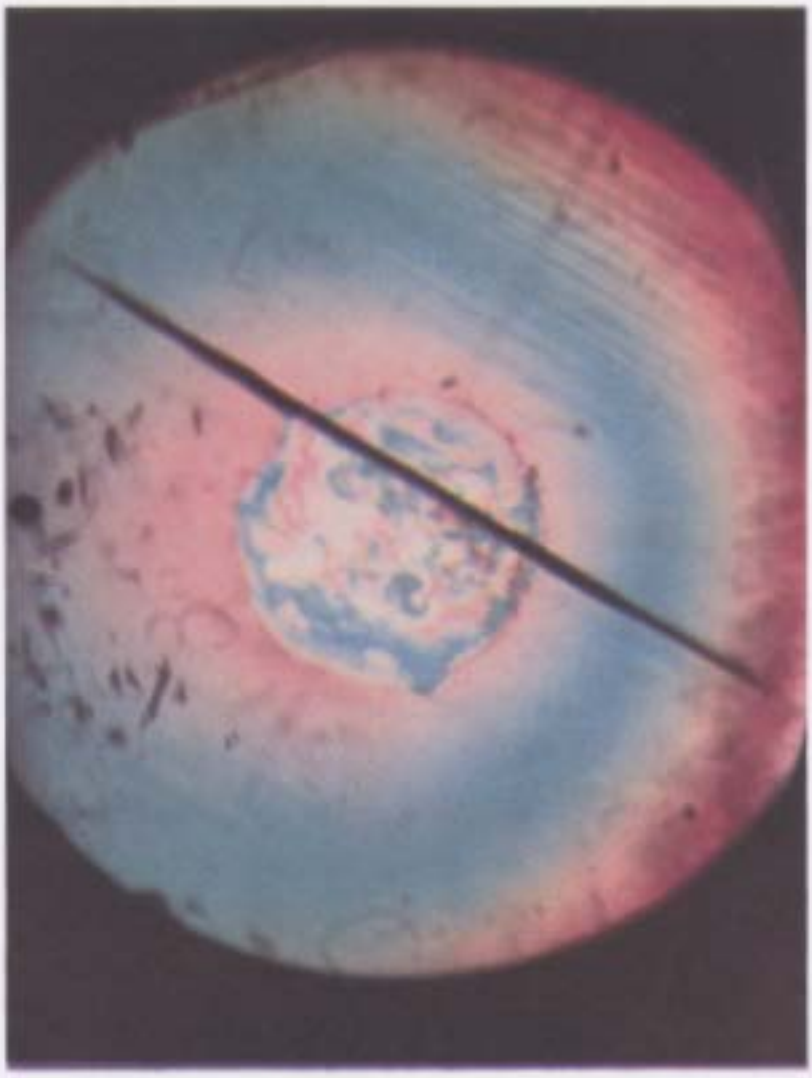

Figure 2-9: Polaroid photo of compressed cone test showing recrystallization (from Offenbach et al., 1972).

2.5 Discussion of Relevant past Indentation Testing Projects

Indentation tests have been conducted by many researchers to investigate the material properties and mechanics involved in ice structure interactions (Michel and Toussaint, 1977; Jordaan et al. 1988; Frederking, 2004; Sodhi, 2001). Some of the first indentation experiments were preformed by simply dropping a cast steel ball, weighing 300 kg, on

natural lake ice (Kheisin and Cherepanov, 1970). These tests were extraordinary in the detailed discussions of the fine-grained nature of the damaged ice generated during the test, and in describing how this fine grain material acts as a lubricant for the ice matrix (Figure 2-10). Kheisin and Cherepanov (1970) also pointed to pressure melting and secondary crystal growth as mechanisms involved in the crushing process.

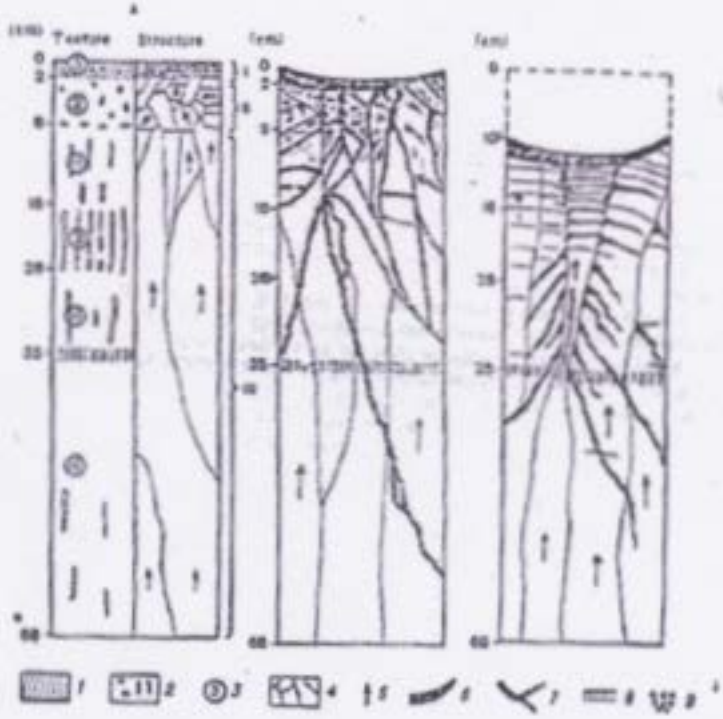

Figure 2-10: Sketch from Kheisin and Cherepanov (1970), showing the ice structure at the impact zone: 1-Ice with small inclusions: 2-Shape and main distribution features of air inclusions in ice: 3-number of inclusions in ice estimated on a three-point scale: 4-boundaries of crystals: 5-direction of the principal crystallographic axis: 6-zone of total crumpling of ice: 7-cracks; 8-direction of cracks in the basal plane: 9-formation of secondary crystals.

The medium scale indentation tests performed by the Hibernia joint venture at Pond Inlet (in tunnels bored into a grounded iceberg 1984 (Masterson et al. 1992)), and the two test series at Hobson's Choice Ice island (Frederking et al., 1990a and 1990b) are considered important steps in the progression of the ice structure interaction model. These tests used indenters with contact areas ranging in size from 0.02 m^2 to 3.0 m^2, with initial indenter velocities of 100 mm/s (Kennedy, 1990). The tests demonstrated a dynamic loading sequence and a layer formation (Figure 2-11 and Figure 2-12) during indentation. They also showed that the level to which each of these phenomena that occurred had a relationship to the velocity of the test and the size of the indenter.

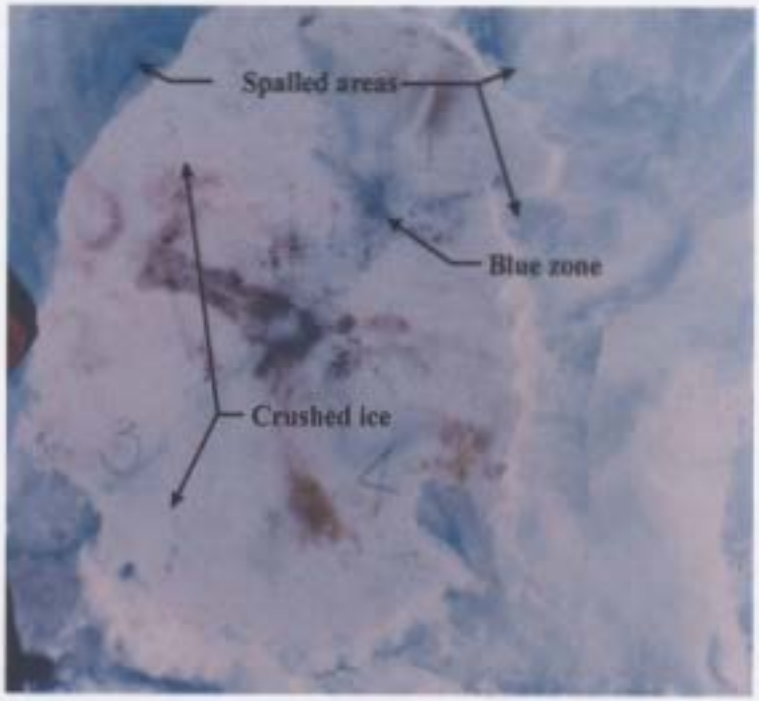

Figure 2-11: Spalled areas and crushed ice observed during field tests at Hobson's choice (from Jordaan, 2001). The blue ice is thought to represent areas that underwent recrystallization during testing.

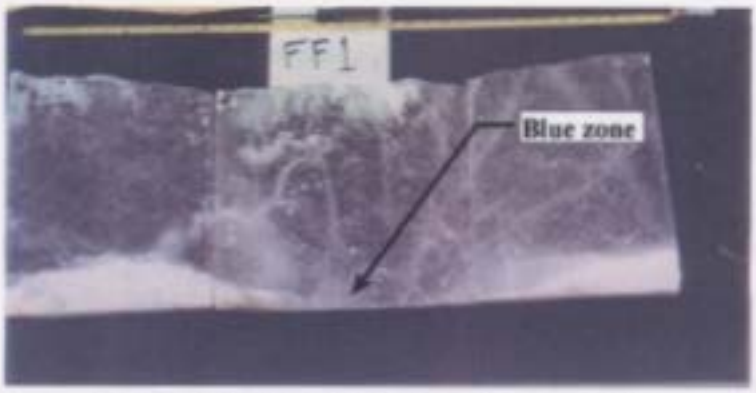

Horizontal thick sections taken from the central region of the ice-indentor interface

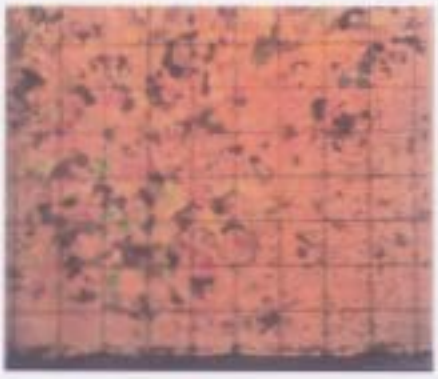

Central region of indentor face (blue zone from above)

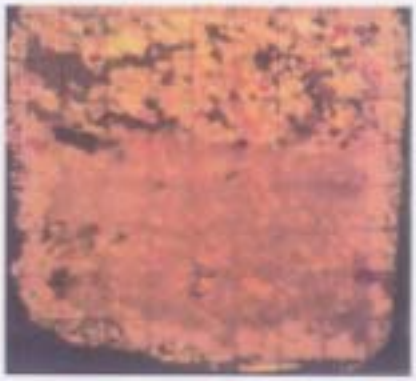

Right side of indentor face (from above)

Figure 2-12: Sections showing clear evidence of layer mechanisms during indentation during field tests at Hobson's choice (from Jordaan, 2001).

The test series completed for this thesis is similar to an earlier project by Barrette et al. (2003) at Memorial University, and draws heavily on experience gained. The aim was to investigate the formation of the layer and how changes in rate and temperature might affect it. The observations from this test program are quite convincing with Figure 2-13 showing remarkable similarity between indention tests of different scales.

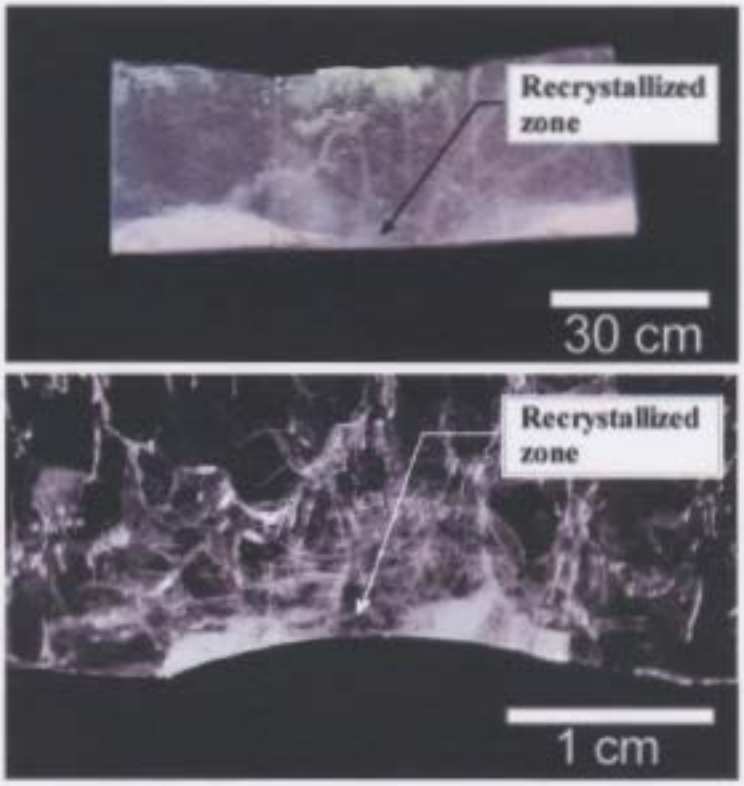

Figure 2-13: Comparison of a medium scale indentation test from Hobson's Choice and a laboratory scale indentation test from Barrette et al. (2003). The two show remarkable similarity, strongly suggesting that the same mechanical phenomenons are at work within the damage zone at both scales.

Chapter 3 Design Load Methodology

Researchers at Memorial Universities Engineering and Applied Science faculty have been heavily involved in providing ice design load estimates for many of the offshore structures currently working within the Newfoundland and Labrador offshore industry. This section will provide a brief description of the design load estimation methodology that was developed and is currently being applied by Jordaan (2001 and 1993).

3.1 Background

Probabilistic methods provide a means to assess or evaluate distribution of **local** and **global** ice loads on offshore structures, and two corresponding pressure-area relationships:

I. **Global loads**: the maximum total force applied to the structure.

II. **Local loads**: the force (or pressure) on a particular area of interest. This is often illustrated using the example of a ships frame spacing.

Probabilistic methods are used in ice mechanics and ice load design to account for the wide range of possible values for any given loading situation. That is, to enable the random nature of ice loading events to be adequately addressed.

For design purposes, an extreme value of a load is chosen. The Canadian Standards Association (CSA) has instituted target safety levels, such that the main target (Safety Class 1) corresponds to an annual probability of failure of 10^{-5}. The CSA standard divides environmental loads into rare and frequent, with a different strategy for determining the design load. Frequent environmental processes are typified by wind and wave loads, in

which cases several extreme storms may occur each year. Rare environmental events are typified by earthquakes and iceberg loads, with a return period of tens of years or longer.

Iceberg loads are considered rare, with annual probabilities of occurrence less than one. Design loads are determined at the 10^{-4} annual exceedance probability and are affected by the following factors:

I. Arrival rate
II. Probability distributions of mass
III. Probability distributions of velocity
IV. Possible eccentricity of impact
V. Shape of iceberg
VI. Ice strength.
VII. Structure Compliance/Geometry

3.2 Design area definitions

In order to estimate accurately both global and local design loads, it becomes necessary to define areas associated with both:

The global interaction area:

Sometimes referred to as the nominal interaction area, it is the area determined by the projection of the structure onto the original shape of the ice feature, without any reduction of the area for spalls and fractures that take place during the interaction. The global interaction area can be determined from the shape of the iceberg and the shape of

the structure. Within this area, there will be areas that carry little or no pressure, as well as the high-pressure zones (Figure 3-1). Design issues related to Global interaction areas are base stability (in shear) and overturning moments.

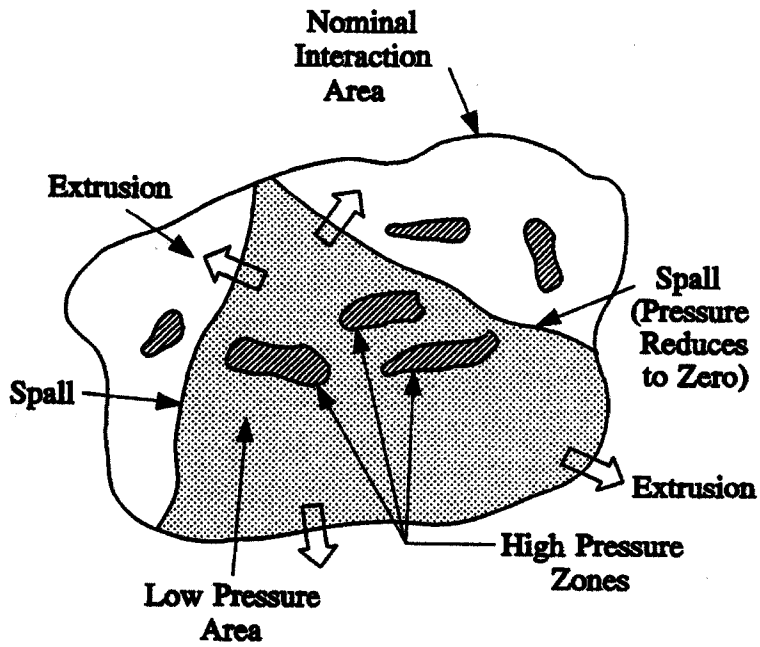

Figure 3-1: Illustration of global interaction area

The local design Area:

Local design area refers to the area of a plate between frames or a panel or substructure that is considered in design. Figure 3-2 illustrates this concept. Design issues related to local design areas are plate/shell punching and shearing.

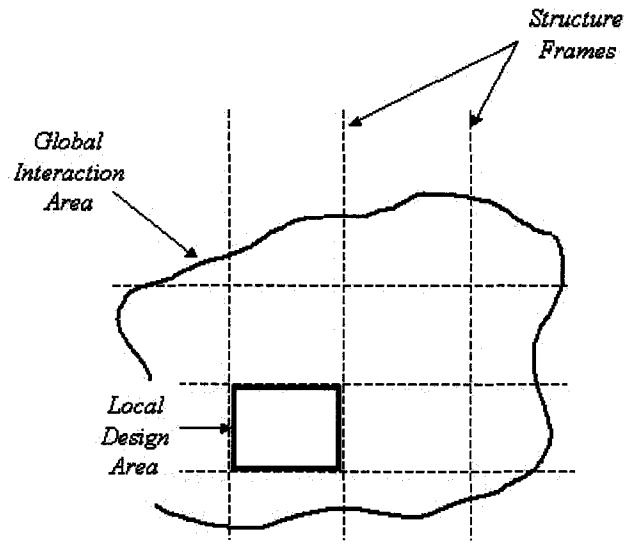

Figure 3-2: Illustration of local design area

3.3 High Pressure Zones

The concept of pressure variation across the compressive interface in ice-structure interactions was first recognized by Kry (1978). This phenomenon is well illustrated in experiments by Ashby et al. (1986) where a sheet of brittle wax was driven against a cylindrical indenter. As illustrated in Figure 3-3 (taken from Ashby et al. 1986), the load at various points in time is transmitted through several distinct points of high pressure. Essentially, the interaction process is defined by a series of randomly distributed and dynamically changing zones of high (or intense) pressure within a larger (background) matrix of lower pressure. Fracturing and spalling of the wax results in the contact point continually changing throughout the interaction.

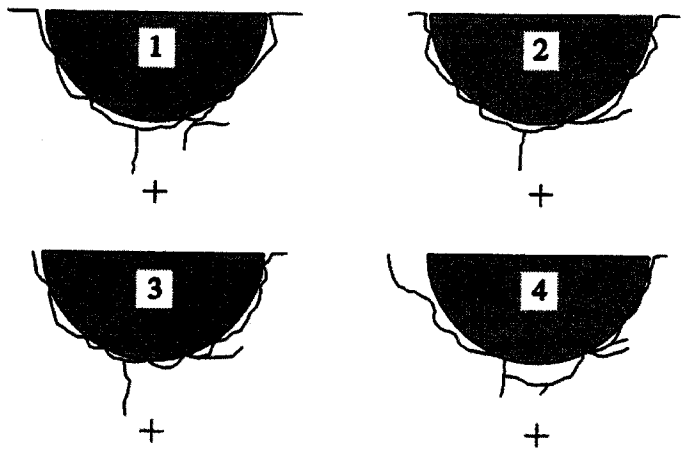

Figure 3-3: Illustration of non-simultaneous failure in brittle wax as observed by Ashby et al. (1986)

A detailed description of non-simultaneous failure relating to ice-structure interactions can be found in Jordaan (2001) among others. This process produces a damage layer within the high pressure zone. The layer consists of areas of recrystallization, micro cracking, crystal defects and pressure melting (discussed in more detail later). Internal flaws, random grain orientation, contact width, ice feature geometry and other random quantities are considered when examining high pressure zone mechanics. Conceptually, high pressure zones formed during ice-structure interactions, illustrated in Figure 3-4, are similar to the high pressure zones formed during the indentation of wax (Figure 3-3).

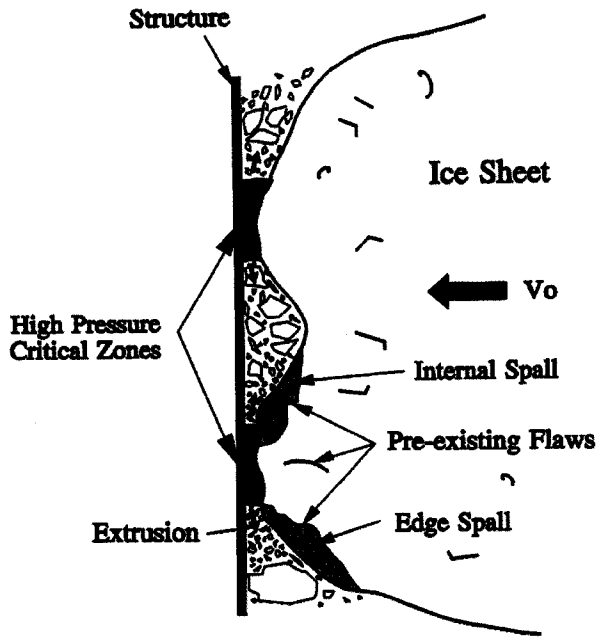

Figure 3-4: Conceptual sketch of how loading is disturbed to a structure through high pressure zones.

3.4 Global Pressure Methodology

Global pressure is modeled using the expression,

$$P = Ca^{D} \ . \qquad \textbf{Equation 3-1}$$

The area, a, is treated as being normalized (i.e. divided by a reference area of, say 1 m^2). Thus, the contact area, a, is dimensionless, and C has the units of pressure (MPa). The parameters C and D are currently modeled using lognormal and normal distributions (relationship using other distributions are undergoing current research by Li and Jordaan as part of a PhD thesis (incomplete at time of writing)), respectively. P currently follows a lognormal distribution as well.

Ship ram data is used to calibrate the design equations. The governing equations of ship motions (Fuglem et al. 1988) during the rams are expressed by.

$$\ddot{x} = \frac{(-k_x x - c_x \dot{x}) - F_h}{m_x}$$ **Equation 3-2**

$$\ddot{y} = \frac{(-k_y y - c_y \dot{y}) - F_v}{m_y}$$ **Equation 3-3**

where,

F_h and F_v are the horizontal and vertical components of force due to ice crushing and friction;

k_x and k_y are the horizontal and vertical spring constants;

c_x and c_y are the horizontal and vertical damping coefficients;

M_x and M_y are the generalized mass at the bow horizontally and vertically.

The force components in Equations 2-2 and 2-3 can be determined using Equation 3-1 and the shape of the bow. The area in Equation 2-1 is a function of penetration coordination (x, y). Therefore, in each of Equations 2-2 and 2-3, there is only one unknown term, namely *x* and *y*, respectively. The equations are solved numerically using the Runge-Kutta procedure in time domain. Monte Carlo simulation is used to generate the number of events of interest. In each event, the parameters *C* and *D* in Equation 3-1 are randomly selected following the chosen distributions with a given mean and standard

deviation. The maximum load determined for each event is compared with the field test data. By varying the mean and deviation of C and D, the best fit to field test data can be calibrated. Experience has shown that with many repetitions, this approach becomes conservative.

Figure 2-5 shows a typical data set for measurements in the 1991 Oden trials. Based on an extremal analysis methodology, the data are sorted and ranked as shown in the right side of the Figure. Vertical bow forces are then simulated using various distributions with different means and standard deviations for C and D. The combination of the mean and standard deviation of C and D resulting in the closest match between the recorded and simulated vertical bow forces is chosen. Figure 3-6 shows one result of simulation using the empirical relationship given by Equation 3-1, as compared to the measured data.

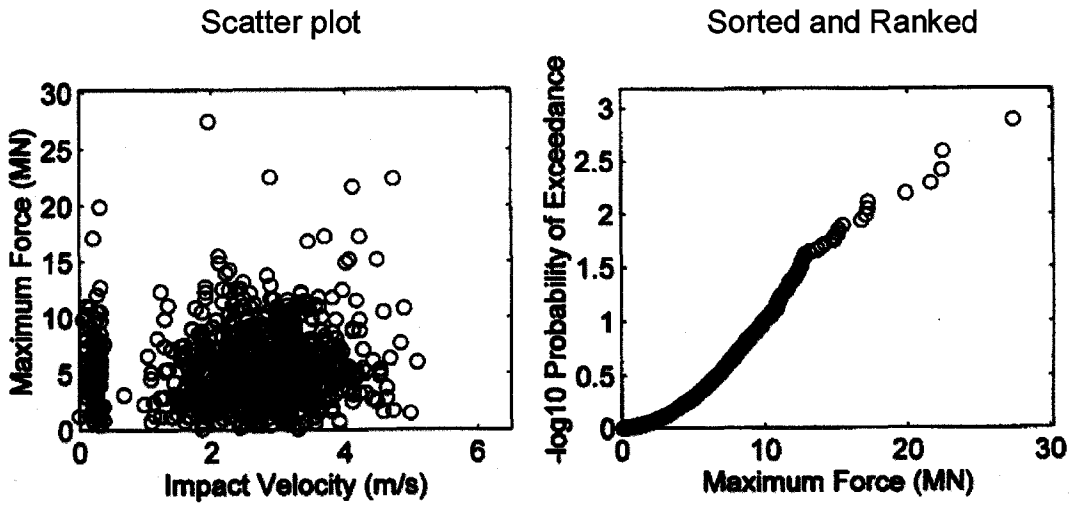

Figure 3-5: Left, scatter plot; right, observed data from the icebreaker Oden (1991)

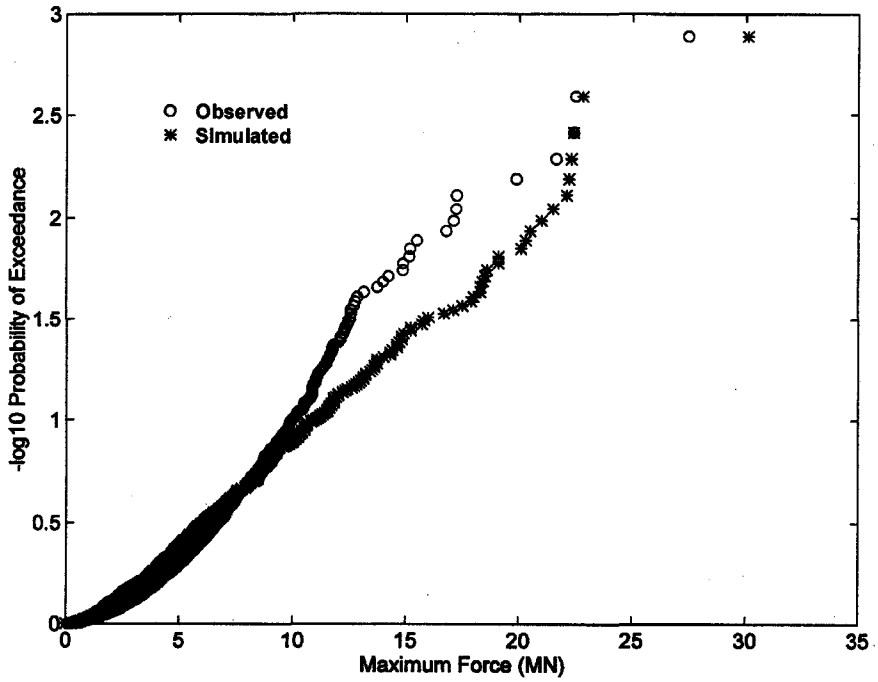

Figure 3-6: Comparison between observed and simulated peak forces for ice interaction events with the icebreaker Oden (1991).

3.5 Local Pressure Methodology

The local ice pressure methodology originated in the concept of extreme value analysis as proposed by Jordaan et al. (1993). The key point was the observation that the ranked data for a specific area (ice pressure on a defined subpanel) was of exponential form in the tail of the distribution. For a series of ship ram events, the ranked pressures on a specific area can be represented using,

$$F_X(x) = 1 - \exp\left(\frac{x - x_0}{\alpha}\right), \qquad \textbf{Equation 3-4}$$

where, x is the local ice pressure and x_0 and α are constants for a given area. Assuming that the impact events follow a Poisson arrival process, the extremal form of the distribution takes the form of,

$$F_Z(z) = \exp[-\mu(1 - F_X(z))], \qquad \textbf{Equation 3-5}$$

where, $\{X, x\}$ denotes the maximum pressure from a single ram event, $\{Z, z\}$ represents the maximum value of $\{X, x\}$ with μ hits. The parameter μ defines the exposure of the panels to hits. Combining the two equations results in,

$$F_X(x) = \exp\left\{-\exp\left[-\frac{z - x_0 - x_1}{\alpha}\right]\right\}, \qquad \textbf{Equation 3-6}$$

where,

$$x_1 = \alpha \ln \mu = \alpha(\ln v + \ln r) \qquad \textbf{Equation 3-7}$$

and v is the number of ship rams and r is the proportion of hits on the panel.

The parameter α represents the decrease of pressure with area. From previous analysis (Jordaan et al., 1993), it was determined that x_0 was approximately zero and that,

$$\alpha = 1.25a^{-0.7}.$$ **Equation 3-8**

Figure 3-7 illustrates the design curve produced from Equation 2-8.

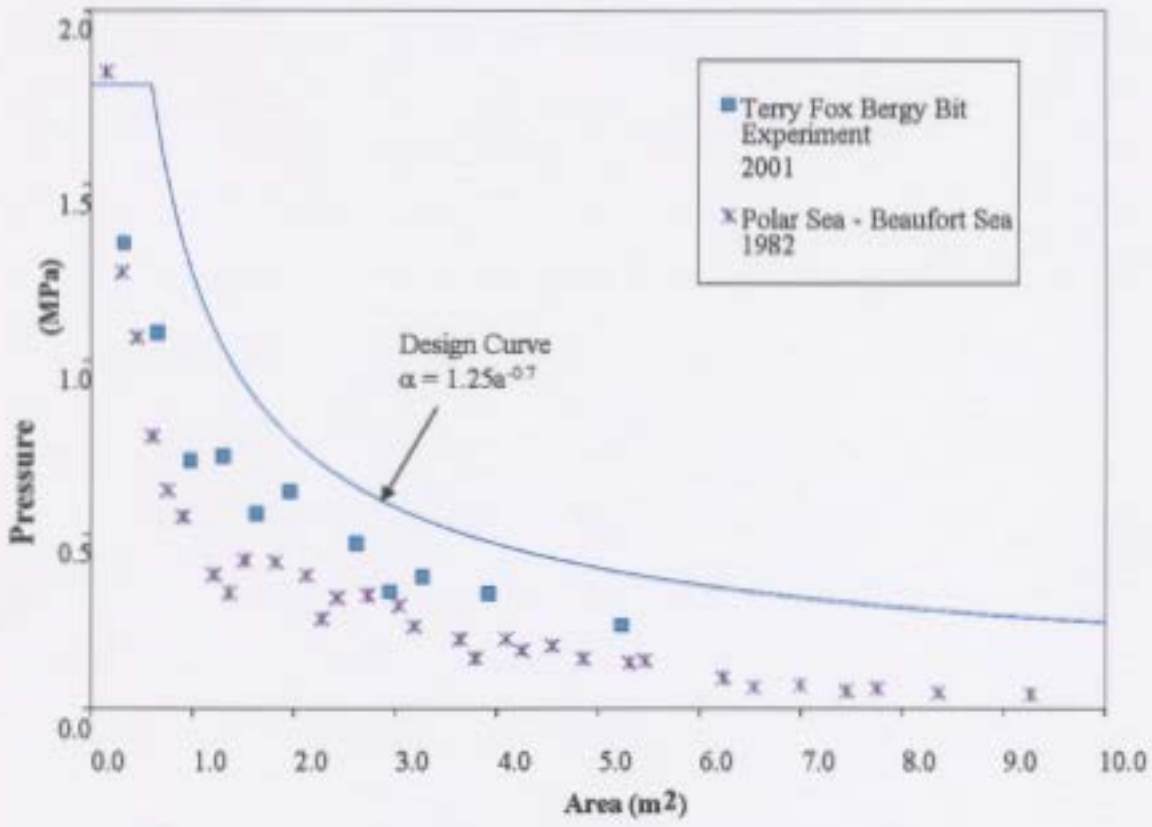

Figure 3-7: Relationship showing the decrease of pressure with area for various ship-ice interaction data sets (from Jordaan et al. 2005)

Chapter 4 Laboratory Investigations

The laboratory work is considered the main component of this thesis. It is also the pilot experimental component of a larger three year, Petroleum Research Atlantic Canada (PRAC)/Natural Sciences and Engineering Research Council of Canada (NSERC) jointly funded project entitled "Experimental Study of Ice Failure Processes for Design Load Estimation".

All tests were reduced scale, laboratory indenter tests, designed specifically to look at fracture and spalling during loading. If one looks at large scale interactions, it is assumed that across the global area of an interaction, there exist a random number of high pressure zones that can fluctuate in intensity and spatially with time. This means that the processes occurring in the high pressure zones of a large scale test are unstable and difficult to study. It is also assumed that damage processes initiate from high pressure zones. An indenter test provides the experimenter with a stable high pressure zone that is forced to exist at the ice-indenter interface. This greatly helps in simplifying the problem of analysis.

The experimental method was designed using the previous work of Barrette et al. (2003) as a starting model. Also considered during experimental design was the idea that these were the initial tests in a 2-3 year testing program, and they should be geared towards providing information to aid in the refinement of future test. This led to a test matrix with no experimental repeats, the idea being that these tests could be used to narrow down

future work, and that more information could be gained through looking at a large number of possibilities.

4.1 Testing Procedure and Data Gathering

The testing program was conducted utilizing the facilities available at the large and small cold rooms within NRC-IOT. The Materials Testing System (MTS) equipment (Figure 4-1) is located within the large cold room and the control systems, data acquisition systems, computers, chart recorders and video monitors are located just outside.

Figure 4-1: MTS test frame located in the large cold room at NRC-IOT

All tests were conducted at -10 ^{0}C, with the samples stored at this temperature prior and post machining, Minimum 2 weeks, to ensure that the samples were at the target test temperature. The samples were stored in air tight plastic bags in camping coolers with a large amount of sacrificial snow to ensure crystal integrity was maintained. The test

setup (Figure 4-2) involved placing a machined test sample (approx. 20cm x 20cm x 10 cm) of polycrystalline ice (explained in detail later) on the test platform so that the indenter would make contact at the desired distance from the edge of the specimen. The indenter contact distance from the sample edge for the intermediate and edge tests was measured using a drafting square and a ruler. The edge was chosen from visual inspection, looking for the edge with the least amount of visual flaws. The center location was taken as the intersection point of diagonals placed on the top of the sample surface. The indenter was than manually lowered such that it was above the sample, but not in contact with it. This space was kept consistent by using thin metal strips as spacers. The strips were bent slightly, and the indenter was brought down until contact with the strip was made. The strip was than removed. The samples were under no confinement during the test. The tests were conducted to a maximum actuator displacement of 5 mm, thus the penetration of each test varied slightly relative to the manual placement of the indenter above the sample. Velocity of the tests varied from 0.2 mm/s to 10 mm/s depending on the test.

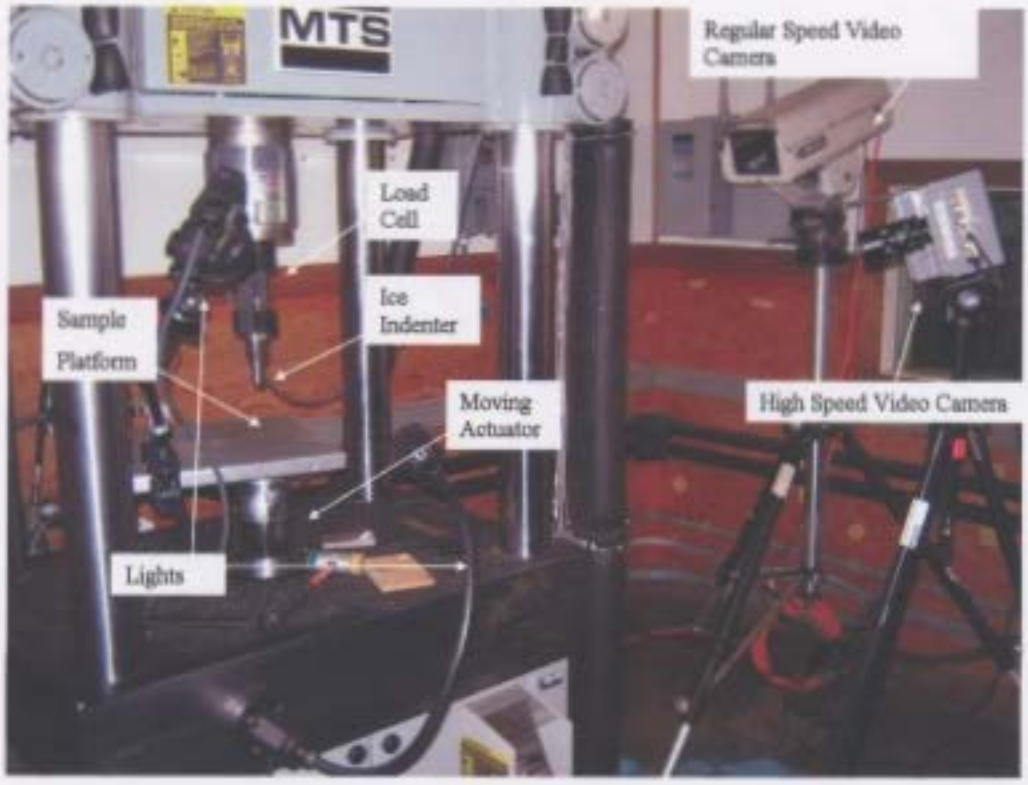

Figure 4-2: General test set-up for the indention tests. A second regular speed video camera was also used, but cannot be seen as it was located at approximately the same location as this picture was taken.

The test was controlled and recorded using the MTS controller and recording equipment. A 25 kN MTS load cell (model number 661.23B-01) was used with a sampling frequency of 20 kHz. The load cell was deemed appropriate based on the expected loads and noise levels. This was then filtered using a 3dB cutoff frequency of 3 kHz. The filter was chosen based on the best available at NRC-IOT to satisfy the Nyquist criterion, and reduce aliasing based on sampling frequency.

The tests were videotaped using 3 video cameras, 1 black and white recording at 30 frames per second (fps), 1 color recording at 30 fps, and 1 high speed black and white

camera recording at 1000, 500 and 125 fps depending on the length of the test in question. The high speed video was analysed using "motion measure" software. A one shot synchronizing pulse was generated on initiation of the MTS, causing a LED located next to the ice sample to flash. This can be seen on the video at the start of the test.

Two indenters were used during the tests. These choices relate directly to the work done by Barrette et al. (2003). In that work, the scaling relationship is studied and was shown with a strong level of confidence that work done on a laboratory indenter scale can be brought up to events of engineering significance. As in Barrette et al. (2003), the indenters used are scaled-down versions of the spherical indenters used in the field (Frederking et al., 1990). Table 4-1 provides details of the indenter used. The shaft of both indenters was painted with a matt black finish to reduce reflective glare from the lights.

Table 4-1: Indenters used during study.

Size	Material	Radius of curvature
10 mm radius	Soft steel	12.8 mm
20 mm radius	Soft steel	25.6 mm

The samples were photographed before and after all tests using digital photography (photographs are provided in an observation section). After the tests the samples were placed in sealed garbage bags and then put into camping coolers for storage. All samples were stored at -10^0 C.

4.2 Thin Sectioning

The samples were thin sectioned approximately 3 weeks after testing (the small delay was due to equipment problems). Thin sectioning was done using the "Double Microtome" technique introduced by Sinha (1977). This involved using a microtome blade (Figure 4-3) to "shave" samples of ice (welded to glass slides) to 1-2 mm in thickness, thus allowing for the crystal structure to be examined. It should be noted that typically the thin section is welded to the glass side by a bead of water around the full perimeter of the sample. In our case, the sample was only welded on 3 sides, leaving the side that was indented un-touched. The thin sections are photographed (Figure 4-4) under:

1. Cross-polarized light (Figure 4-5): facilitating easy viewing of the various crystals. (Ice has a preferred optical crystal axis, the c-axis, so that crystals with the c-axis oriented in different directions will show different color under cross-polarized light).
2. Normal light with a side light oriented at approx 45 degrees pointed at the sample (Figure 4-6): This highlights any micro cracking that may be present in the thin section as the side light will reflect off the crack surfaces.

Figure 4-3: Microtome setup showing the blade with shaved ice, and a thin section on a glass plate. The thin section will continue to be shaved until it reaches a thickness of less than 2 mm.

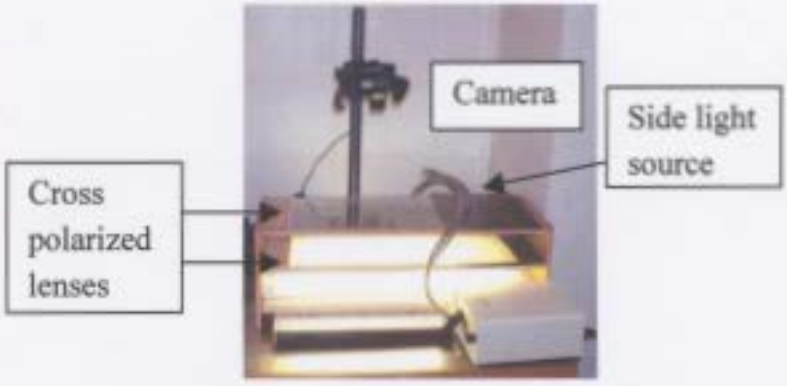

Figure 4-4: Thin section photo station: The thin section is placed between the 2 polarized lenses to produce the colourful photos and on top of the platform for the side reflection photos.

Figure 4-5: Typical thin section photographed under cross polarized light conditions.

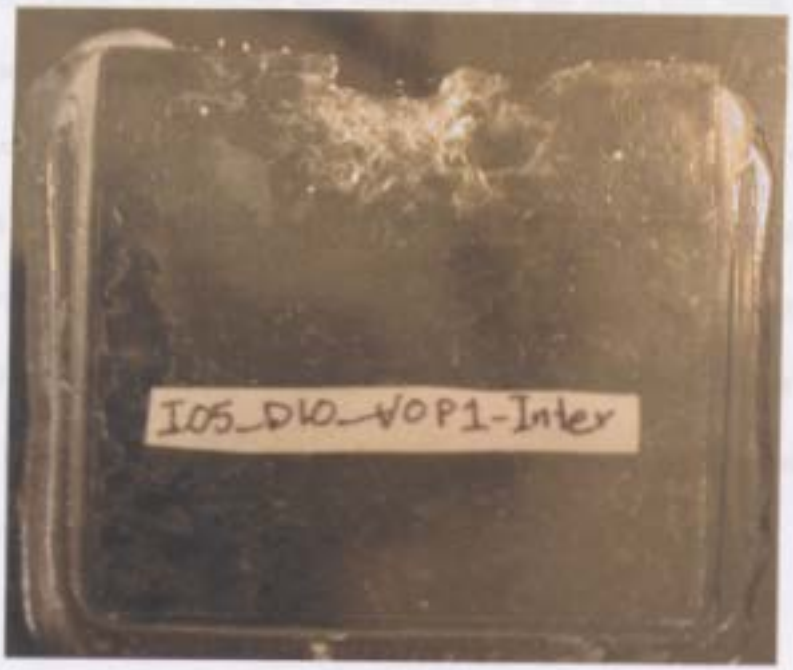

Figure 4-6: Typical thin section photographed under side reflective light conditions.

4.3 Step by step summary of test procedure

1. Machine sample
2. Measure and photograph the sample
3. Position sample on testing platform
4. Adjust the indenter height using spacers
5. Set MTS controller to specific test parameters
6. Roll video cameras
7. Simultaneously initiate test and commence load acquisition
8. Photograph and store tested sample.
9. Thin section and photograph samples (thin sections were than placed in storage)

4.4 Test Details

The test matrix (Table 4-2) shows the variations of the tests that were conducted. The indenter distance to the edge was varied to investigate any potential edge effect. The indenter displacement rates for the slow and medium velocities were chosen to be consistent with the scaling rules used by Barrette et al. (2003). In that study the fastest rate was equivalent to the medium speed in this test series. The fastest rates used by Barrette (2003) indicate a transition zone between creep and brittle material deformation of the ice. The higher rate for this series was chosen to investigate the material properties beyond that transition, and into the brittle deformation region.

Table 4-2: Test Matrix

			Number of Tests		
Indenter Diameter	Indenter Speed (mm/sec)		Indenter distance to the edge		
			Center (10 cm from edge)	Intermediate (5cm from edge)	Edge (2 cm from edge)
10 mm	5.0	Fast	**1**	**1**	**1**
10 mm	1.0	Medium	**1**	**1**	**1**
10 mm	0.1	Slow	**1**	**1**	**1**
20 mm	10.0	Fast	**1**	**1**	**1**
20 mm	2.0	Medium	**1**	**1**	**1**
20 mm	0.2	Slow	**1**	**1**	**1**

Test naming convention

The naming convention inherently gives details about the test in question. The tests will be refereed to by name, and it will aid the reader to understand this convention. Table 4-3 provides examples to follow.

Table 4-3: Naming Convention (2 examples)

Test name: **I05_D20_V10P0_C**			
I05	**D20**	**V10P0**	**C**
Test Type & Year	Indenter Diameter	Indenter velocity	Indenter Location
Indenter test, 2005	20 mm	10.0 mm/s	Center (10 cm from edge)
Test name: **I05_D10_V0P1_E**			
I05	**D10**	**V0P1**	**E**
Test Type & Year	Indenter Diameter	Indenter velocity	Indenter Location
Indenter test, 2005	10 mm	0.1 mm/s	Edge (2 cm from edge)

4.5 Preparation of Ice Sample

Introduction

There is a need to provide a standard description of ice preparation so that experimental results can be compared and reviewed objectively. Techniques for preparing fine grained homogenous, isotropic low porosity ice have been described by Garcia (1984), Jacka and Lile (1983), Cole (1979). The techniques used at Memorial University have been described Barrette (2003). The techniques used during this project are very similar to that described by Barrette. A summary is provided below.

Ice Production Process

A synopsis of the ice sample preparation steps is shown in Table 4-41. The ice was produced for this project at the cold room facilities NRC-IOT.

Table 4-4 Flow chart for the ice sample preparation

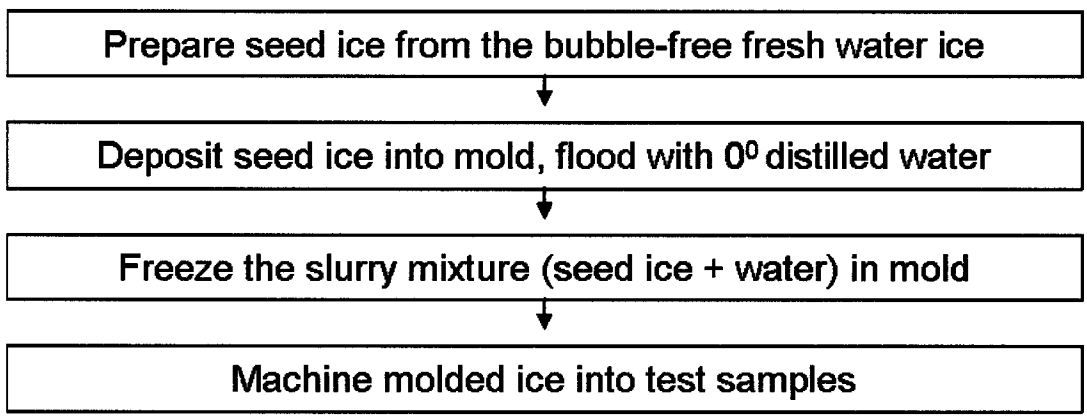

Production of seed ice

The seed ice for making granular ice blocks (poly-crystalline ice) has to be free of air bubbles so that the ice sample that is produced will also be bubble free (very difficult to achieve, but the aim is to minimize the air present in the testing sample). The seed ice used in this project was acquired from a commercial ice supplier as 300 lbs blocks of clear ice produced for use in the ice sculpture industry. This is not a standard practice, as most times the ice used for seed is grown from distilled water. This option was chosen as a means to reduce the time needed to prepare for the testing program, and is expected to have been of minimum consequence in the overall response of the ice as the water used to make the ice blocks was degassed and filtered (to produce clear ice for the sculptures).

In order to produce the seed ice (Figure 4-7), large bubble free ice blocks are first cut with a chain saw into manageable blocks. The blocks are then further reduced on a band saw into strips of ice approx 20 mm x 80 mm x 5 mm. The strips are then fed into an ice crusher (as found in food service). The crushed ice is then side sieved in order to obtain the desired grain size. The seed used for this testing was that retained on a standard ASTM International 4.75-3.35 mm sieve. It is important to maintain a clean environment during the sieving process to minimize contamination. This was done at -10^0C.

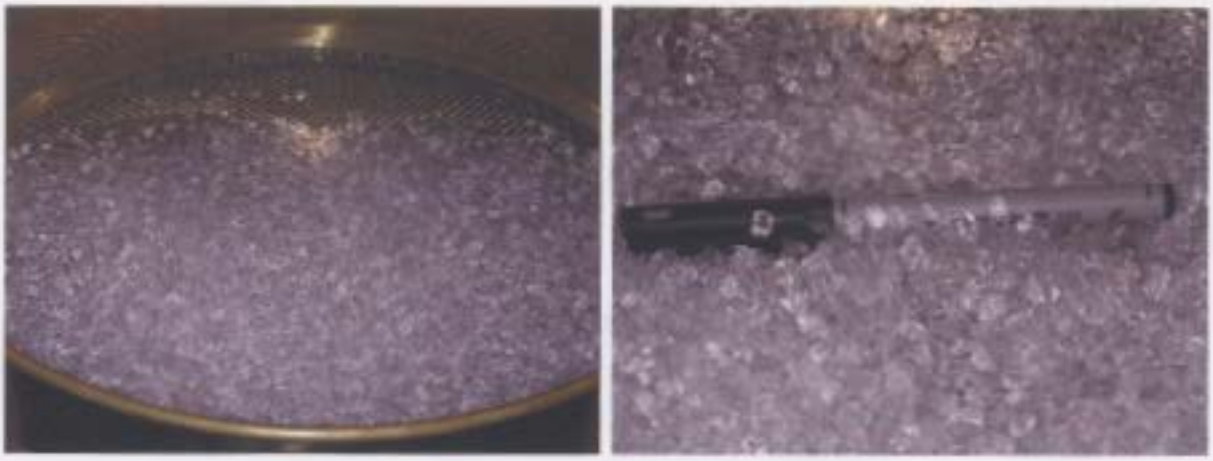

Figure 4-7: Polycrystalline seed ice on ASTM International 4.75-3.35 mm sieve

Molding

Molding is the process by which the large polycrystalline ice blocks are produced. The critical step in this process is the evacuation of air from inter-seed voids and from the water used to flood the mold. A vacuum molding system was designed for this purpose and is located in the anti-room (0^0 C) next to the large cold room at IOT. This will be described in detail below

Various types of molds and procedures have been established and introduced in the literature. Glen (1953) introduced a brass mold and a vacuum for the production of test ice. His system produced cloudy ice due to the random orientation of crystal grains and the presence of bubbles. Goughnour (1967) did not use a vacuum system, although the water was seeded, for the production of test ice; this resulted in ice with columnar grain.

The molding process used for this project is outlined as follows:

1. Place mold (Figure 4-8) in cold room overnight to ensure that it gets down to temperature. This is tested by placing several seeds along the outside of the mold making sure that they do not show any signs of melting.
2. Fill the mold with seed (approximately 1-50 quart cooler full).
3. Carefully place a thin layer of snow (finely crushed ice produced as a by-product of the sieving process, guaranteeing that it will not contaminate the sample) over the seed. This ensures that no sharp edges from the seed will come into contact with the latex membrane used to hold the vacuum.
4. Place a bead of vacuum grease around the lip of the mold, and then stretch a cut off weather balloon (latex membrane) over the mold, making sure of a good seal with the vacuum grease. Hold this in place with large rubber bands. The mold is than vacuumed to approximately 2-3 mm Hg.
5. 6.0 litres of zero degree distilled de-aerated (Figure 4-9) water is drawn into the mold under vacuum.
6. An insulated cover is placed over the flooded mold ensuring that freezing takes place from the bottom up. Any air that may remain is pushed to the top of the ice block during freezing, facilitating trimming later on.
7. The mold requires a minimum of 3 full days to freeze at -10^0 C. The mold was left upturned at 0^0 C until the ice block released. This was facilitated by the downward taper shape of the mold shape.

Figure 4-8: Polycrystalline ice block mold. (Note: the hose and valve to the left, used for vacuuming out air, and flooding with de-aerated water.

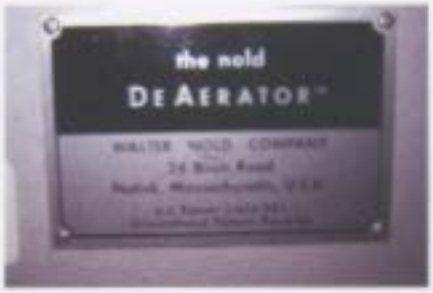

Figure 4-9: Nold DeAerator System located at NRC-IOT

Machining

The samples used for testing had to be machined from the large blocks produced from the mold (Figure 4-10). This technique was preferred to casting samples as it allows for selective trimming of any poor quality ice, and increases control of the sample finish. For this project the test samples measured approximately 20cm x 20cm x 10cm.

The Machining process used for this project is outlined as follows:

1. Cut the large blocks into manageable blocks on band saw, continuing to work the smaller blocks until they were approximately square and measuring 25cm x 25cm x 15cm. Each mold was able to produce 2 blocks.
2. Using the milling machine (located in the cold room at IOT) and a surface cutter, the large rough blocks were then machined to the final size (Figure 4-11). The milling machine could remove approximately 3-4 mm maximum per pass. The technique used did produce precisely flat surfaces, but did not produce perfectly square blocks.

Figure 4-10: From mold block to test sample

Figure 4-11: Machining test sample using the milling machine in the large cold room at NRC-IOT

Chapter 5 Individual Test Observations

This project was designed with much of the focus placed on visual data obtained through high speed video, regular video, and digital photographs. This section will provide a sample of the observations made for each test (complete observations are found in appendix A). This includes a table detailing the events and times noted on the high speed video (regular speed camera for the longer tests). These times are then transferred to the load trace using Matlab. The load traces are manually adjusted to begin at zero by using Matlab to observe the point that the load graph deviates from its baseline. The video times are adjusted to zero based on the first observed frame of contact. This adjustment is necessary as an initial space exists between the indenter and the sample that must be closed before the indenter makes contact with the specimen. This space is necessary to ensure that the indenter is up to the required velocity at time of contact (i.e., no error in velocity related to acceleration). The zeroing cuts off this initial movement, and because the video and load sensor could not be set off at the same time, they have to be separately adjusted to zero. Photographs of the test samples before and after testing, and the photographs of the thin sections are included.

note
Not all peaks showed definitive expulsions on the video, and some were observed to a lesser degree. For the sake of this project, the events recorded were deemed significant by the relatively larger magnitude then was observed throughout the duration of the test. This means that all spikes on graphs were not associated with a significant event as is defined related to this project. The periods between significant events was characterized by vary degrees of clearing at the indenter contact zone; from continuous flow of particles at high speeds, to" popping" small ejections at lower speeds.

5.1 Example of Individual Test Observations: Test I05_D10_V5p0_I

Figure 5-1: I05_D10_V5p0_I Post test pictures; the left side shows clearly that relatively large pieces of ice were injected away from the indenter. The right side shows that within the indenter footprint, areas of white crushed ice, and areas of clear ice are present.

I05_D10_V5p0_I - Test observations:

1. High speed projectile extrusions
2. Indenter "bored" into the sample causing continuous expulsion of crushed ice with periodic large "violent" ejections of larger particles with high velocity
3. Loud continuous cracking noises

Table 5-1: I05_D10_V5p0_I- High speed video observations

HSV Observation	Start Time as seen from HSV (seconds)	Normalized Time (seconds)
Indenter contact	0.085	0
significant expulsion	0.111	0.026
significant expulsion	0.287	0.20
significant expulsion	0.428	0.34
significant expulsion	0.563	0.48
significant expulsion	0.732	0.65
significant expulsion	0.994	0.91
significant expulsion	1.125	1.04

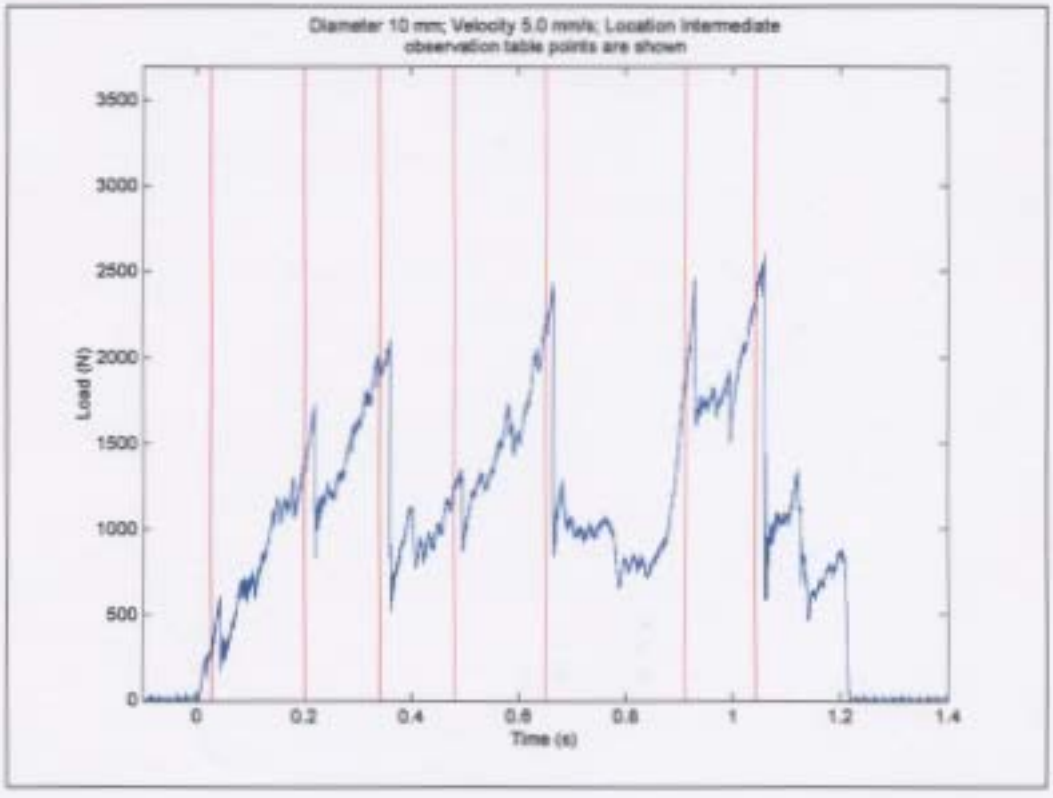

Figure 5-2: I05_D10_V5p0_I -Load trace with vertical lines indicating the time of observed significant events from the high speed camera.

Figure 5-3: I05_D10_V5p0_I -Thin section pictures (indented from top). The left side shows the thin section under cross polarized light. The right side shows the thin section under a side reflected light.

Chapter 6 General Test Observations

6.1 Edge Effects and Rate of load Increase

Performing tests at the same velocity, but at differing locations provides insights into edge effects, large scale fracturing and the rate of load change. By comparing the 3 tests of common velocity and looking for similarities and differences, interesting trends become apparent.

The most noticeable trend is that the initial change in load with time slope for the tests of the same velocity, but at different locations, is similar. That is, for any given loading rate, there exists a characteristic rate of load increase. The common slope continues until the distance to a free edge (the edge effect) becomes significant (Figures 6-2 and 6-3), and large scale fractures occur. This is a significant observation, as the scale effect in ice engineering, the resulting magnitude of pressure will decrease with increasing ice contact area, is directly related to fracture. As seen in Figure 6-1, fracture events, whose occurrence is correlated to level of confinement, present a limit to the potential load. Thus, the edge effect (an indirect measure of confinement) plays a role in the maximum potential load experienced. The edge effect should also become enhanced as the area increased, this was not clearly evident from the tests conducted, but warrants further research.

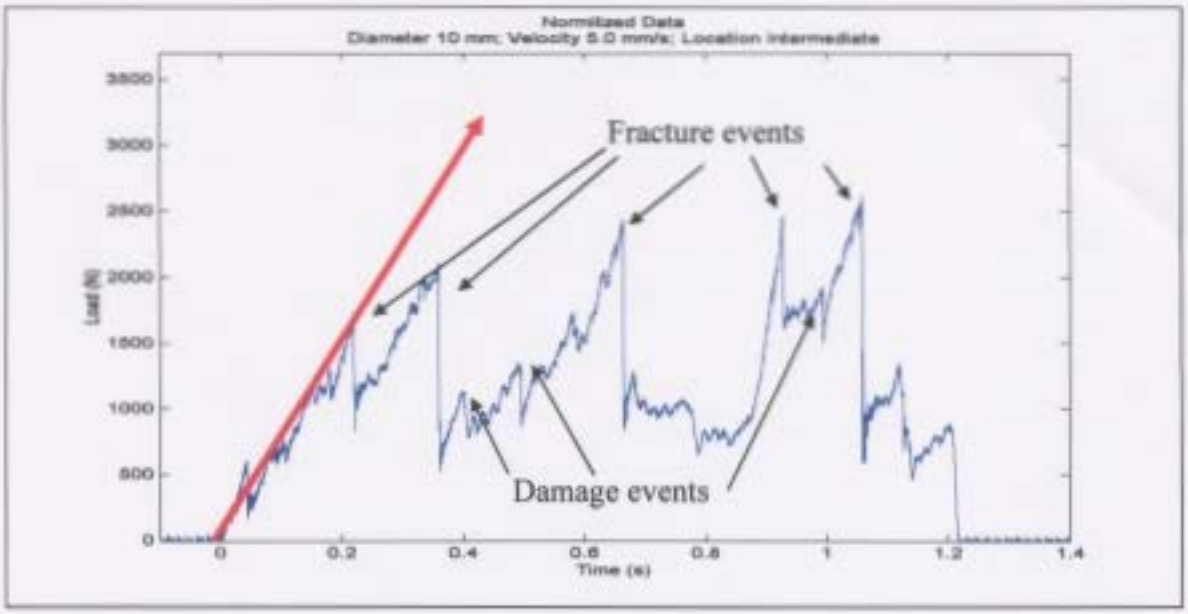

Figure 6-1: The load during ice structure interactions is limited by layer damage mechanisms and large scale fractures. The red line indicates the potential for a large load increase if fractures did not occur. This study has shown that the distance to a free surface is influential in fracture formation, and indirectly to the maximum load reached.

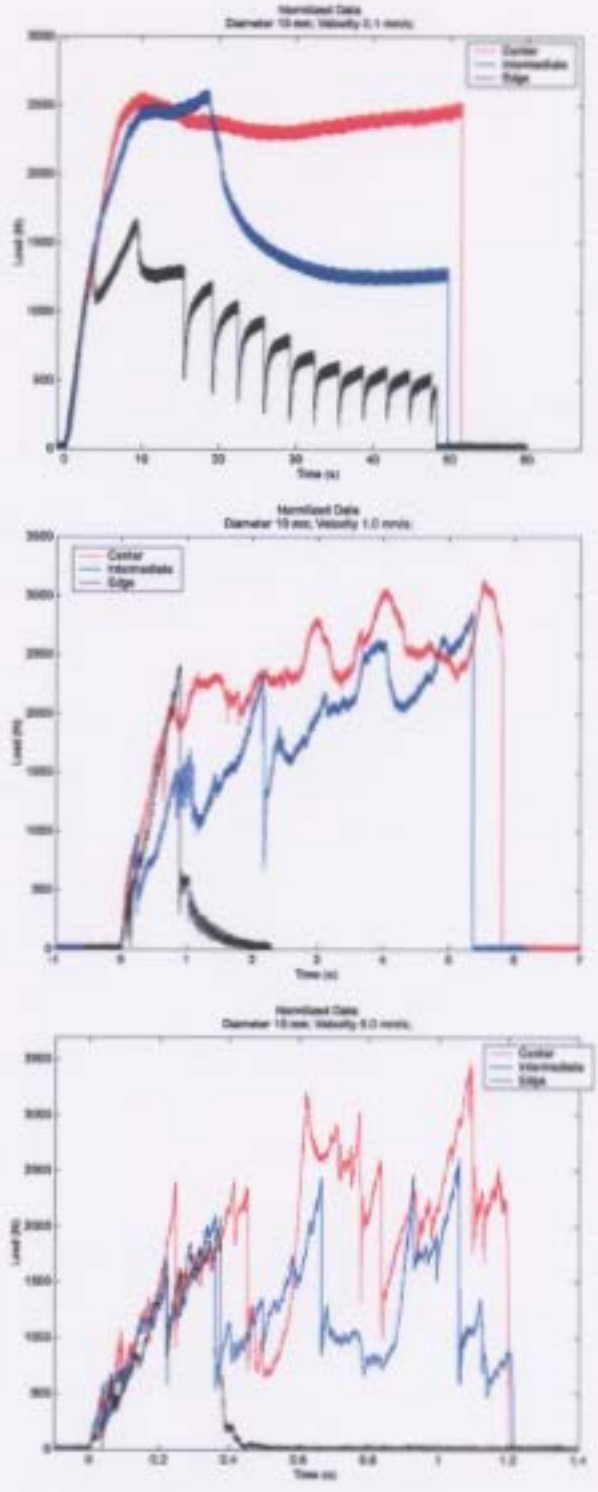

Figure 6-2: Comparison of tests performed with the same indentation velocity (10 mm indenter). Notice that the initial slope of all 3 tests per graph is the same.

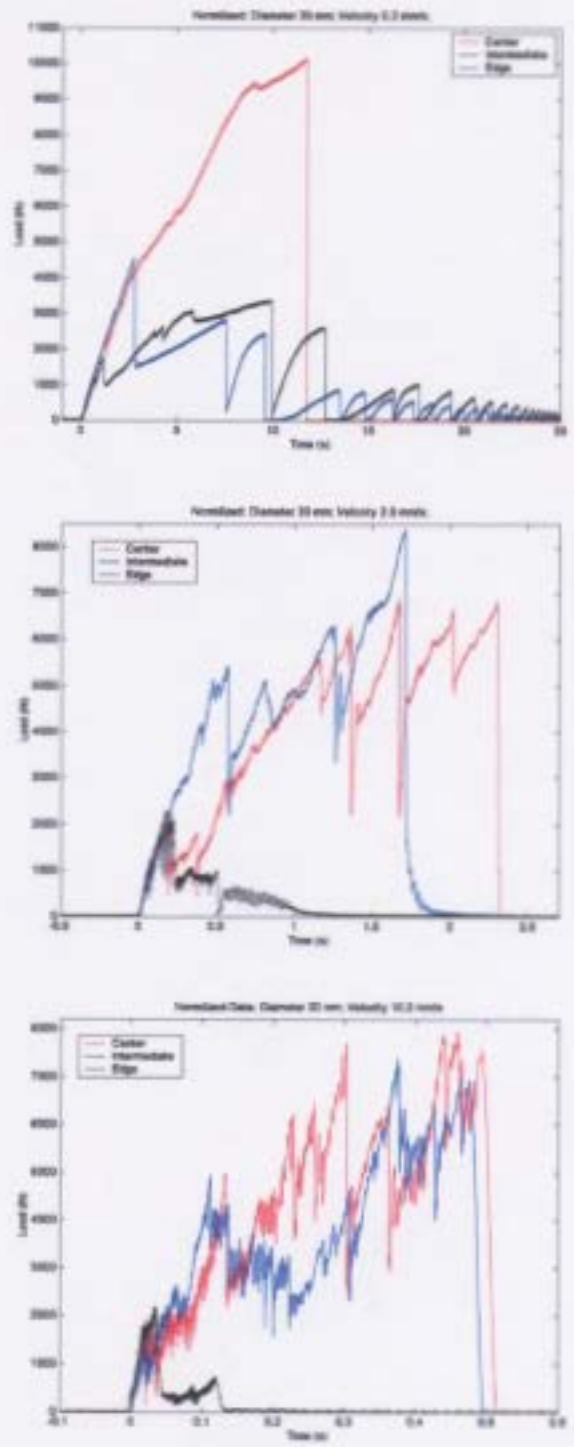

Figure 6-3 Comparison of tests performed with the same indentation velocity (20 mm indenter). Notice that the initial slope of all 3 tests per graph is the same.

6.2 Damage Classification Under Differing Test Conditions

This testing program was designed to examine how varying testing conditions would affect the test outcome and type of deformation. An important step to achieve this is to examine each test, classify the type of damage that took place, and identify significant trends. Tables 6-1 to 6-6 enable easy comparison between tests. Observations for these tables were made through observing the tests while in progress, and then studying the high speed camera data. It is beyond the scope of this project to take detailed measurements regarding items such as the location of fracture initiation or the actual sizes if the spalled peaces. It is apparent though from qualitative observations that the fractures tended to initiate near the center of the indenter and that the larger indenters tended to result in larger spalls.

Table 6-1: Damage Classification: Center location Sorted.

Test Number	Indenter Diameter	Test Speed	Test Location	Dominant Damage Description (ranked 1-3 for mild-severe)		
				Large Fractures	Local Spalling	Crushing
I05_D20_V0p2_C	20 mm	Slow	Center	y	2	3
I05_D20_V2p0_C	20 mm	Medium	Center	n	3	2
I05_D20_V10p0_C	20 mm	Fast	Center	n	3	1
I05_D10_V0p1_C	10 mm	Slow	Center	n	1	3
I05_D10_V1p0_C	10 mm	Medium	Center	n	2	3
I05_D10_V5p0_C	10 mm	Fast	Center	n	3	1

Table 6-2: Damage Classification: Intermediate location Sorted

Test Number	Indenter Diameter	Test Speed	Test Location	Damage Description (ranked 1-3 for mild-severe)		
				Large Fractures	Local Spalling	Crushing
I05_D20_V0p2_I	20 mm	Slow	Intermediate	y	1	3
I05_D20_V2p0_I	20 mm	Medium	Intermediate	y	2	2
I05_D20_V10p0_I	20 mm	Fast	Intermediate	n	3	3
I05_D10_V0p1_I	10 mm	Slow	Intermediate	y	1	3
I05_D10_V1p0_I	10 mm	Medium	Intermediate	n	2	3
I05_D10_V5p0_I	10 mm	Fast	Intermediate	n	3	2

Table 6-3: Damage Classification: Edge location Sorted

Test Number	Indenter Diameter	Test Speed	Test Location	Damage Description (ranked 1-3 for mild-severe)		
				Large Fractures	Local Spalling	Crushing
I05_D20_V0p2_E	20 mm	Slow	Edge	y	1	2
I05_D20_V2p0_E	20 mm	Medium	Edge	y	1	2
I05_D20_V10p0_E	20 mm	Fast	Edge	y	3	2
I05_D10_V0p1_E	10 mm	Slow	Edge	y	1	1
I05_D10_V1p0_E	10 mm	Medium	Edge	y	1	2
I05_D10_V5p0_E	10 mm	Fast	Edge	y	2	3

Table 6-4: Damage Classification: Fast Indentation Velocity Sorted

Test Number	Indenter Diameter	Test Speed	Test Location	Damage Description (ranked 1-3 for mild-severe)		
				Large Fractures	Local Spalling	crushing
I05_D20_V10p0_C	20 mm	Fast	Center	n	3	1
I05_D20_V10p0_I	20 mm	Fast	Intermediate	n	3	3
I05_D20_V10p0_E	20 mm	Fast	Edge	y	3	2
I05_D10_V5p0_C	10 mm	Fast	Center	n	3	1
I05_D10_V5p0_I	10 mm	Fast	Intermediate	n	3	2
05_D10_V5p0_E	10 mm	Fast	Edge	y	2	3

Table 6-5: Damage Classification: Medium Indentation Velocity Sorted

Test Number	Indenter Diameter	Test Speed	Test Location	Damage Description (ranked 1-3 for mild-severe)		
				Large Fractures	Local Spalling	crushing
I05_D20_V2p0_C	20 mm	Medium	Center	n	3	2
I05_D20_V2p0_I	20 mm	Medium	Intermediate	y	2	2
I05_D20_V2p0_E	20 mm	Medium	Edge	y	1	2
I05_D10_V1p0_C	10 mm	Medium	Center	n	2	3
I05_D10_V1p0_I	10 mm	Medium	Intermediate	n	2	3
I05_D10_V1p0_E	10 mm	Medium	Edge	y	1	2

Table 6-6: Damage Classification: Slow Indentation Velocity Sorted

Test Number	Indenter Diameter	Test Speed	Test Location	Damage Description (ranked 1-3 for mild-severe)		
				Large Fractures	Local Spalling	crushing
I05_D20_V0p2_C	20 mm	Slow	Center	y	2	3
I05_D20_V0p2_I	20 mm	Slow	Intermediate	y	1	3
I05_D20_V0p2_E	20 mm	Slow	Edge	y	1	2
I05_D10_V0p1_C	10 mm	Slow	Center	n	1	3
I05_D10_V0p1_I	10 mm	Slow	Intermediate	y	1	3
I05_D10_V0p1_E	10 mm	Slow	Edge	y	1	1

From examining the above tables and the graphs in Figure 6-1, it is apparent that several generalizations can be made:

1. With all other things equal, the probability of large fracture increases as distance to the edge decreases.
2. Slow speed tests have a higher probability of fracture than high speed tests.
3. Slow speed tests undergo continuous small extrusion (local crushing) that appears ineffective in "clearing" the indenter. This leads to build up of energy in the system that is released in violent bursts causing large fractures.
4. Fast tests undergo continuous extrusion in the form of local spalling, effectively relieving the energy in the system in a series of small bursts.

6.3 High Speed Video: A Closer Look

The use of high speed video to observe loading events during indentation is an interesting and promising method of data collection. There is the inherent difficulty of how to present this data effectively to the reader. It is impossible to include the videos, and there is no numerically effective method to fully represent this data. This section aims to provide the reader with a glimpse of information available through two step by step case studies that examine how the load-time traces and screen shots are analyzed together. The video was shot at 1000 frames per second. It should be noted here that the data on the load trace and the high speed camera had to be manually correlated (as explained earlier). This introduces a small level of error (on the order of plus or minus 1 frame) but the evidence strongly suggests that the noticeable load fluctuations, or events, visible on

the graphs correlate well with significant visual events from the video, and that spalling and fractures results in the large drop in loads.

Case 1: High speed ejection spall

Step 1. Load trace: Generated using matlab from data obtained from the MTS machine load cell at NRC-IOT.

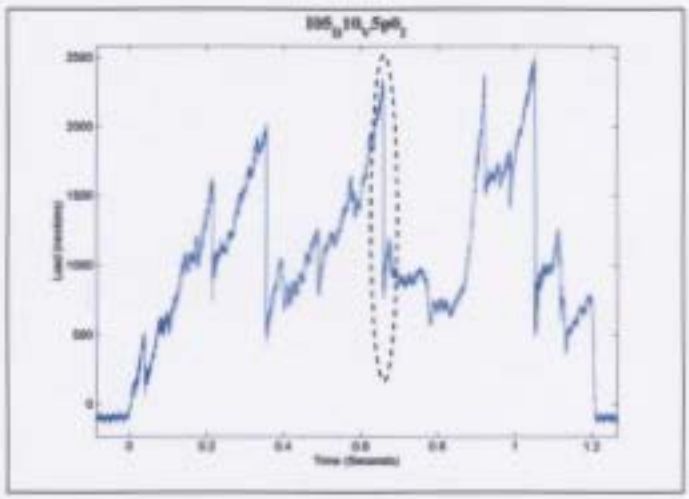

Figure 6-4 Complete Load trace for test I05 D10 V5p0 I with highlighted event

Step 2. Blow up the circled region on above graph

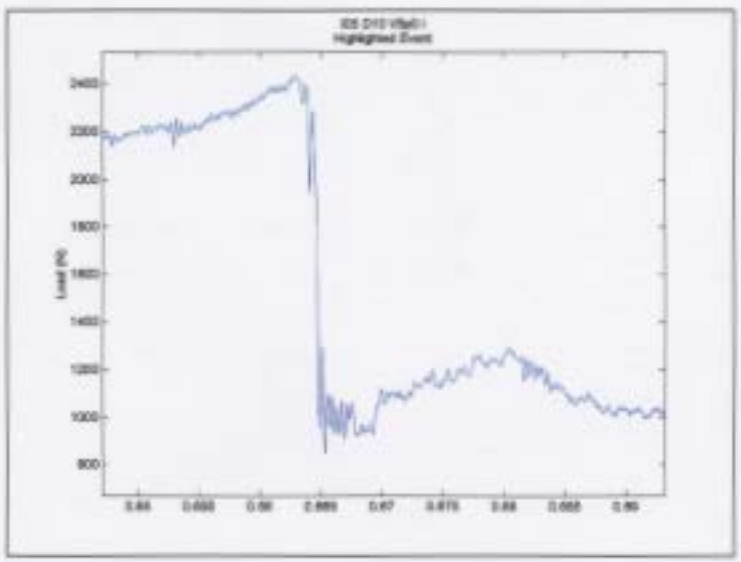

Figure 6-5: Test I05 D10 V5p0, highlighted event, focusing on time 0.650 - 0.69 s

Step 3. Screen shots from the high speed video

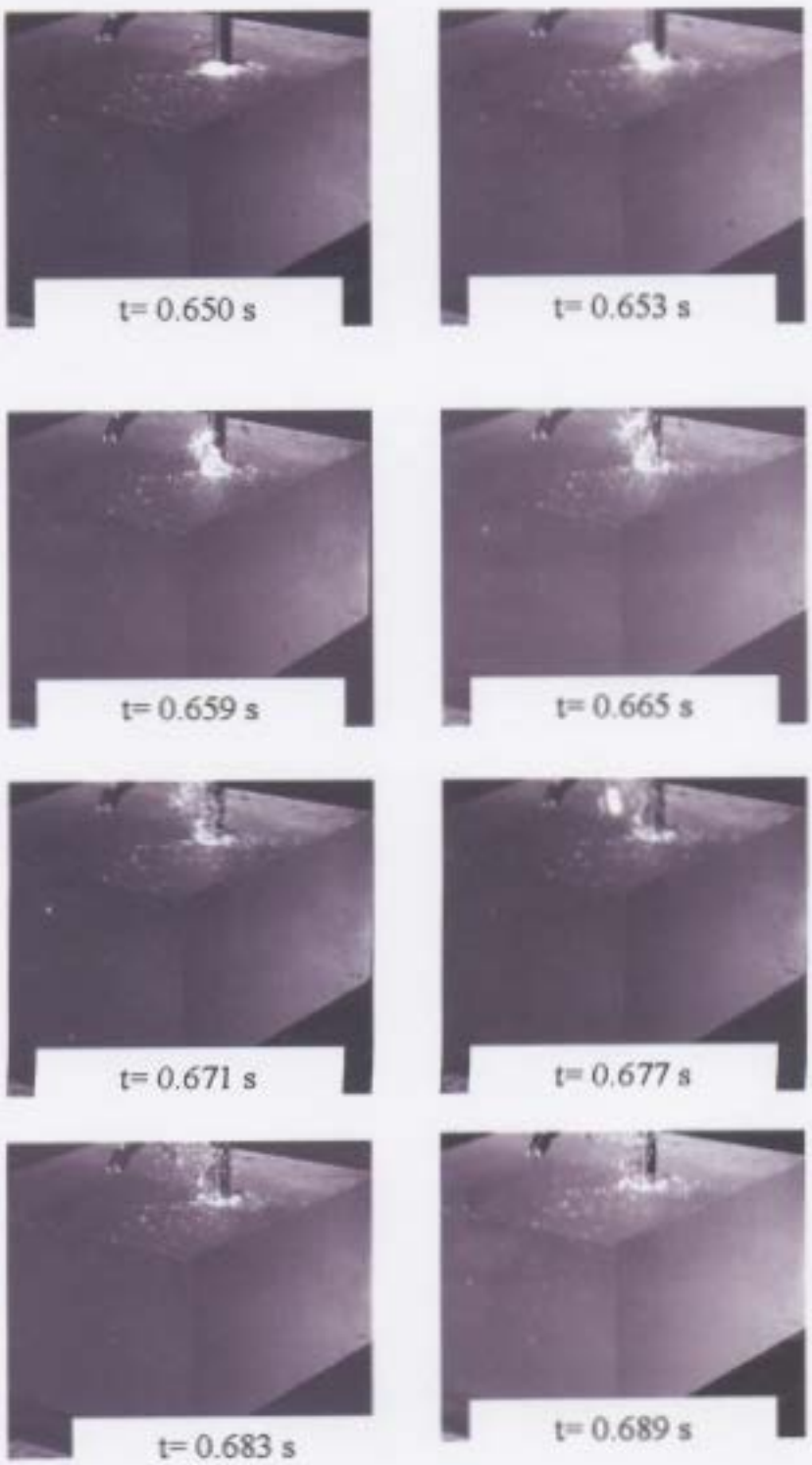

Figure 6-6: Screen shots of the circled event. It shows that the large load drop is directly associated with a spall ejection process.

Case 2: Edge Fracture

Step 1. Load trace: Generated using matlab from data obtained from the MTS machine load cell at NRC-IOT.

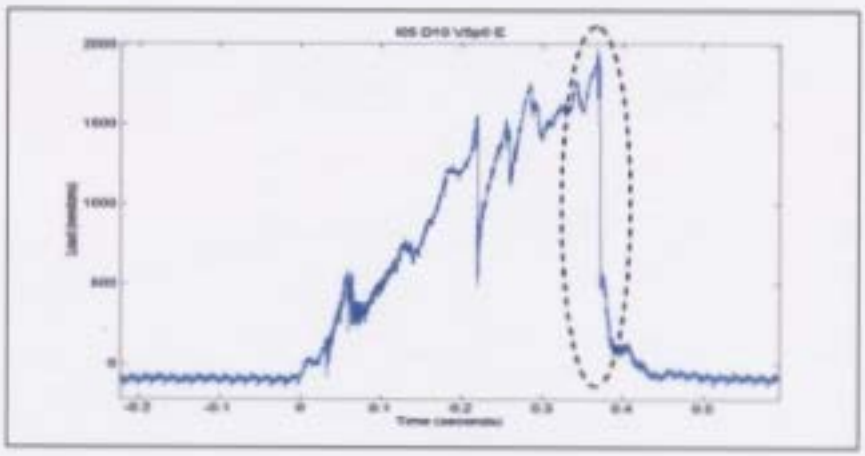

Figure 6-7: Complete Load trace for test I05 D10 V5p0 E with highlighted event

Step 2. Blow up the circled region on above graph.

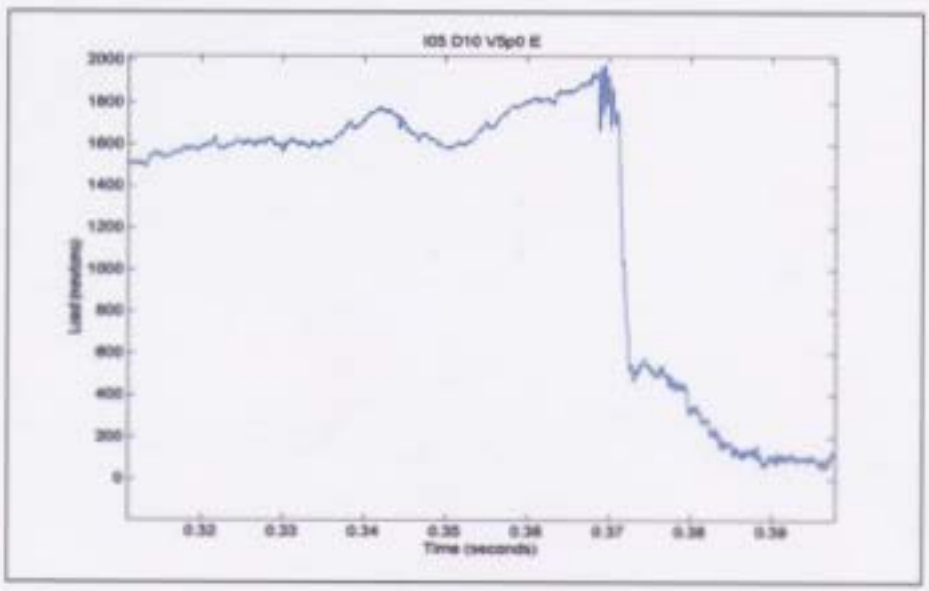

Figure 6-8: Test I05 D10 V5p0, highlighted event, focusing on time 0.342 - 0.375 s.

Step 3. Screen shots from the high speed video.

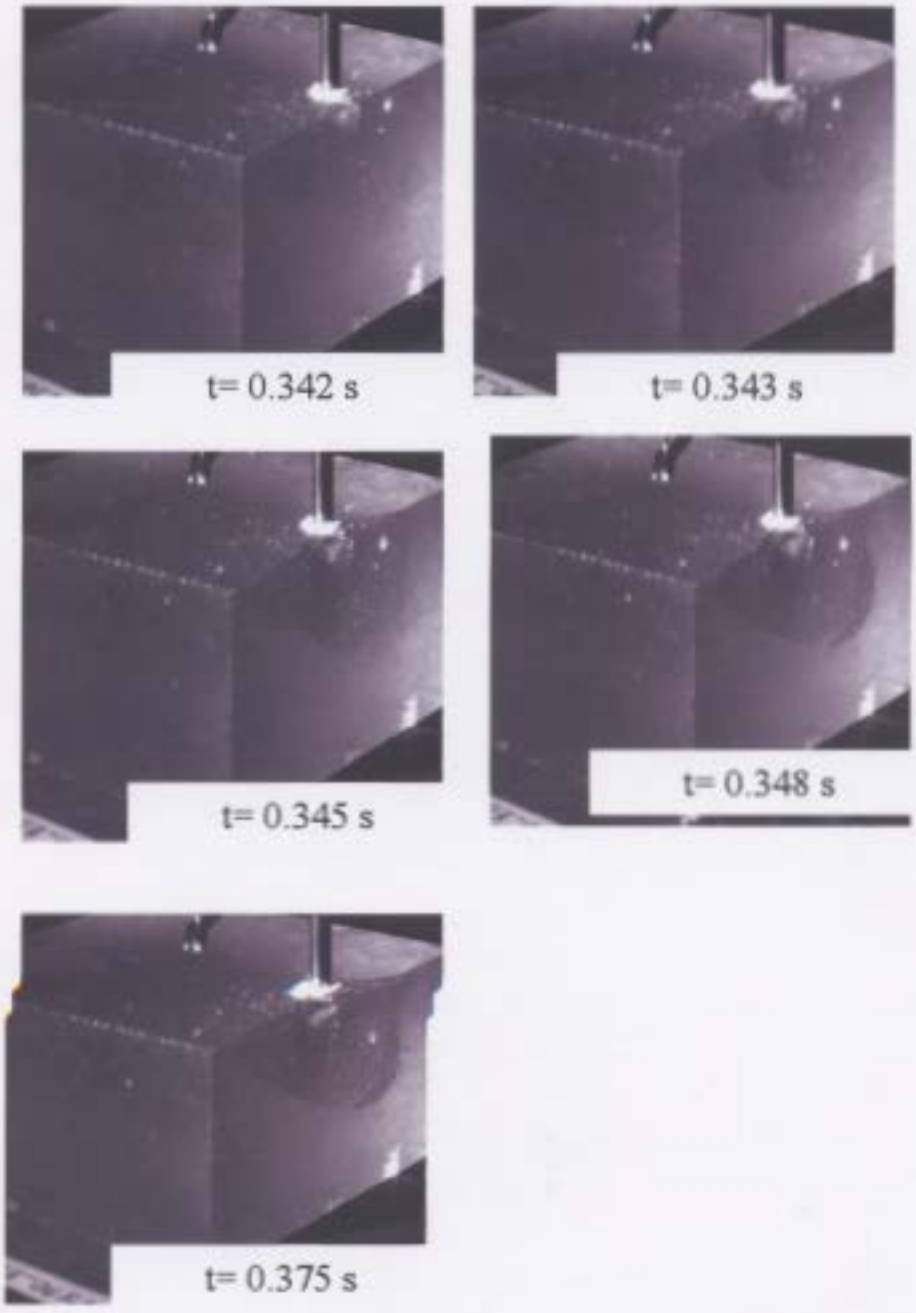

Figure 6-9: Screen shots of the circled event. It shows that the large load drop is *directly associated with an edge fracture.*

Chapter 7 Damage Layer: Observations and Evidence

7.1 Introduction

The damage layer, as described in detail earlier, manifests itself as a zone mechanical damage processes, varying depending on relative location to a high pressure zone (Figure 7-1). This section will present observational evidence for the existence of a damage layer, and the varying components. It should be noted that although this section aims to provide examples of the specific damage processes, they do not exist alone during the processes. Damage is a complex interaction of several processes.

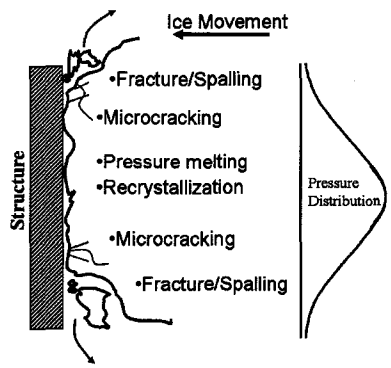

Figure 7-1: Zones of Damage associated with High Pressure Zones

7.2 Fracturing

Evidence of large fractures was abundant, with every edge location causing fracture, half the intermediate location test causing fracture, and one central location test causing fracture. Figure 7-2 is included here as an example.

Figure 7-2: Example of fracture observed during testing

7.3 Spalling

Spalling is more or less fracture, but in this report it is distinguished from large scale fractures. The term spalling is used to describe the smaller flakes that are ejected (mostly from the top surface, very close to the indenter). Figure 7-3 shows a flake being "spalled off" during indentation.

Figure 7-3 : High speed video screen shot showing an ice flake being ejected as a result of spalling near the indenter

7.4 Micro-cracking

Micro-cracking referees to the small cracks that form within the ice sample, very close to the indention site. Micro-cracks are quite visible from the side reflective thin sections. It is of importance to note where this cracks form in relation to the ice crystals, evidence from this study strongly points to a relationship between crystal boundaries and micro-crack propagation. Figure 7-4 shows this phenomenon well.

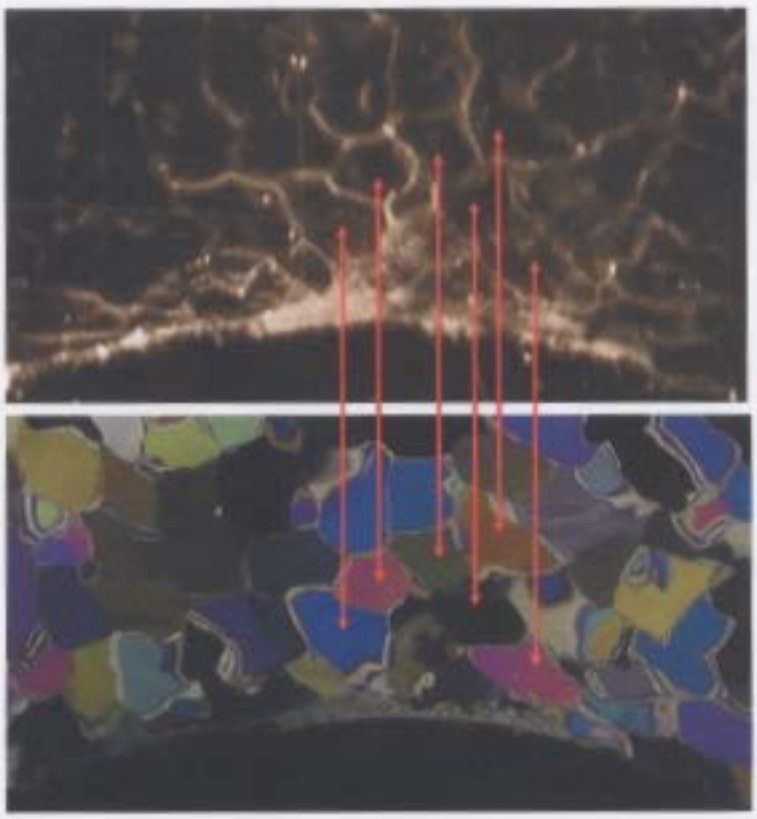

Figure 7-4: The red lines correlate grains from the thin section photographed under reflective light conditions (top) and cross polarized light (bottom) conditions. It clearly shows that the outline defined by the micro-cracking is related to grain boundary location, at least within the lower portion of the damage.

7.5 Recrystallization without micro-cracking

The evidence for recrystallization is found in the fine detail of the thin sections, specifically the area directly in front of the indenter. Many of the thin sections show that the area in front of the indenter, under cross polar light conditions, contains many tiny crystals. This is often caused by crushed ice, and highly micro-cracked ice, but within some of the reflected light thin sections, it can be seen that this is not always the case. Many of the reflected light thin sections show that this area is actually clear ice. Since the ice was originally made of 4 mm crystals, the presence of the new smaller crystals of clear ice is the result of recrystallization as a result of damage (Figure 7-5).

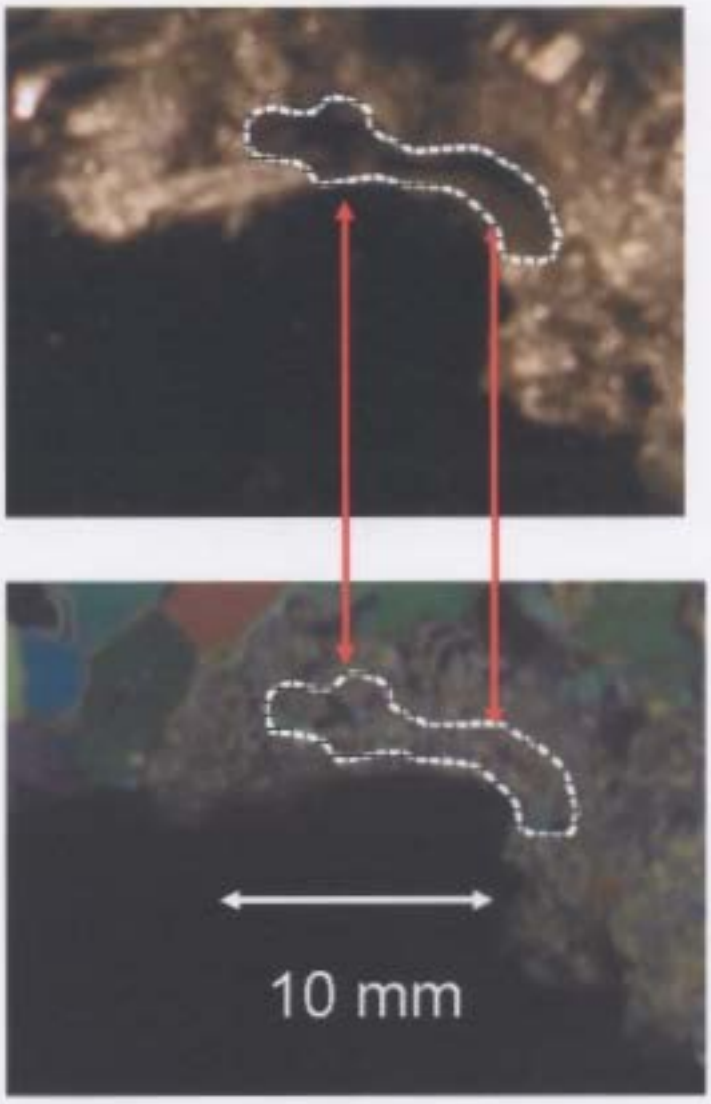

Figure 7-5: The outlined area, that consists of many small crystals (lower picture), is made up off clear ice (top picture), evident by the lack of micro- cracks. This is clearly evidence for the presence of recrystallization processes at the indenter interface.

Chapter 8 Discussion and Conclusions

8.1 Recommendations for future work

This was a test series and certain lessons were learned that are extremely valuable to a future set, or as George Box (Professor Emeritus-University of Wisconsin) has been known to say, "The best time to do an experiment is after it has been done".

This experimental program was designed as a pilot project, and although there is scientific merit in the experimental results of this testing program, the recommendations for future projects is certainly of equal importance. This section is dived into a section outlining recommended changes to the experimental procedure, and a section recommending potential new experiments.

Experimental procedure recommendations

1. Ice growth is of utmost importance, and it can become the dominant factor in controlling the experimental progress.
    a. The time taken to grow samples of testable ice was reduced by purchasing the large industrial blocks of air free ice; it is recommend that this be continued in the future.
    b. The time taken to crush air free ice and subsequently hand sieve it the desired seed size was very time consuming, and produced a lot of waste ice. A more suitable crusher with finer adjustment should be considered to remedy this issue.

c. It was very time consuming to actually seed a block of ice, and then the sample had to be left to freeze for at least 3 days. This process could be sped up with additional molds. For example, if 3 molds were available, as one mold was being seeded, another mold could be in the freezing stage and the other could have a sample being ejected, allowing for continuous production.

2. Sample machining is a time consuming process, and in any future projects, samples should be used to the full potential. Within this project, 1 machined sample was used for each test. As Figure 8-1 illustrates, it was possible to use a sample for more than one test during all of the edge tests, and potentially some of the intermediate tests. In the future it is recommended to test more than one side of the sample under such circumstances.

Figure 8-1: Illustrating the potential of testing on more than one side of a sample.

3. The samples during testing moved from the initial location on the sample platform during indentation. This is a consequence of the testing conditions chosen, but it will certainly introduce a level of uncertainty into the tests that should be effectively dealt with in future studies to strengthen the validity of the edge tests. It is however, difficult to control. In future testing of this nature, the sample should be secured to the platform in a manner that would not affect the sample's unconstrained condition. Two suggestions on how to accomplish this are:
    a. "Weld" the sample to the platform using a small bead of water around the perimeter.
    b. Place the sample on a platform with a higher coefficient of friction. "Grip tape" is one potential solution.

4. During some of the testing, it was noted that corners and edges on the bottom of the sample (the side in contact with the platform) were fracturing and breaking off. Two potential amendments to the procedure to prevent this from happening are:
    a. Make one final "cleaning" pass on the bottom surface of the sample on the milling machine directly prior to testing
    b. Use a platform that has been milled to a higher tolerance.

5. The high speed camera used was very good visually, but it did have the constraint of not providing a means for allowing trigger signal synchronization with the load cell. This would have made analysis of the data easier and provided for greater

accuracy in correlating events between both data sets. Cameras are available that have this ability and in the future they should be used. It would also be beneficial to invest in software that will enable easier editing and trimming of the videos.

6. The data acquisition rate, and filter used were based primarily on those available to us for use at NRC-IOT. This is an issue that would have to be further investigated.

7. The use of a high speed camera for the slower velocity tests proved rather fruitless as the capacity of the memory storage disk for the camera used was not capable of recording the full duration of the longer, slower tests. This issue would have to be addressed. A larger memory card or direct links into a computer hard drive appear to be reasonable solutions.

Future experiment recommendations

1. This test series raised the issue of edge effects relating to loading and fracture. To further investigate this issue the following is suggested:
    a. The speed of indention and the indenter size are kept constant.
    b. The only variable would be the indenter location (Figure 8-2). Note, this was done to a degree during this test series, but a larger number of intermediate distances would help constrain the problem, and lead to a more complete understanding.

c. The experiment should be carried out until a large global fracture occurs

d. Load should be measured

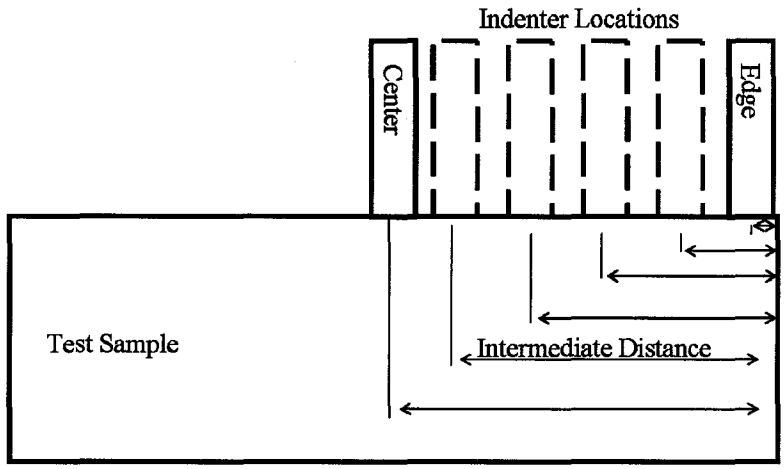

Figure 8-2: Illustrative sketch of suggested test set-up

This experiment will help develop a numerical relationship between edge distance loading and fracture as is hypothesised in Figure 8-3.

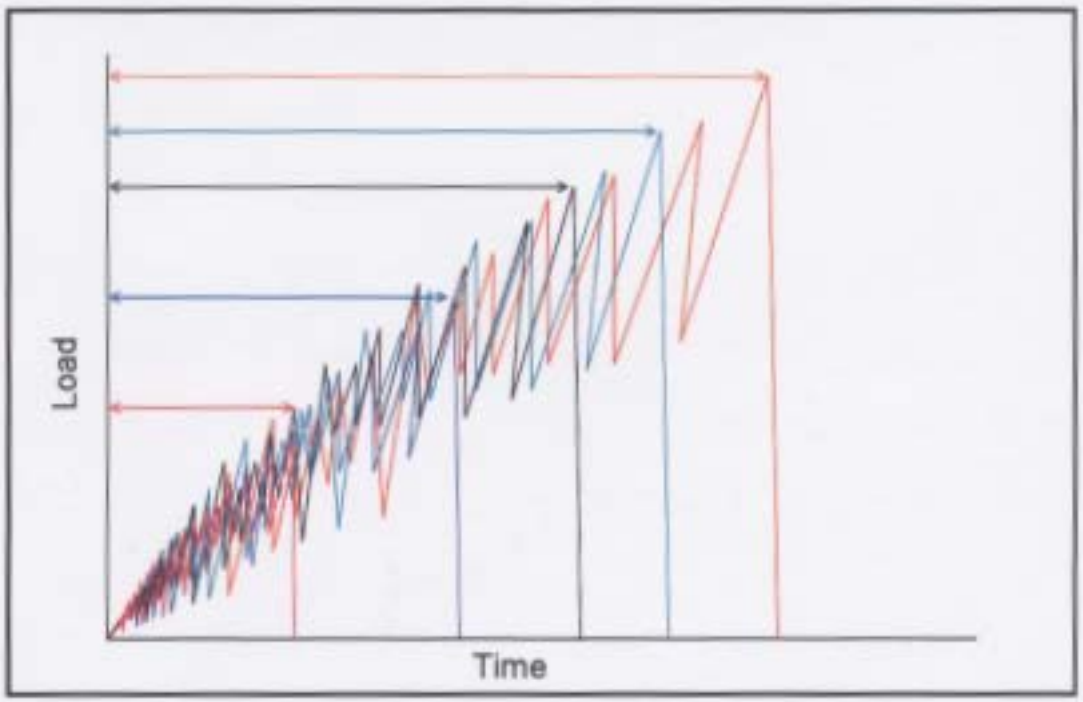

Figure 8-3: Illustration of potential load traces showing how the maximum load before fracture might vary depending on the indenter distance from the edge. (Lowest load being at the edge going to largest load at the center)

2. The high speed camera proved to be a valuable tool in observing the behaviour of the ice during indentation. This idea could be carried forward to a larger area experiment where a load could be applied across a whole face and a high speed camera could be used to watch how spalling locations, and similarly high pressure zones, change spatially with time.

It is suggested that to aid in fracture and spall initiation, a truncated pyramid shape be used, with the loading applied to the top plane. A square based truncated pyramid could be used as a control, and aspect ratio affects could be

studied quite elegantly by changing the shape of the base from square to rectangular in various configurations.

3. A third recommendation is to complete the above 2 test series while using a pressure sensor to map the spatial and temporal dynamics of high pressure zones. This experiment is currently being looked into with the Tekscan I-Scan Pressure measurement system being investigated. It is suggested that a high speed camera be utilized during these tests.

8.2 Practical implications

These experiments have effectively shown that fracture plays an important role in load reduction during continuous interaction, and in the scale effect. The scale effect itself is well known to be an important consideration in design situations, but it may not be clear how the results of an indentation test series can be related to design. Comparisons between an indenter test and a structure being impacted by a large ice sheet can be made. As seen in Figure 8-4, a stationary structure being impacted by a large floe is directly comparable to an indenter test. In the case of the Molikpaq structure, it was very thin in comparison to the impacting sheet; in this case it resembles a center indenter test. The lessons learned regarding the consequences of a fracture during indention tests (see figure 6-1) can be applied to artic structures.

Figure 8-4: The Molikpaq in the Beauforte Sea. Illustrating how a stationary structure being impacted by a large floe is comparable to an indenter test.

8.3 Conclusions

Evidence from this report supports the theory of a damage layer induced at the ice structure interface, and provides useful insight into the mechanisms involved in this process. This is highlighted by the powerful evidence visible in the thin sections and variable modes of interaction visible from the high speed camera during the different rates. The existence of such a strong correlation between grain boundaries and micro cracks are also of interest.

Compelling evidence linking the dynamic loading sequence, a well documented phenomenon of ice interaction, to fracture and spalling events is also visible in the comparison between load traces and the high speed videos. This was a theory that has been discussed before, but to the author's knowledge, this was the first time that such persuasive evidence has been presented.

The prelude to the existence of a numerical relationship between the distances to a free edge on fracture processes has also been shown.

References

Ashby, M.F., Palmer, A.C., Thoules, M., Goodman, D.J., Howard, M., Hallum, S.D., Murrell, S.A.F., Jones, N., Sanderson, T.J.O., Ponter, A.R.S., 1986. Nonsimultaneous failure and ice loads on artic structures. *Offshore Technology Conference, pp 399-404.*

Barnes, P. and Tabor, D. 1966. Plastic flow and pressure melting in the deformation of ice I. *Nature 210*: 878–882.

Barnes, P., Tabor, D. and Walker, J.C.F. 1971. The friction and creep of polycrystalline of ice. *Proceedings of the Royal Society of London A324*: 127–155.

Barrette, P., Pond, J., Li, C., Jordaan, I., 2003. Laboratory-scale indentation of Ice. PERD/CHC report 4-81.

Barrette, P. 2003. Laboratory manual for ice production, testing and examination. Ocean engineering research center. Faculty of engineering and applied science, Memorial University of Newfoundland. Internal document.

Blenkarn, K.A., 1970. Measurement and analysis of ice forces on Cook Inlet Structures. In *Proceedings of the 2nd Offshore Technology Conference Symposium (OTC)*, Vol. 2, Houston, #1261, 365-378.

Cole, D. M. 1979. Preparation of polycrystalline ice specimens for laboratory experiments. *Cold Regions Science and technology*, vol. 1, pp 153-159.

Frederking, R.M.W, 2004. Ice pressure variations during indentation. *Proceedings of the 17th International Association for Hydraulic Engineering and Research Symposium, Vol.2,* pp. 307-314.

Frederking, R.M.W., Blanchet, D., Jordaan, I.J., Kennedy, K., Sinha, N.K., Stander, E., 1990a. Field tests on Ice Indentation at medium scale, Ice Island. National Research Council of Canada Report CR 5866.1

Frederking, R.M.W., Jordaan, I.J. and McCallum, J.S. 1990b. Field tests of ice indentation at medium scale Hobson's Choice Ice Island. In *Proceedings of the 10th International Association for Hydraulic Engineering and Research Symposium*, Vol. 2,

Espoo, 931–944.

Fuglem, M.F., Muggeridge, K. and Jordaan, I.J. 1998. Design load calculations for iceberg impacts, Proceedings of the 8th International Offshore and Polar Engineering Conference, Montreal, Canada, Vol. 2, pp.460-467. *Int. Journal of Offshore and Polar Engineering*, 1999,9(4):298-306

Garcia, N. B. 1984. Specimen preparation for ice research. *Cold Regions Science and technology*, vol. 10, pp 273-275.

Glen, J. W. 1975. The mechanics of ice. *Cold Reg. Res. Eng. Lab. Monogr. II-C2b, Hanover, N.H.*

Glen, J. W. 1953. Mechanical properties of ice and their relation to glacier flow. *Ph. D. Thesis.* University of Cambridge.

Goughnour, R. 1967. The soil-ice system and the shear strength of frozen soil. *Ph. D. Thesis.* Michigan State University.

Jacka, T.H. and Lile, R.C. 1983. Sample preparation techniques and compression apparatus for ice flow studies. *Cold Regions Science and technology*, vol. 8, pp 235-240.

Jefferies M.G. and Wright W.H., 1988. Dynamic Response of Molikpaq to Ice structure *OMAE, Houston, Texas.*

Johnson, M. 1988. Uniaxial and triaxial testing of ice on the materials testing system. Memorial University, Dept of Engineering *Internal Document.*

Jordaan, I.J., Li, C., Sudom, D., Stuckey, P., Ralph., 2005. Principles for local and global ice design using pressure-area relationships. Presented at the *18th International Conference on Port and Ocean Engineering Under Arctic Conditions (POAC).*

Jordaan, I. J., 2001. Mechanics of ice-structure interaction. *Engineering Fracture Mechanics, vol. 68, pp 1923-1960.*

Jordaan, I.J., Maes, M.A., Brown, P.W., Hermans, I.P., 1993, Probabilistic analysis of local ice pressures. *Journal of Offshore Mechanics and Artic Engineering, vol. 115, pp 83-89*

Jordaan, I.J., Maes, M.A. and Nadreau, J.P., 1988. The crushing and Clearing process of ice in fast spherical indentation test. *Proc. 7th Int. Conf. on Offshore Mechanics and Artic Engineering, Houston, vol. 4,* PP. 111-116.

Kennedy, P.K., 1990. Dynamic activity and ice crushing behaviour in medium-scale ice-structure interactions. *Master Thesis,* Memorial University of Newfoundland.

Kheisin, D.E. and Cherepanov, N.W. 1970. Change of ice structure in the zone of impact of a solid body against the ice cover surface. In *Problems of the Arctic and Antarctic,* Issues 33–35 (A.F. Treshnikof), Israel Program for Scientific Translations 239–245.

Kry, P.R., 1978. A statistical prediction of effective ice crushing stresses on wide structures. *Proceddings of the 5th International IAHR Conference, Part 1. Lulea, Sweden,. pp 33-47.*

Lockett, F. J., 1972. Nonlinear Viscoelastic Solids. *Academic Press, London and New York,* pp 195

Masterson, D.M., Nevel, D.E., Johnston, R.C., Kenney, J.J., Spencer, P.A., The medium scale iceberg impact test program. *Proceedings,* IAHAR *Ice Symposium. Banff, Alberta, 1992.*

Michel, B., 1978. Ice Mechanics. *Le Presses De L'Universite Laval, Quebec,* pp 499.

Michel, B., Toussaint, N., 1977. Mechanisms and theory of indentation of ice plates. *Journal of Glaciology 19, No. 81,* pp 285-301.

Offenbacher, E.L., Roselman, I.C. and Tabor, D., 1972. Friction, Deformation and Recrystallization of Single Crystals of Ice Ih Under Stress. *Physics of Chemistry and Ice, Papers presented at the symposium on the physics and Chemistry of ice, Ottawa, Canada.*

Peyton, H.R. 1966. Sea ice strength. *Univ. of Alaska Geophysical Institute Report AG R-182.*

Pounder, E.R., 1965. The Physics of Ice, *Pergamon Press Ltd.,* pp 151.

Sanderson, T.J.O. 1988. Ice mechanics: Risks to Offshore Structures. *Graham and Trotman, Boston,* pp. 253.

Schulson E.M., 1999. The Structure and Mechanical Behavior of Ice. *JOM, vol* 51 (2), pp. 21-27

Sinha, N.K., 1979. Grain Boundary sliding in polycrystalline materials. *Philosophical Magazine*. A 40 (6) pp. 825-842

Sinha, N.K. 1977. Technique for studying the structure of sea ice. *Journal of Glaciology 18*: 315–323.

Sodhi, D.S., 2001. Crushing failure during ice-structure interaction. *Engineering Fracture Mechanics, vol. 68,* pp. 1889-1921.

Timoshenko, S., and Goodier, J.N., 1951. Theory of Elasticity, Second Edition, *McGraw Book Company, Inc. Tokyo*, pp. 506.

(http://www.cnlopb.nl.ca/ Dated: May 19, 2004)

Appendix A Test Observations

Test: I05_D10_V5p0_C

Figure Error! No text of specified style in document.**-1: I05_D10_V5p0_C Post test pictures; the left side shows clearly that relatively large pieces of ice were injected away from the indenter. The right side shows that within the indenter footprint, areas of white crushed ice, and areas of clear ice are present.**

I05_D10_V5p0_C -Test Observations:

1. High speed projectile extrusions
2. Indenter "bored" into the sample causing continuous expulsion of crushed ice with periodic large "violent" ejections of larger particles with high velocity
3. Loud continuous cracking noises

I05_D10_V5p0_C- High speed video observations

HSV Observation	Start Time as seen from HSV (seconds)	Normalized Time (seconds)
Indenter contact	0.060	0
Significant expulsion	0.780	0.062
Significant expulsion	0.197	0.181
Significant expulsion	0.235	0.219
Significant expulsion	0.441	0.425
Significant expulsion	0.765	0.749
Large flake lifting of top of sample	0.823	0.807
Significant expulsion	1.083	1.067

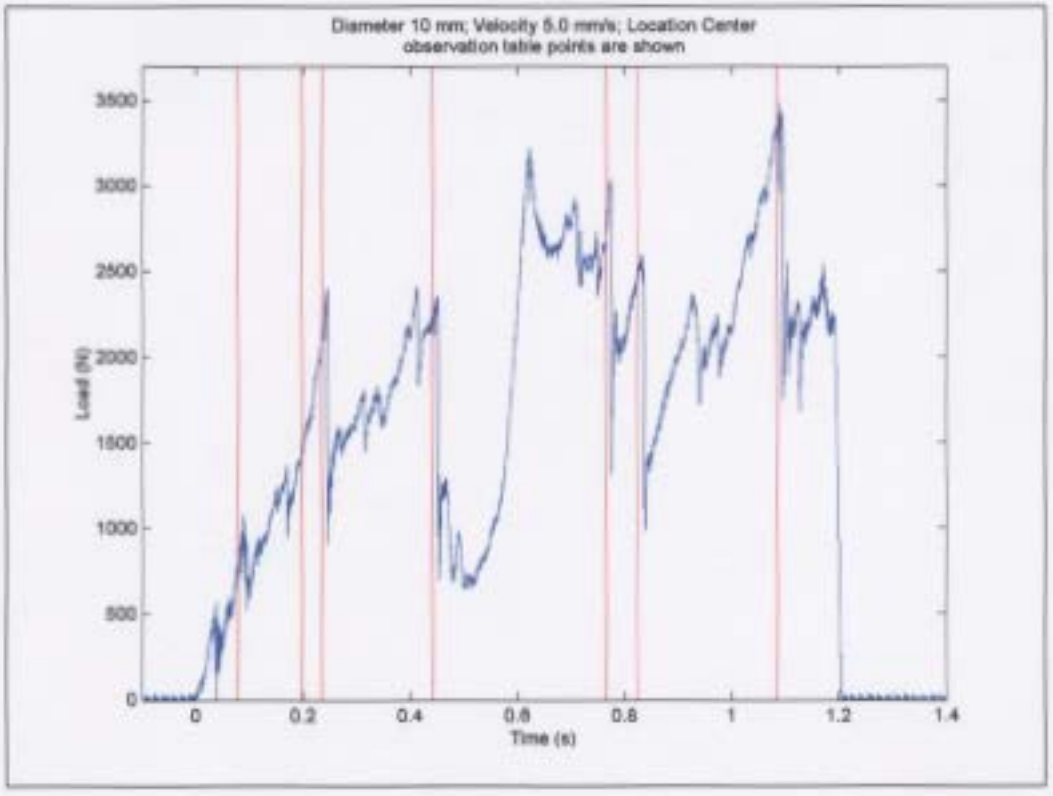

I05_D10_V5p0_C; Load trace with vertical lines indicating the time of observed events from the high speed camera

I05_D10_V5p0_C Thin section pictures; (indented from top) the left side shows the thin section under cross polarized light. The right side shows the thin section under a side reflected light.

Test: I05_D10_V5p0_I

I05_D10_V5p0_I Post test pictures; the left side shows clearly that relatively large pieces of ice were injected away from the indenter. The right side shows that within the indenter footprint, areas of white crushed ice, and areas of clear ice are present.

I05_D10_V5p0_I - Test observations:

1. High speed projectile extrusions
2. Indenter "bored" into the sample causing continuous expulsion of crushed ice with periodic large "violent" ejections of larger particles with high velocity
3. Loud continuous cracking noises

I05_D10_V5p0_I- High speed video observations

HSV Observation	Start Time as seen from HSV (seconds)	Normalized Time (seconds)
Indenter contact	0.085	0
significant expulsion	0.111	0.026
significant expulsion	0.287	0.20
significant expulsion	0.428	0.34
significant expulsion	0.563	0.48
significant expulsion	0.732	0.65
significant expulsion	0.994	0.91
significant expulsion	1.125	1.04

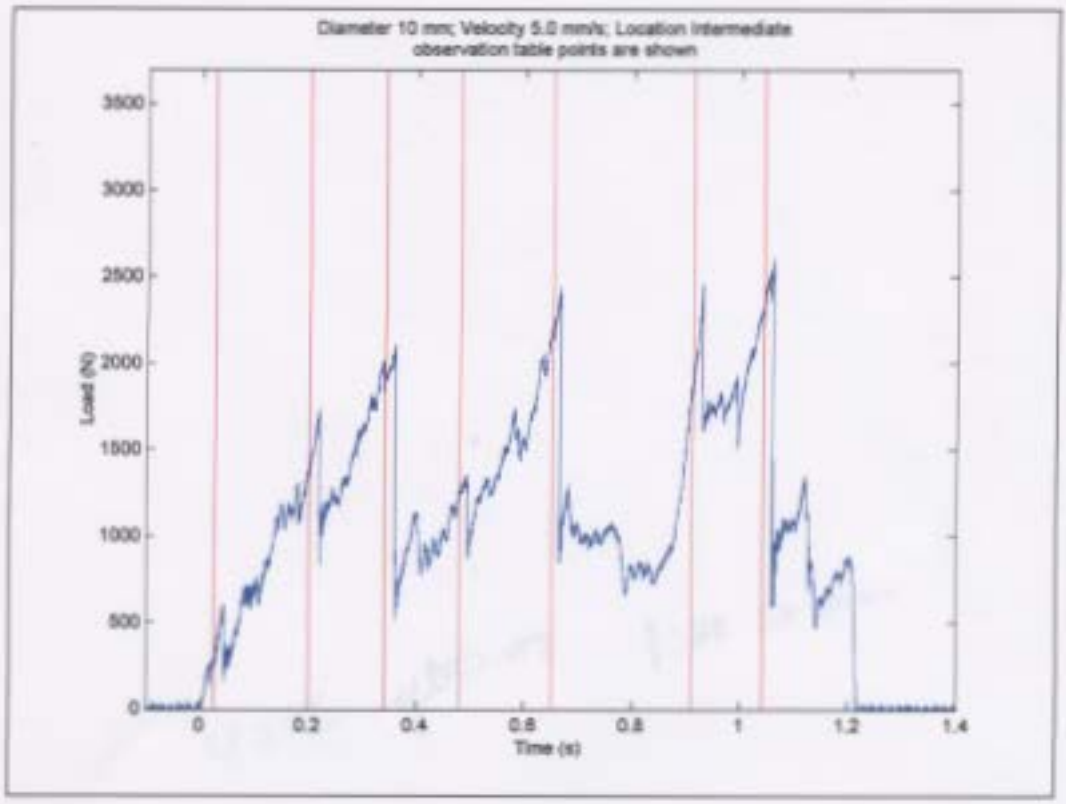

I05_D10_V5p0_I -Load trace with vertical lines indicating the time of observed events from the high speed camera.

I05_D10_V5p0_I -Thin section pictures (indented from top). The left side shows the thin section under cross polarized light. The right side shows the thin section under a side reflected light.

Test: I05_D10_V5p0_E

I05_D10_V5p0_E- Post test pictures. The left side shows clearly that a large edge fracture caused an ice piece to be ejected. The right side shows that within the indenter footprint, the fracture that broke away was roughly in the center of the indenter, and that the fracture did not extend all the way to the bottom of the sample.

I05_D10_V5p0_E- Test observations:

1. High speed projectile extrusion
2. Loud continuous cracking/popping noises
3. Large edge fracture formed quickly and the ejected particle was rounded
4. After the large fracture, the sample was "pushed" or slid along the platform in a stick-slip fashion

I05_D10_V5p0_E- High speed video observations

HSV Observation	Start Time as seen from HSV (seconds)	Normalized Time (seconds)
Indenter contact	0.09	0
Significant expulsion	0.278	0.188
Significant expulsion	0.316	0.226
Large crack begins	0.427	0.337
Large crack breaks free	0.433	0.343
Crack releases and begins to fall	0.46	0.37

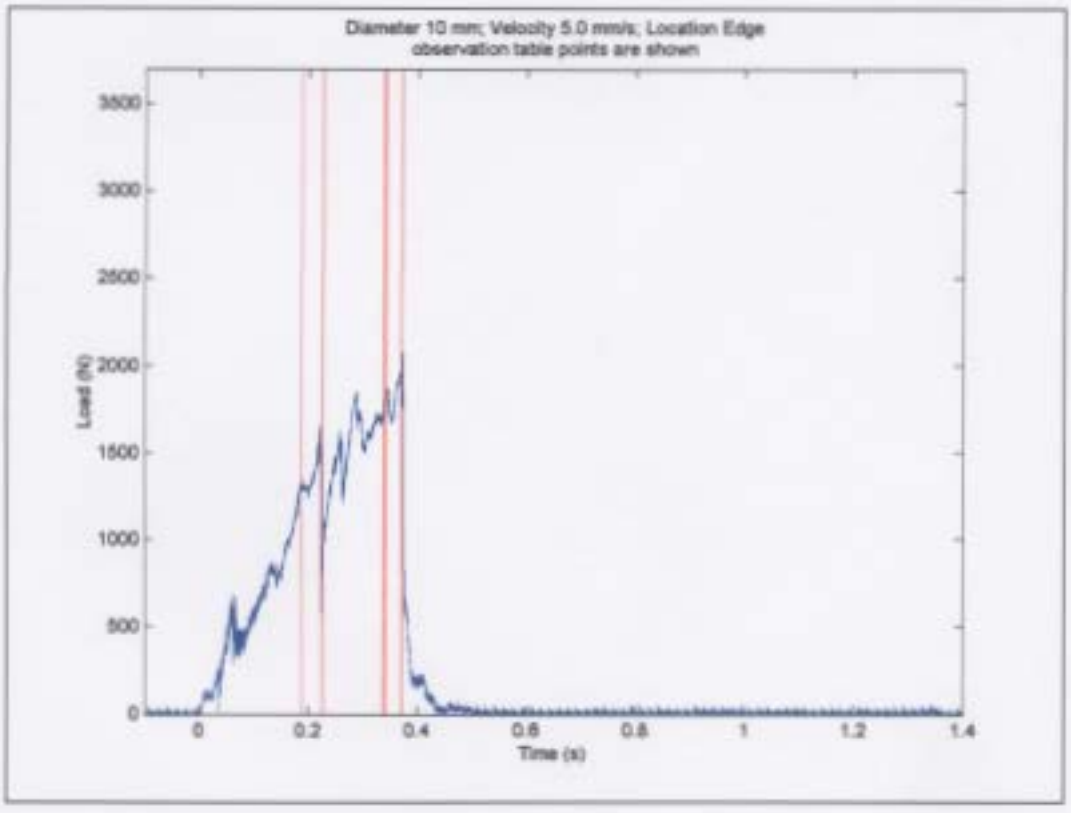

I05_D10_V5p0_E -Load trace with vertical lines indicating the time of observed events from the high speed camera

I05_D10_V5p0_E- Thin section pictures (indented from top). The left side shows the thin section under cross polarized light. The right side shows the thin section under a side reflected light.

Test: I05_D10_V1p0_C

I05_D10_V1p0_C-Post test pictures. The left side shows that although some ice particles were ejected, not to the same extend as the faster tests above. The right side shows that within the indenter footprint, areas of white crushed ice, and areas of clear ice are present. It also shows the large area of Hertz fracture present in the area surrounding the indenter.

I05_D10_V1p0_C-Test observations:

1. Loud continuous cracking/popping noises associated with continual crushing and extrusion
2. Large flake spall (approx 2inch in width) formed and was ejected from the top surface
3. Zone of penetration of the cracking was relatively shallow, extending only a few centimetres (approx 1-2cm) into the sample

I05_D10_V1p0_C- High speed video observations

HSV Observation	Start Time as seen from HSV (seconds)	Normalized Time (seconds)
Indenter contact	0.184	0
Lower corner blow out	0.772	0.588
Significant expulsion	1.286	1.102
Significant expulsion	1.748	1.564
Significant expulsion	1.914	1.73
Significant expulsion	2.574	2.39
Start of 2nd HSV file	0	3.068
Significant expulsion	1.11	4.178

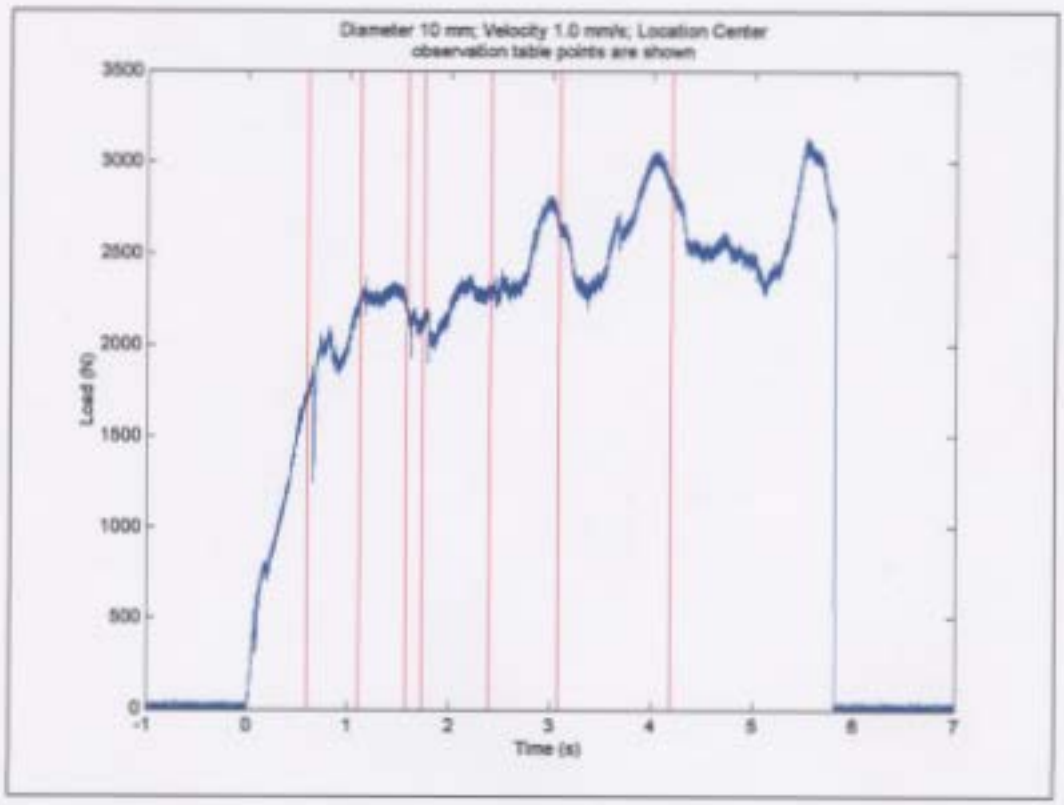

I05_D10_V1p0_C-Load trace with vertical lines indicating the time of observed events from the high speed camera.

Figure Error! No text of specified style in document.**-2: I05_D10_V1p0_C-Thin section pictures (indented from top). The left side shows the thin section under cross polarized light. The Right side shows the thin section under a side reflected light.**

Test: I05_D10_V1p0_I

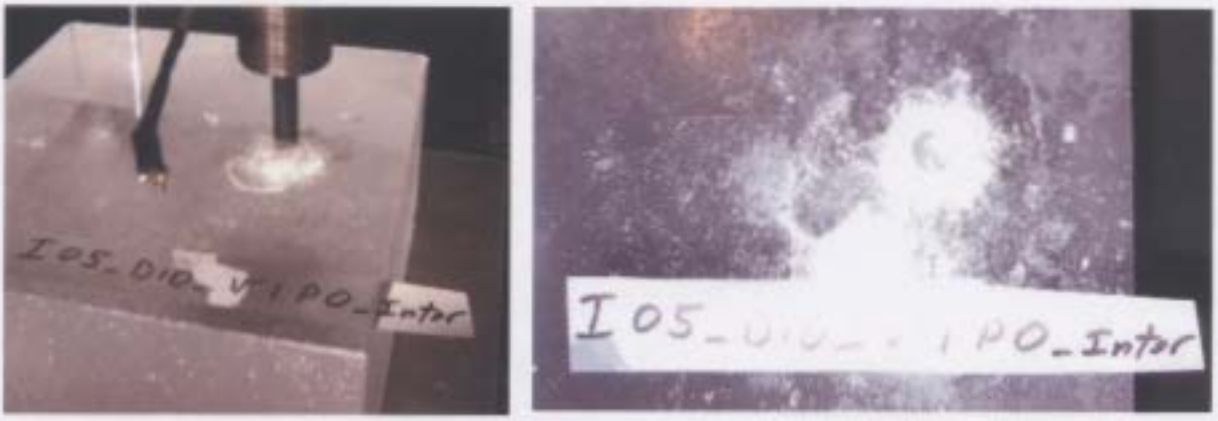

Figure Error! No text of specified style in document.**-3: I05_D10_V1p0_I- Post test pictures. The left side shows although some ice particles were ejected, not to the same extend as the faster tests above. The right side shows that within the indenter footprint, areas of white crushed ice, and areas of clear ice are present. It also shows the large area of Hertz fracture present in the area surrounding the indenter.**

I05_D10_V1p0_I- Test observations:

1. Loud continuous cracking/popping noises associated with continual crushing and extrusion
2. Large flake spall (approx 2inch in width) formed and was ejected from the top surface
3. Zone of penetration of the cracking was relatively shallow, extending only a few centimetres (approx 1-2cm) into the sample

I05_D10_V1p0_I - High speed video observations

HSV Observation	Start Time as seen from HSV (seconds)	Normalized Time (seconds)
Indenter contact	0.196	0
Significant spalling extrusion	0.338	0.142
Significant spalling extrusion	1.154	0.958
Significant spalling extrusion and crack growth	1.19	0.994
Large expulsion	1.2	1.004
Large expulsion	2.28	2.084
Large expulsion	3.212	3.016

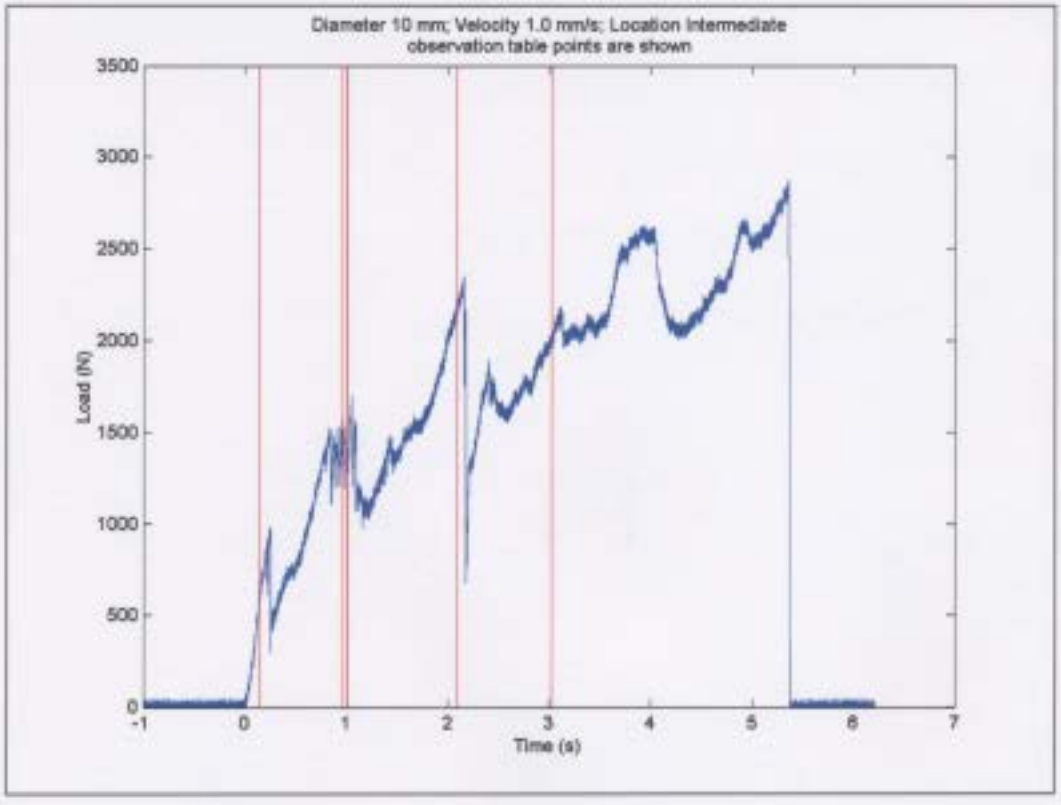

I05_D10_V1p0_I- Load trace with vertical lines indicating the time of observed events from the high speed camera

I05_D10_V1p0_I- Thin section pictures (indented from top). The left side shows the thin section under cross polarized light. The right side shows the thin section under a side reflected light. It should be noted the elongated grains in the bottom left side of the left picture are due to the flooding process during seeding. Every attempt was made to eliminate this, but it still occurs in some samples. Also, the large top-bottom cracks seen in the right picture are artefacts of the thin-section process.

Test: I05_D10_V1p0_E

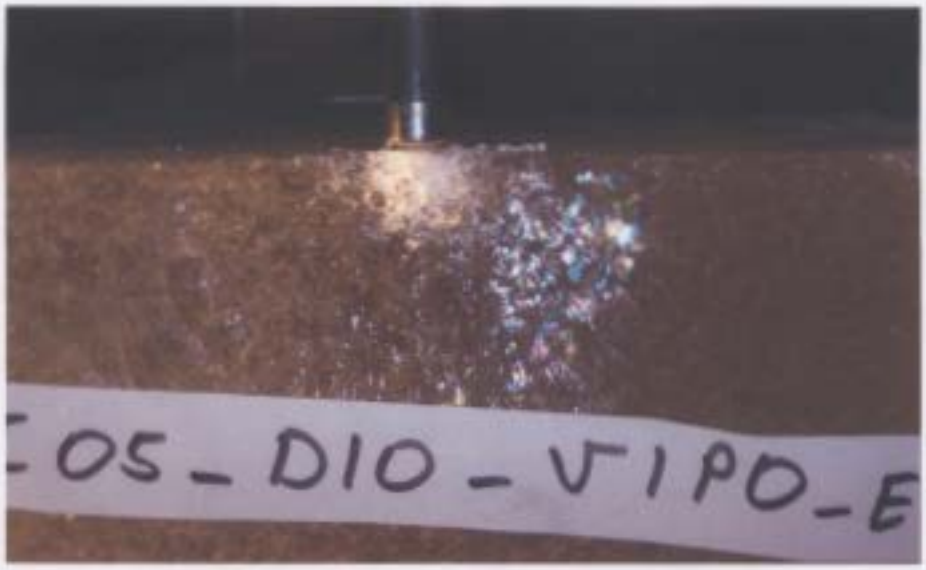

I05_D10_V1p0_E- Post test pictures. This picture shows a very nice close up of the area directly under the indenter. Note the semi-circle shape of the edge crack, the appearance that the ice is "wet" in the picture although it is dry, and the white zone of micro-cracking directly beneath the indenter to a depth of approx 1 cm (the diameter of the indenter is 1 cm for scale).

I05_D10_V1p0_E- Test observations:

1. Loud continuous cracking/popping noises
2. Large edge fracturing occurring very quickly and cleanly
3. After the large fracture, the sample was "pushed" or slid along the platform in a stick slip fashion

I05_D10_V1p0_E- High speed video observations

HSV Observation	Start Time as seen from HSV (seconds)	Normalized Time (seconds)
Indenter contact	0.214	0
Crack begins to form at bottom of sample	0.378	0.164
Crack begins to form at top center edge of sample	0.66	0.446
Large radial edge crack forms	1.005	0.791
Large radial edge spall falls away	1.012	0.798
Mass expulsion as spall off piece falls and crushed ice is extruded	1.03	0.816
More material falls from crushed zone	1.178	0.964

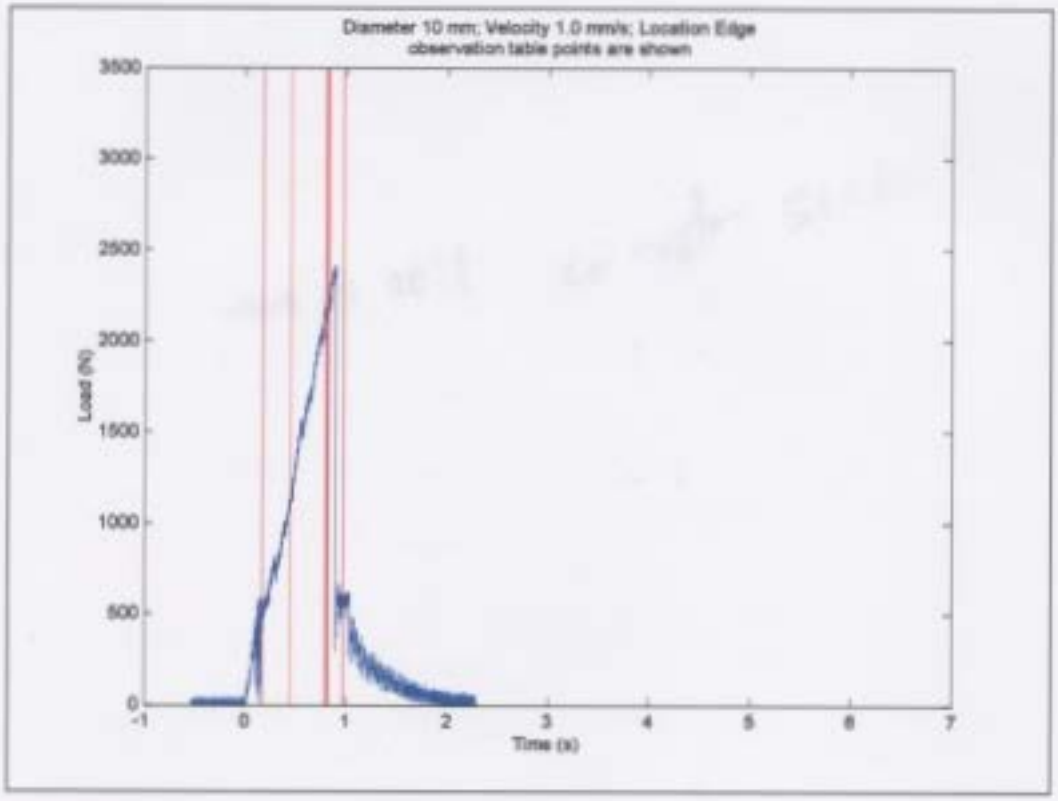

Figure Error! No text of specified style in document.**-4: I05_D10_V1p0_E- Load trace with vertical lines indicating the time of observed events from the high speed camera**

I05_D10_V1p0_E- Thin section pictures (indented from top). The left side shows the thin section under cross polarized light. The right side shows the thin section under a side reflected light.

Test: I05_D10_V0p1_C

I05_D10_V0p1_C- Post test pictures. Note the existence of Hertz like fracture in the right side picture.

I05_D10_V0p1_C- Test observations

1. Loud continuous cracking/popping noises.
2. The test was very consistent from start to finish with no visible "events"
3. The crushed ice did not "flow out" from the indenter, but instead, it occurred with lots of cracking suggesting small scale spalling
4. Very apparent "clear ice zone" seen in indenter footprint

I05_D10_V0p1_C- Regular speed video observations

Regular Video Observation (the test was too slow for HSV)	Normalized Time (seconds)

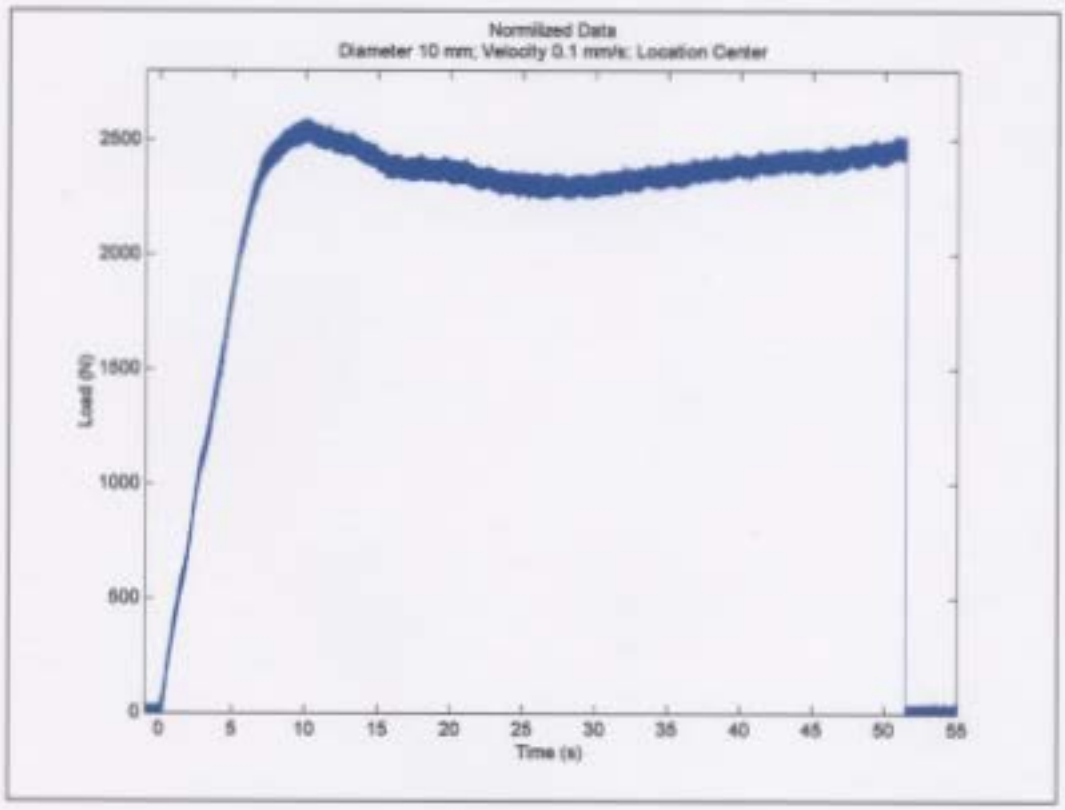

I05_D10_V0p1_C- Load trace. Note the resemblance to a typical ice creep curve (as discussed previously in the ice mechanics section)

I05_D10_V0p1_C- Thin section pictures (indented from top). The left side shows the thin section under cross polarized light. The right side shows the thin section under a side reflected light. This set of thin sections shows a very convincing zone of undamaged, recrystallized ice in the indenter contact region.

Test: I05_D10_V0p1_I

I05_D10_V0p1_I- Post test pictures. This picture shows a very nice close up of the area directly under the indenter. Note the semi circle shape of the edge crack, the appearance that the ice is "wet" in the picture although it is dry, and the white zone of micro-fractioning directly beneath the indenter to a depth of approx 1 cm (the diameter of the indenter is 1 cm for scale).

I05_D10_V0p1_I- Test observations:

1. Loud continuous cracking/popping noises
2. Large edge fracturing occurring relatively slowly, and propagating in discrete "jumps".
3. Zone of damage extends 2-3 cm below indenter

I05_D10_V0p1_I- Regular speed video observations

Regular Video Observation (the test was too slow for HSV)	Normalized Time (seconds)
Start	0
Large interior fracture appears	16.6
Large interior fracture jumps 1-2 cm in length	18.9
Large interior fracture jumps 0.5 cm in length	19.1
Large fracture reaches the edge and breaks through	21.0

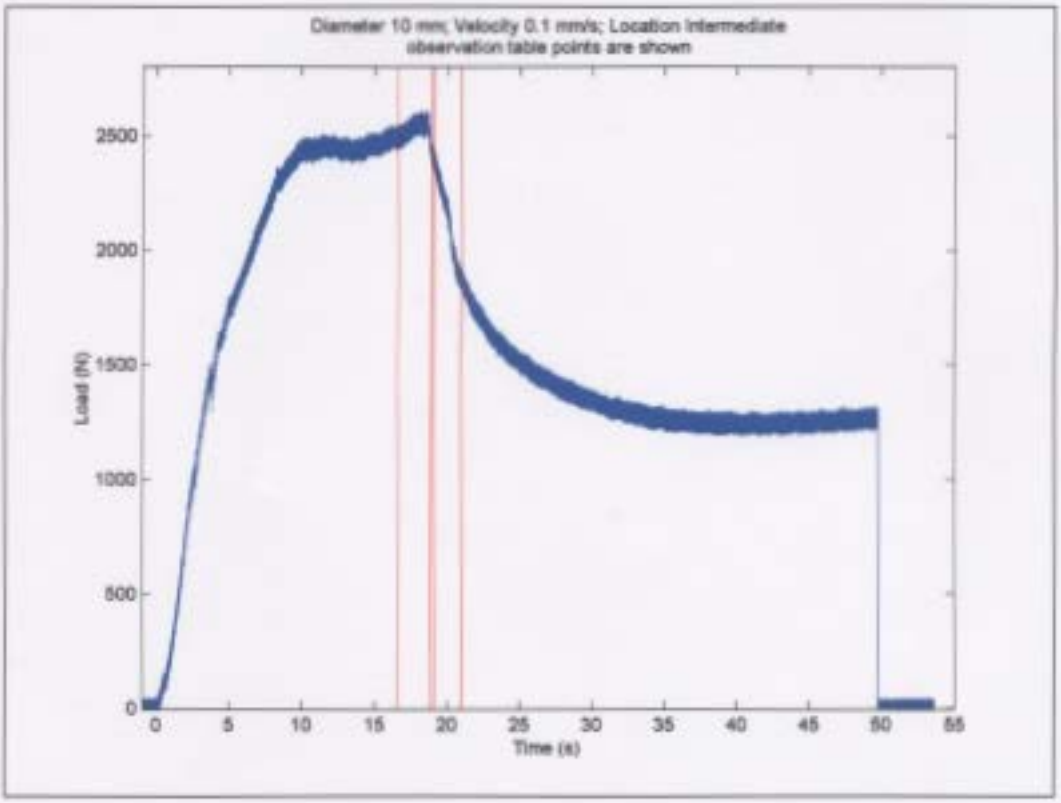

I05_D10_V0p1_I- Load trace with vertical lines indicating the time of observed events from the regular speed camera. Note that the load drop was not as sharp as it is for the faster tests, even with the large scale fracture.

I05_D10_V0p1_I- Thin section pictures (indented from top). The left side shows the thin section under cross polarized light. The right side shows the thin section under a side reflected light.

Test: I05_D10_V0p1_E

Figure Error! No text of specified style in document.**-5: I05_D10_V0p1_E- Post test pictures. This set of pictures illustrates well the zone of damage under the indenter.**

I05_D10_V0p1_E- Test observations

1. Loud continuous cracking/popping noises
2. Large edge fracturing

I05_D10_V0p1_E- Regular speed video observations

Regular Video Observation (the test was too slow for HSV)	Normalized Time (seconds)
Test start	0
Internal crack (5 mm in length) appears	1.4
Crack reaches edge	2.1
Crack "jumps" about 2 mm around perimeter	7.1
Large fracture chunk breaks free on all sides of crack	8.1
Chunk falls away	14.1
Indention continues with sample sliding along platform	

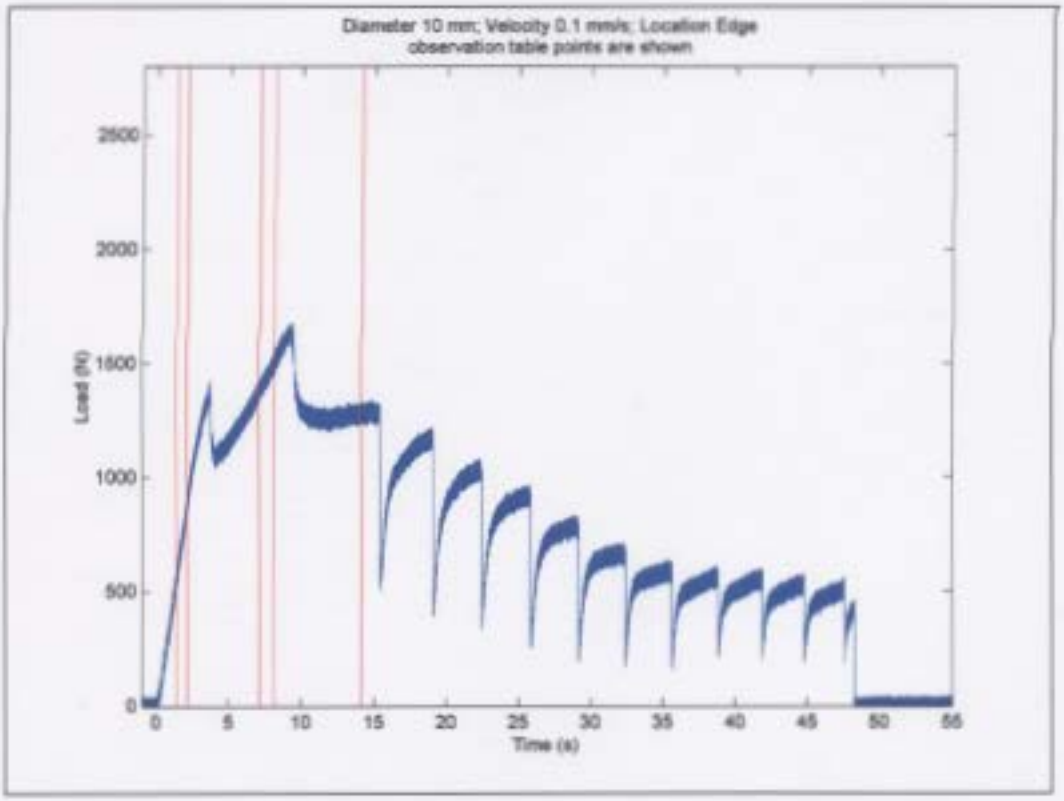

I05_D10_V0p1_E- Load trace with vertical lines indicating the time of observed events from the high speed camera.

I05_D10_V0p1_E- Thin section pictures (indented from top). The left side shows the thin section under cross polarized light. The right side shows the thin section under a side reflected light.

I05_D20_V10p0_C

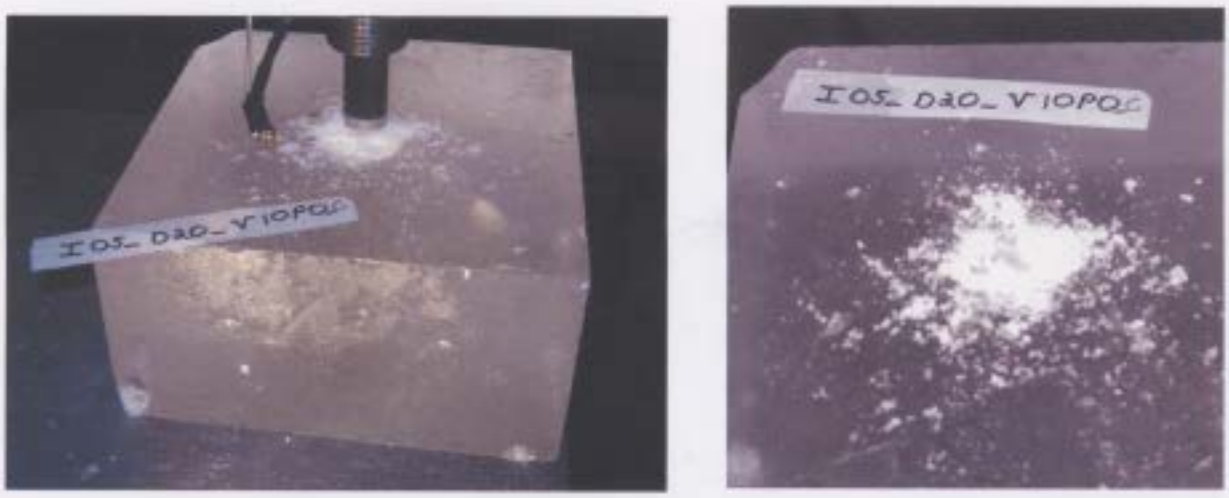

I05_D20_V10p0_C- Post test pictures. The left side shows clearly that relatively large pieces of ice were injected away from the indenter. The right side shows that within the indenter footprint, areas of white crushed ice, and areas of clear ice are present.

I05_D20_V10p0_C- Test observations:

1. Corner (back left in top picture) was cracked prior to testing)
2. Indenter "bored" into the sample causing continuous expulsion of crushed ice with periodic large "violent" ejections of larger particles with high velocity
3. Loud continuous cracking noises

I05_D20_V10p0_C- High speed video observations

HSV Observation	Start Time as seen from HSV (seconds)	Normalized Time (seconds)
Indenter contact	0.296	0
End of 1st HSV file	0.324	0.028
2nd HSV file	0	0.028
Significant expulsion	0.101	0.129
Significant expulsion	0.202	0.23
Significant expulsion	0.223	0.251
Significant expulsion	0.27	0.298
End of 2nd HSV file	0.324	0.352
3rd HSV file	0	0.352
Significant expulsion	0.009	0.361
Significant expulsion	0.082	0.434

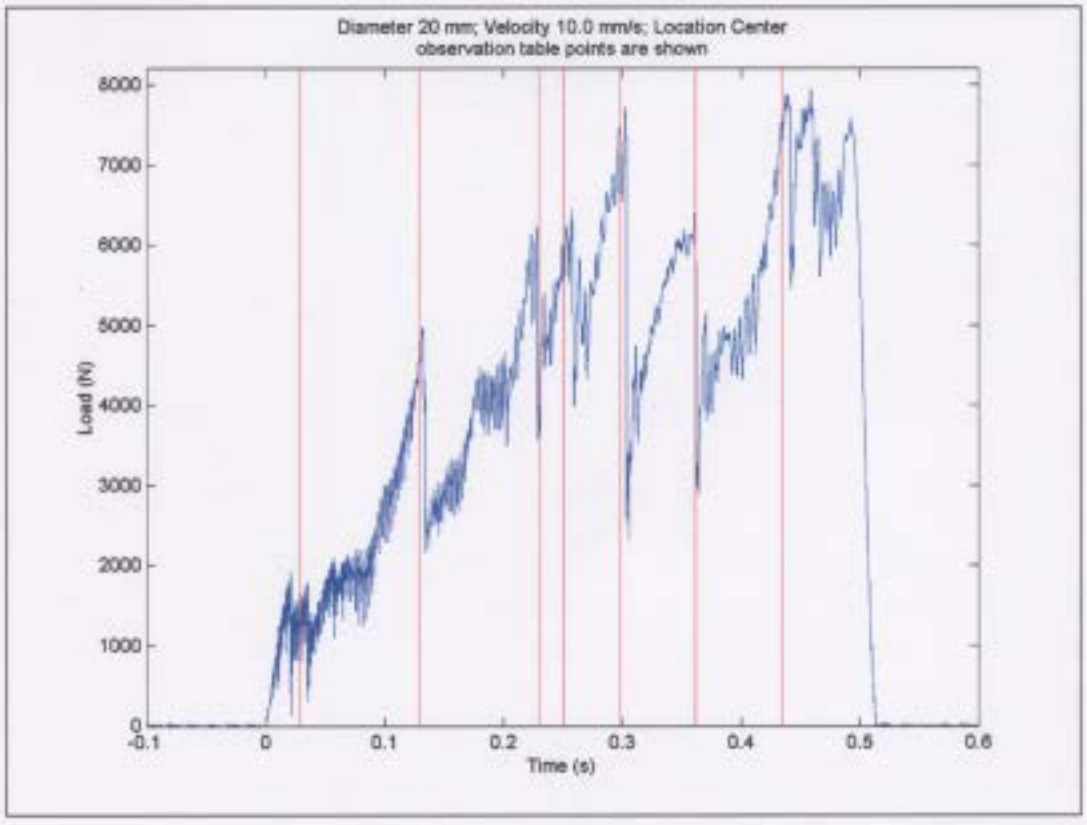

I05_D20_V10p0_C-Load trace with vertical lines indicating the time of observed events from the high speed camera. This is a particularly fine example of when the observed events correlate to the load trace.

I05_D20_V10p0_C- Thin section pictures (indented from top). The left side shows the thin section under cross polarized light. The right side shows the thin section under a side reflected light (note that the micro-cracks at depth are forming around grain boundaries).

Test: I05_D20_V10p0_I

I05_D20_V10p0_I- Post test pictures. The left side shows clearly that relatively large pieces of ice were injected away from the indenter. The right side shows that within the indenter footprint, areas of white crushed ice, and areas of clear ice are present.

I05_D20_V10p0_I- Test observations:

1. Indenter "bored" into the sample causing continuous expulsion of crushed ice with periodic large "violent" ejections of larger particles with high velocity
2. Loud continuous cracking noises
3. Large chip/flake was ejected from the top of the sample near the indenter

I05_D20_V10p0_I- High speed video observations

HSV Observation	Start Time as seen from HSV (seconds)	Normalized Time (seconds)
Indenter contact	1.282	0
Significant expulsion	1.32	0.038
Significant expulsion	1.386	0.104
Significant expulsion	1.412	0.13
Significant expulsion	1.43	0.148
Significant expulsion	1.447	0.165
Significant expulsion	1.588	0.306
2nd HSV file	0	0.344
Significant expulsion	0.03	0.374
Significant expulsion	0.075	0.419

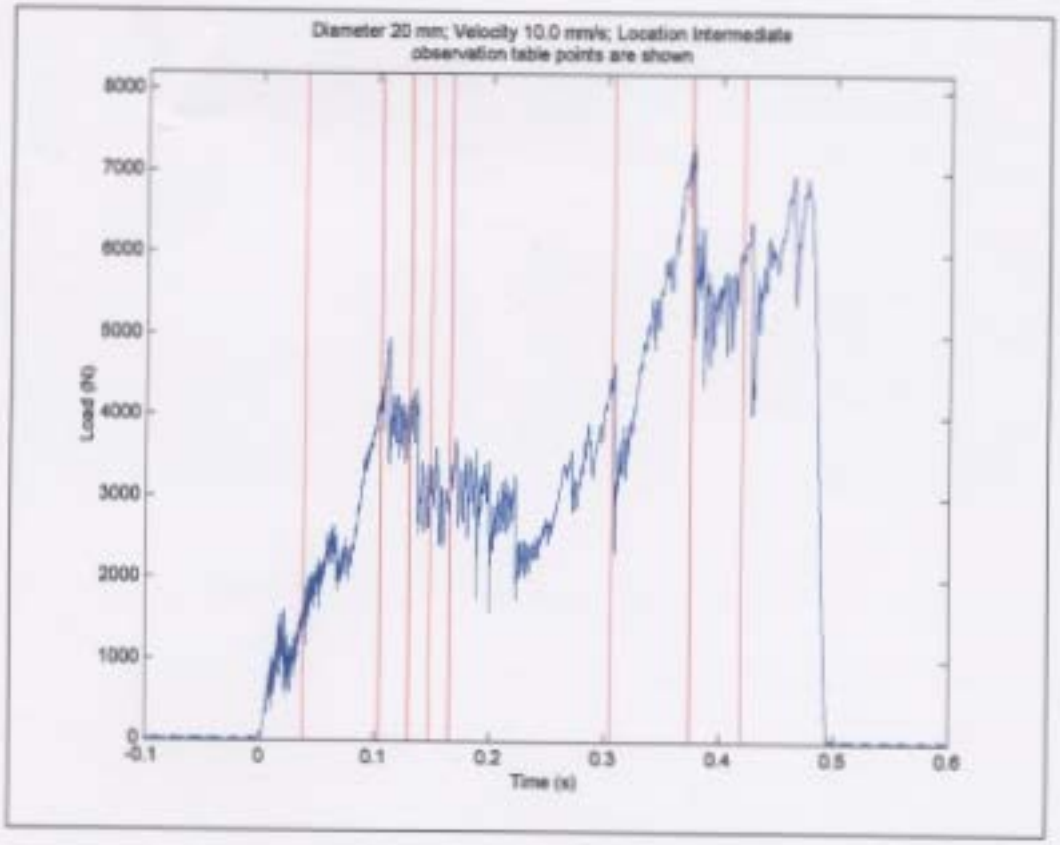

Figure Error! No text of specified style in document.**-6: I05_D20_V10p0_I- Load trace with vertical lines indicating the time of observed events from the high speed camera.**

I05_D20_V10p0_I- Thin section pictures (indented from top). The left side shows the thin section under cross polarized light. The right side shows the thin section under a side reflected light.

Test: I05_D20_V10p0_E

I05_D20_V10p0_E- Post test pictures. The left side shows the large edge spall that fractured off. The right side shows that within the indenter footprint, areas of white crushed ice, and areas of clear ice are present. It also shows that the edge crack forms at roughly the center of the indenter footprint.

I05_D20_V10p0_E- Test observations:

1. Large edge fracture happened very quickly
2. Loud continuous cracking noises
3. The sample underwent "stick-slip" movement relative to the platform after the large spall fell away

I05_D20_V10p0_E- High speed video observations

HSV Observation	Start Time as seen from HSV (seconds)	Normalized Time (seconds)
Indenter contact	1.422	0
Radial crack begins	1.455	0.033
Fracture breaks through to sides	1.464	0.042
Spalled piece falls away	1.47	0.048
Sample begins to slide on platform	1.501	0.079

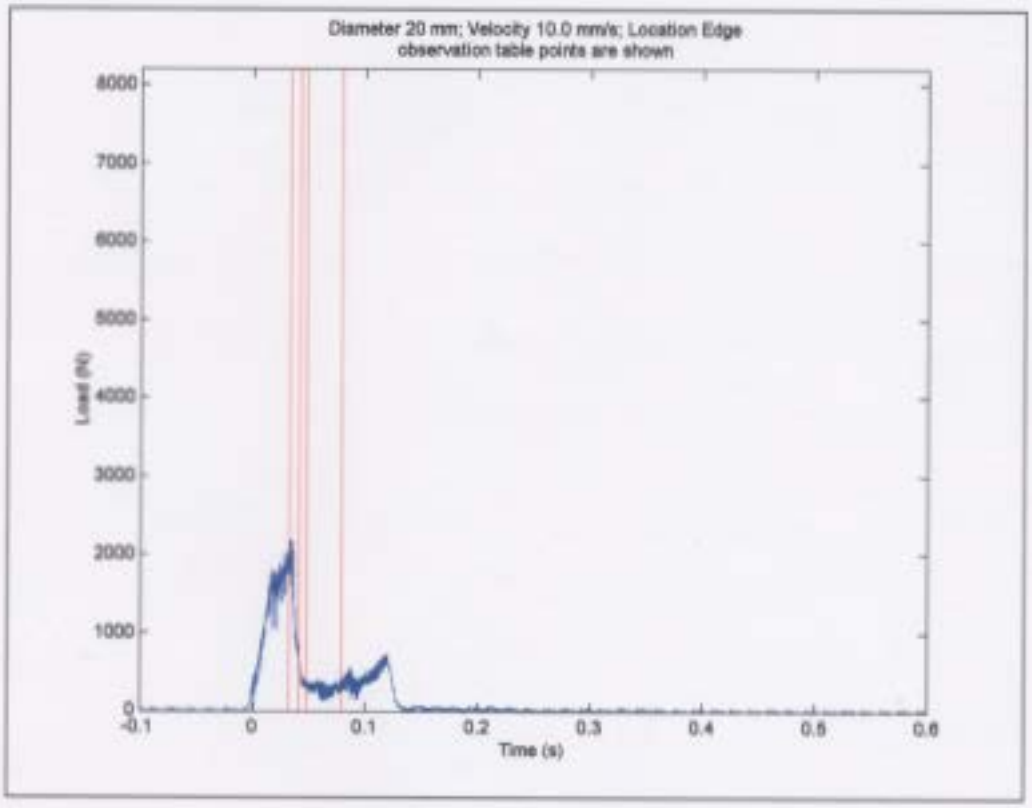

I05_D20_V10p0_E- Load trace with vertical lines indicating the time of observed events from the high speed camera. Notice that before the large spall happens (time 0.01-0.04 seconds), the load ramps upwards and then undergoes a cyclic loading. This was a period of some small but high speed extrusion and rapid growth of a zone of "white" near the indenter.

I05_D20_V10p0_E- Thin section pictures (indented from top). The left side shows the thin section under cross polarized light. The right side shows the thin section under a side reflected light. This shows shallow penetration of the indenter due to sliding of the specimen after the large fracture. The large elongated crystals in the cross polarized picture are related to the seeding process.

Test I05_D20_V2p0_C

I05_D20_V2p0_C- Post test pictures. This was the first test completed, and the process of taking pictures was not refined. This is the only post test picture from this experiment. It illustrates well the idea of clear ice (recrystallized in the high pressure zone) and white ice (crushed and extruded to the side of the high pressure zone).

I05_D20_V2p0_C- Test observations:

1. High velocity extrusions
2. Loud continuous cracking noises
3. The sample had a visible "channel" located within it (due to seeding process)

Note: No thin sections available for this test

I05_D20_V2p0_C- High speed video observations

HSV Observation	Start Time as seen from HSV (seconds)	Normalized Time (seconds)
Indenter contact	2.798	0
Medium size expulsion	2.966	0.168
Small expulsion	3.152	0.354
Small expulsion	3.232	0.434
End of first HSV file	3.252	0.454
Start of Second HSV file	0	0.454
Small expulsion	0.168	0.622
Crushing extrusion	0.168	0.622
Significant expulsion	0.676	1.13
Small expulsion	0.864	1.318
Significant expulsion	0.888	1.342
Significant expulsion	1.192	1.646
Significant expulsion	1.322	1.776
Significant expulsion	1.538	1.992

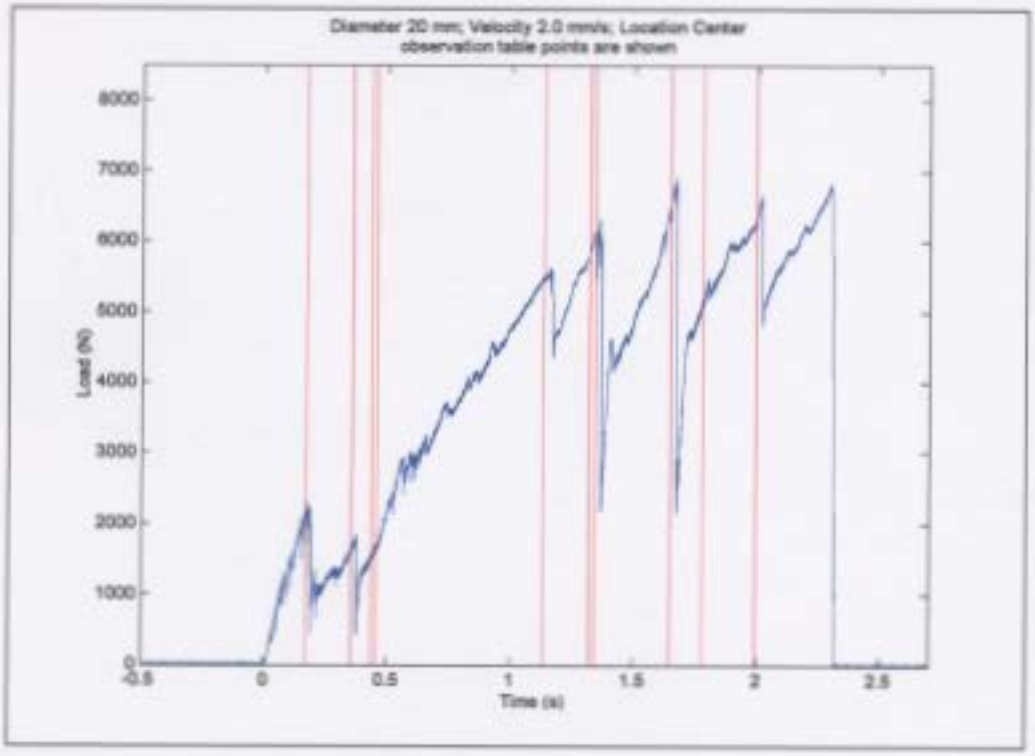

I05_D20_V2p0_C- Load trace with vertical lines indicating the time of observed events from the high speed camera.

I05_D20_V2p0_I

Figure Error! No text of specified style in document.**-7: I05_D20_V2p0_I- Post test pictures. This was one of the most violent fractures. Clear and white zones were visible within the indenter footprint even in such a broken test sample.**

I05_D20_V2p0_I- Test observations:

1. Large fracture happened very quickly, but flickers of light (possible internal cracks) were visible prior to fracture
2. Loud continuous cracking noises
3. The Load dropped to zero after this fracture, as the size and force of it cleared all the ice away from the indenter

I05_D20_V2p0_I- High speed video observations

HSV Observation	Start Time as seen from HSV (seconds)	Normalized Time (seconds)
Indenter contact	2.678	0
Significant expulsion	3.218	0.54
End of 1st HSV file	3.252	0.574
2nd HSV file	0	0.574
Significant expulsion	0.204	0.778
Significant expulsion	0.346	0.92
Significant expulsion	0.63	1.204
Significant expulsion	0.864	1.438
Large splitting fracture begins	1.101	1.675
Block has begun to spread open and slid	1.125	1.699

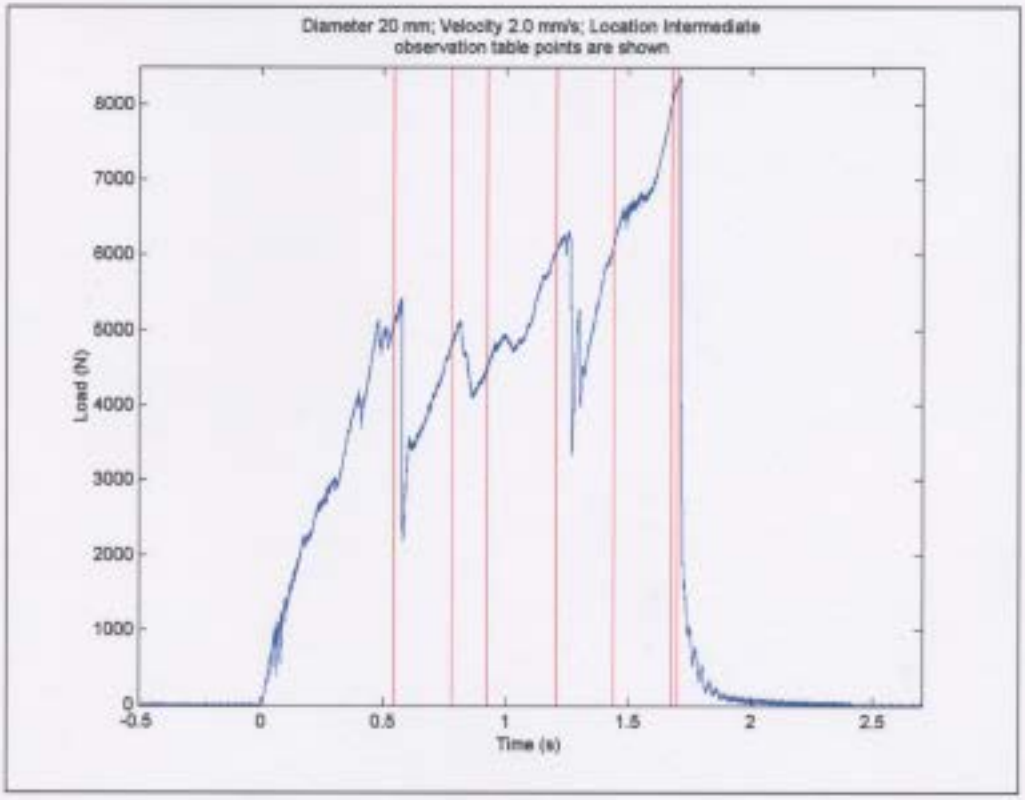

I05_D20_V2p0_I- Load trace with vertical lines indicating the time of observed events from the high speed camera.

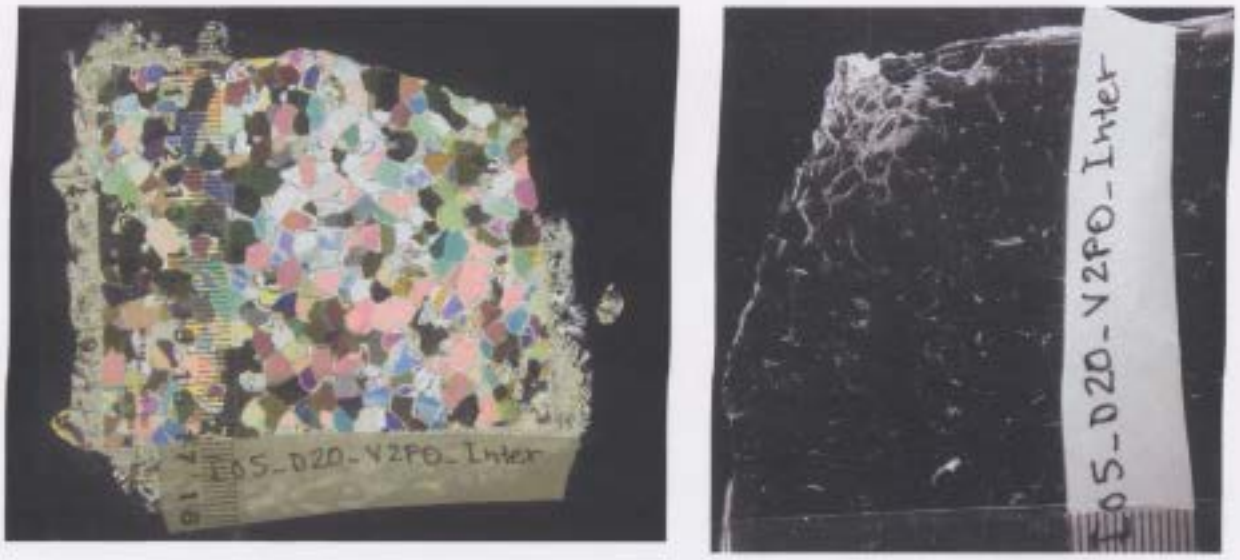

I05_D20_V2p0_I- Thin section pictures (indented from top). The left side shows the thin section under cross polarized light. The right side shows the thin section under a side reflected light. The odd shape of the thin section is related to a fracture that began at the indenter contact. The sample was flipped during photographing.

Test: I05_D20_V2p0_E

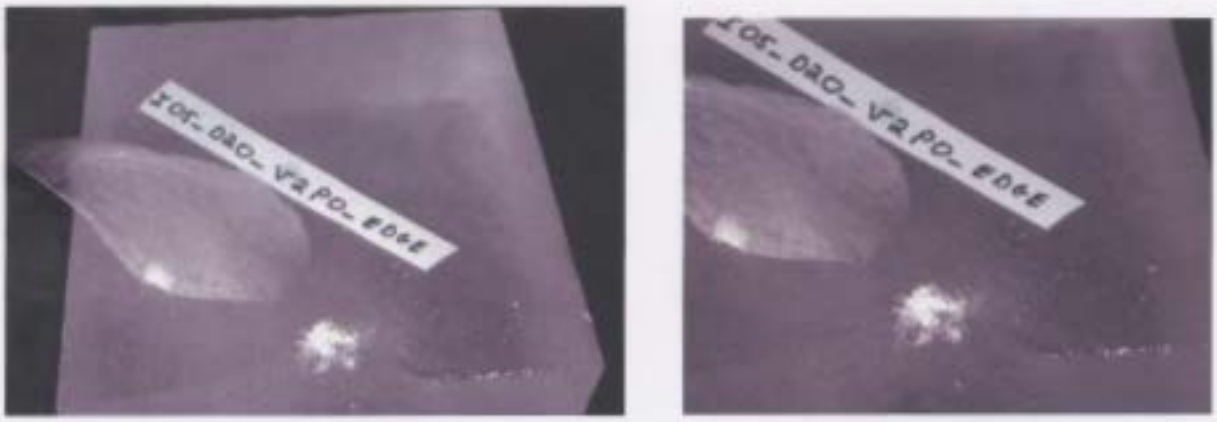

Figure Error! No text of specified style in document.**-8: I05_D20_V2p0_E- Post test pictures. Radial shape of spalled piece is visible.**

I05_D20_V2p0_E- Test observations:

1. Large fracture happened very quickly, the spalled off piece was razor thin at the bottom
2. Loud continuous cracking noises
3. The sample underwent "stick-slip" movement relative to the platform after the large spall fell away

I05_D20_V2p0_E- High speed video observations

HSV Observation	Start Time as seen from HSV (seconds)	Normalized Time (seconds)
Indenter contact	2.702	0
Small Expulsion	2.804	0.102
Start of large radial crack growth	2.889	0.187
End of large radial crack growth	2.905	0.203
Crushing and spall falls away from parent	2.905- 3.252	0.203-0.55
End of first HSV file	3.252	0.55
Start of Second HSV file	3.252	0.55
Continued crushing and horizontal "stick slip of sample	3.252 until the end of the test	0.55 until the end of the test

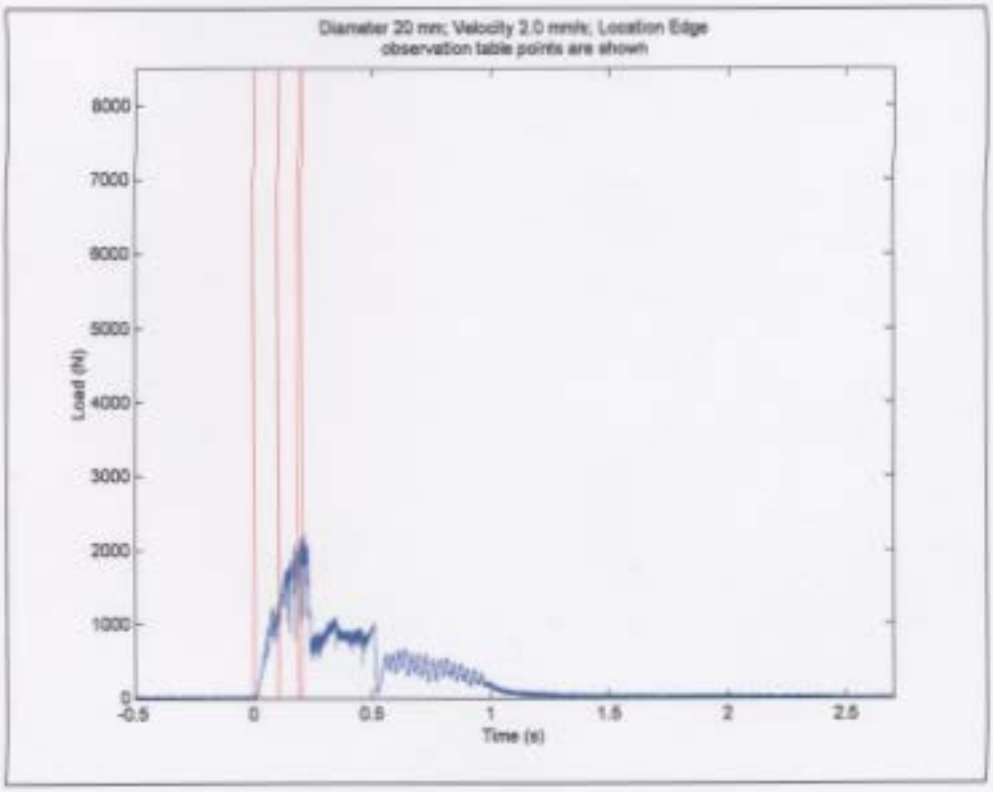

I05_D20_V2p0_E- Load trace with vertical lines indicating the time of observed events from the high speed camera.

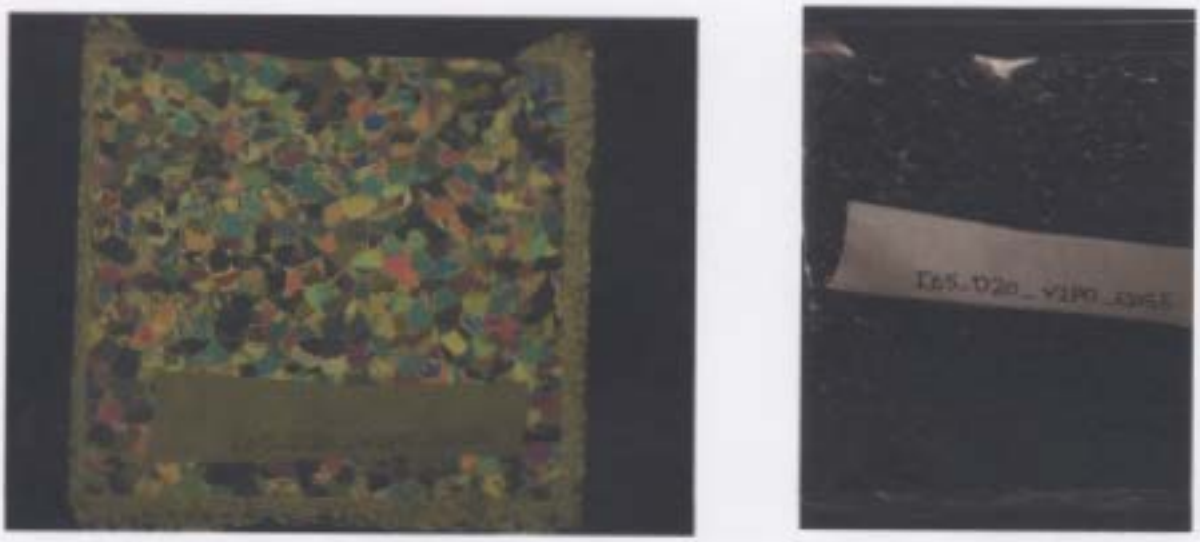

I05_D20_V2p0_E-Thin section pictures (indented from top). The left side is the thin section under cross polarized light and the right side is the thin section under side reflective light.

Test: I05_D20_V0p2_C

I05_D20_V0p2_C- Post test pictures. This was the only centrally located test to fracture. Note the large area of damage.

I05_D20_V0p0_C- Test observations

1. Large fracture happened very quickly, and involved a violent release of energy
2. A lot of activity in the white zone around indenter, but not much material ejected
3. Large amount of micro-cracking around the indenter, accompanied by "cracking and popping" noise

I05_D20_V0p2_C- Regular speed video observations

Regular Video Observation (the test was too slow for HSV)	Normalized Time (seconds)
Start	0
1st internal fracture becomes apparent within sample	10.6
2nd Internal fracture becomes apparent within sample	11.4
Sample splits apart into 3 pieces	11.7

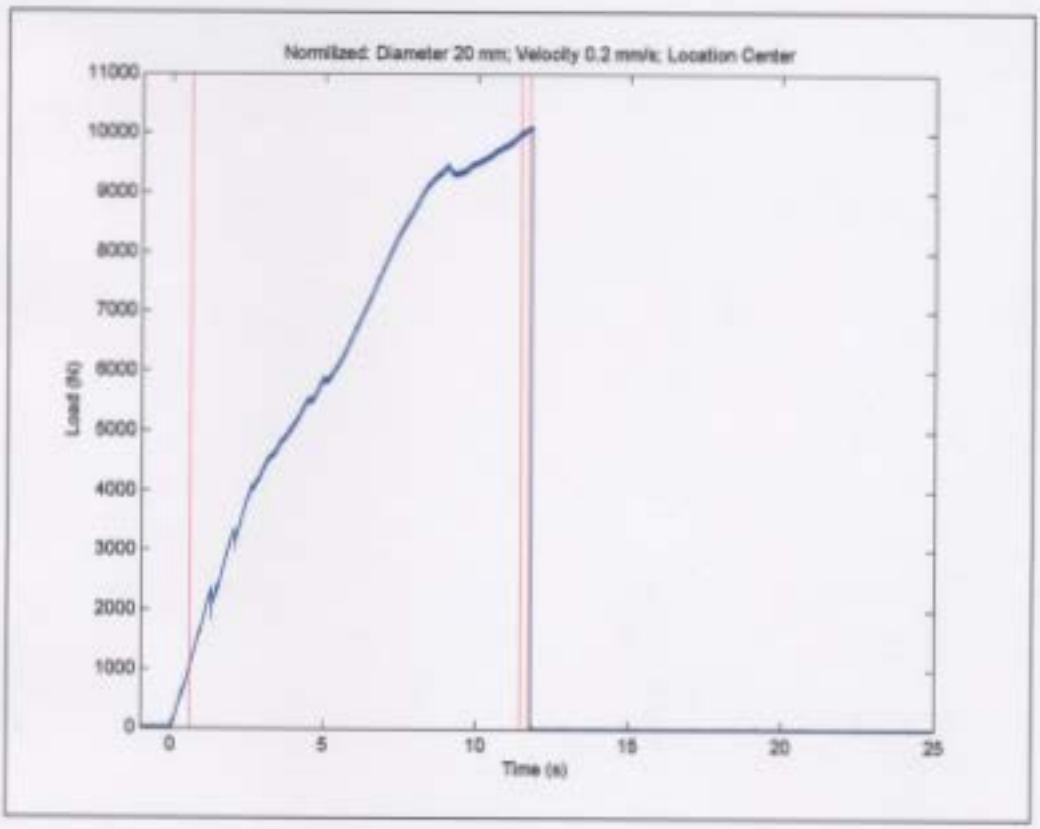

I05_D20_V0p2_C- Load trace with vertical lines indicating the time of observed events from the high speed camera

I05_D20_V0p2_C- Thin section pictures (indented from top). The left side is the thin section under cross polarized light and the right side is the thin section under side reflective light. Note the large zone of micro-cracking.

Test: I05_D20_V0p2_I

I05_D20_V0p2_I- Post test pictures. The left side shows the depth of the damaged zone. The sample cracked into 3 pieces, the large one visible in the top right and 2 smaller pieces of approximately the same size.

I05_D20_V0p2_I- Test observations:

1. Large fracture happened very quickly, with interior flickers of light prior to large fracture
2. Loud continuous cracking noises
3. The sample underwent "stick-slip" movement relative to the platform after the large spalled off piece of ice fell away

I05_D20_V0p2_I- Regular speed video observations

Regular Video Observation (the test was too slow for HSV)	Normalized Time (seconds)
Indenter contact	0
Interior crack flicker	2.3
Large 3 way crack appears	2.5
Cracks begin to open up	7.2
Complete separation of cracks	9.3

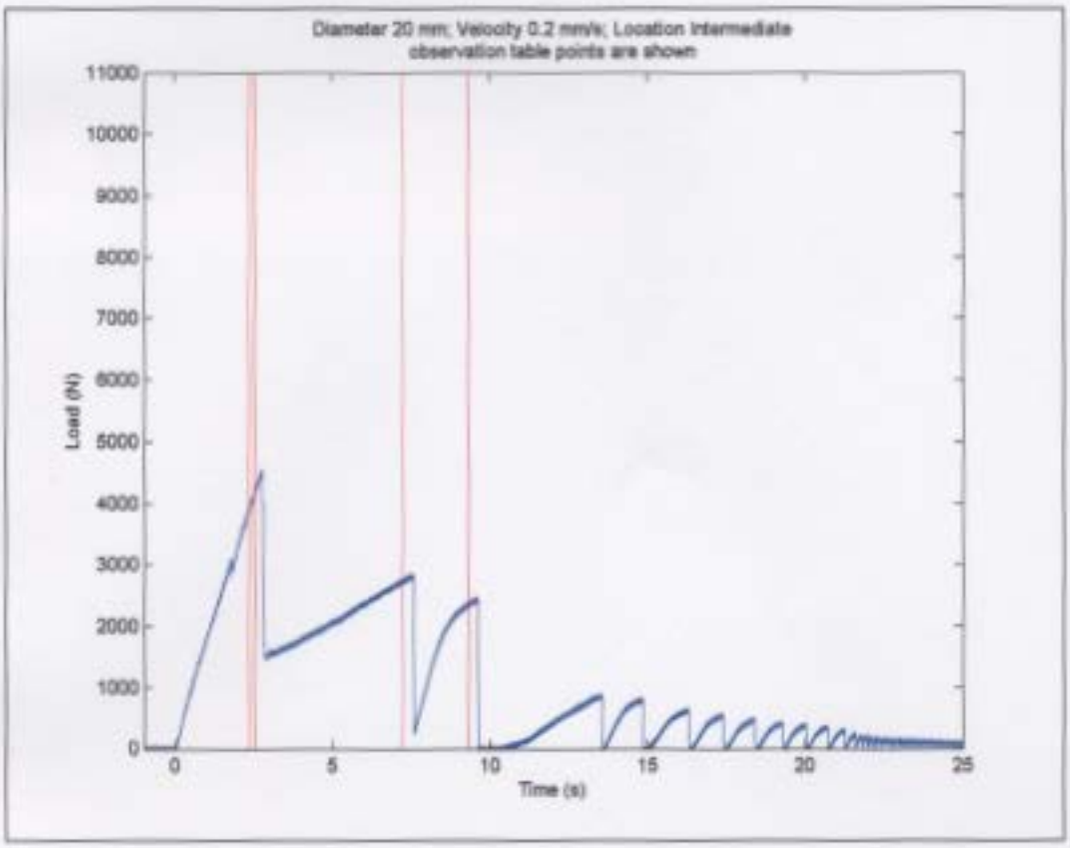

Figure Error! No text of specified style in document.**-9: I05_D20_V0p2_I- Load trace with vertical lines indicating the time of observed events from the high speed camera.**

I05_D20_V0p2_I- Thin section pictures (indented from top). The left side shows the thin section under cross polarized light. The right side shows the thin section under a side reflected light. The odd shape of the thin section is related to a fracture that began at the indenter contact.

Test: I05_D20_V0p2_E1

I05_D20_V0p2_E1- Post test pictures. Edge fracture is visible

I05_D20_V0p2_E1- Test observations:

1. Large fracture happened very quickly
2. Lots of crushed damage around indenter
3. Loud continuous cracking noises
4. The sample underwent "stick-slip" movement relative to the platform after the large spall fell away

I05_D20_V0p2_E1- Regular speed video observations

Regular Video Observation (the test was too slow for HSV)	Normalized Time (seconds)
Indenter contact	0
Edge fracture appears	1.0
Flake drops off	3.3
2nd edge fracture appears	5.5
2nd edge fracture grows in a "jump"	5.6
2nd edge fracture grows in a 2nd "jump"	5.7
2nd flake is ejected at a high speed	10.1
Crushing continues with stick-slip of sample	Till end

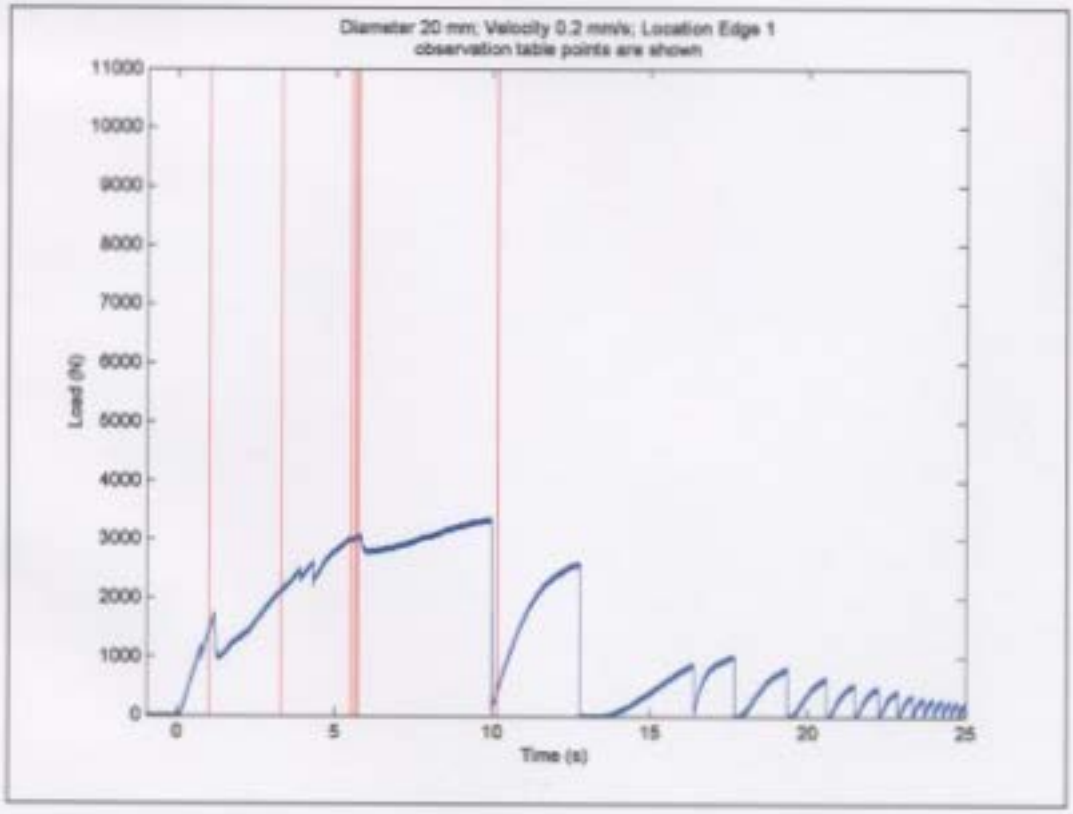

I05_D20_V0p2_E1- Load trace with vertical lines indicating the time of observed events from the high speed camera.

I05_D20_V0p2_E1- Thin section pictures (indented from top). The left side is the thin section under cross polarized light and the right side is the thin section under side reflective light.

Test: I05_D20_V0p2_E2

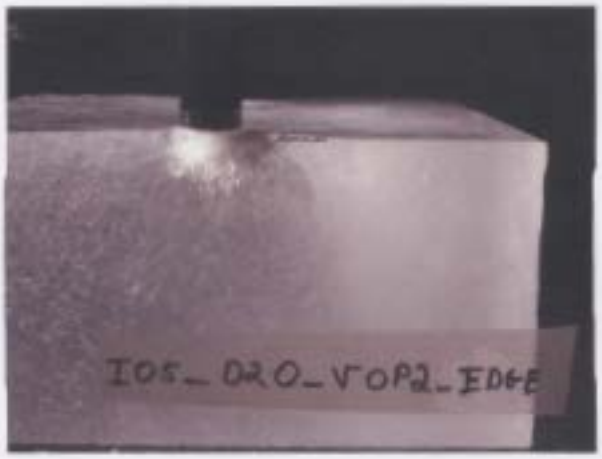

I05_D20_V0p2_E2- Post test pictures. This is the 2nd test on the same block.

I05_D20_V0p2_E2- Test observations:

1. Large fracture happened very quickly, the spall was razor thin at the bottom
2. Loud continuous cracking noises
3. The sample underwent "stick-slip" movement relative to the platform after the large spall fell away

I05_D20_V0p2_E2- Regular speed video observations

Regular Video Observation (the test was too slow for HSV)	Normalized Time (seconds)
Indenter contact	0
Edge fracture appears	0.7
Edge fracture grows in "jump"	0.8
Large flake ejected	2.4
Crushed ice ejected from damaged zone	5
Large slip movement of sample	7.1
Crushing continues with stick-slip of sample	Till end

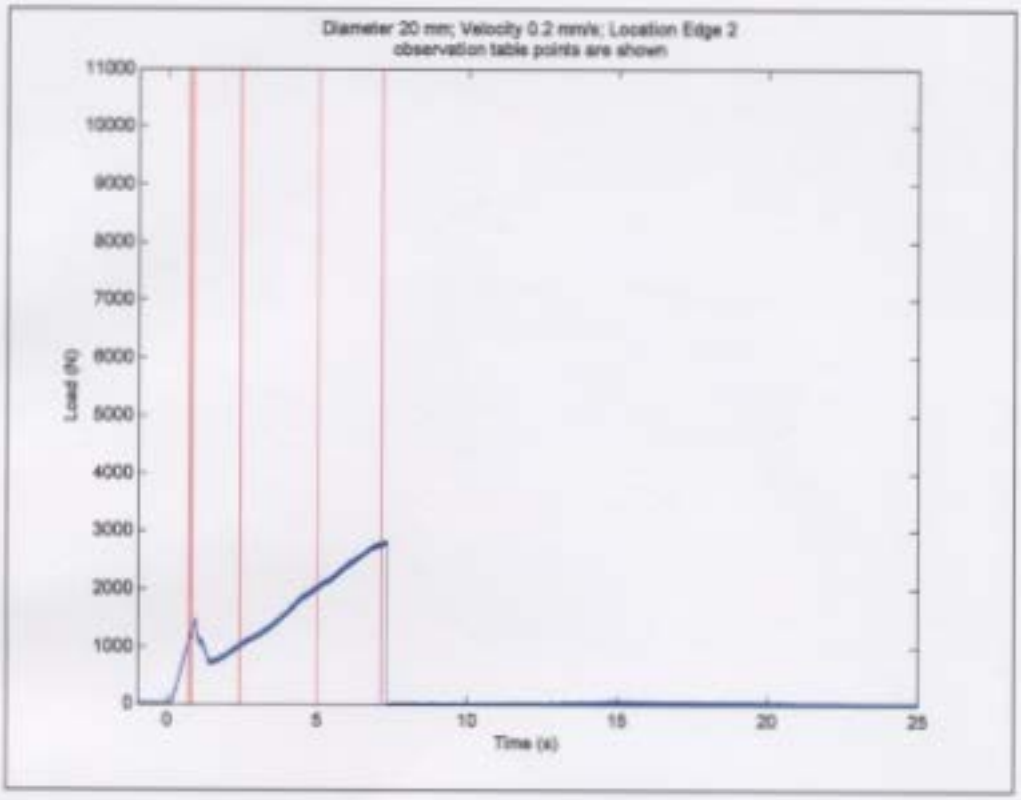

I05_D20_V0p2_E2-Load trace with vertical lines indicating the time of observed events from the high speed camera.

I05_D20_V0p2_E2- Thin section pictures (indented from top). The left side is the thin section under cross polarized light and the right side is the thin section under side reflective light. This is a particular good example of inter-grain boundary cracking.